UNIVERSITY OF COPENHAGEN
FACULTY OR DEPARTMENT

Master's Thesis

Diana Spurzem

Representativity of albedo measurements of Automated Weather Stations in Greenland

Supervisor: Aslak Ginsted, Baptiste Vandecrux

Submitted on: 31 May 2021

Abstract

The Greenland Ice Sheet is a key component of Earth's climate system that has been evidently influenced by global warming. Determined by an interconnected climate system, the changes of the ice sheet are involved in feedback mechanisms that can enhance further warming of the Earth. The surface's albedo marks one essential feedback mechanism. In order to better emphasize scientific research of climate change impacts, it is essential to constantly monitor the Greenland ice sheet. Two predominant sources of climate-related data about the Greenland ice sheet are automated weather stations and remote sensing products. An ongoing concern in the field is the comparability of the differently retrieved data. Weather stations have a limited footprint on what they measure in situ, which might not correspond to the actual circumstances of the site. This makes it challenging to process the data in terms of representativity. Because satellites measure way larger footprints, a point-to-pixel comparison can disagree. A homogenous ground surface indicates similar conditions within a certain area. A heterogeneous surface however might distort the results. Global warming can enhance this matter by increasing the surface melt in Greenland and therefore decreasing the amount of homogenous snow surfaces. To confront the issue, this study evaluated the representativity of 40 automated weather stations in Greenland to detect whether they represent their local environment well. It is expected to give further access to the aspects on (1) how representative the individual weather stations are for their surrounding area; (2) which local conditions occur when the station is representative or not representative and (3) how this is influenced by the melt season. The analysis was done using Landsat 8 high resolution data in an area corresponding to a 1km^2 MODIS grid pixel to approach the viewpoint of point-to-pixel comparison. The 40 weather stations were categorized into three groups, characterizing how representative they are in terms of albedo. The results showed that stations located on a homogenous snow cover all year around are highly representative. This occurred for all weather stations located at an altitude above 1500m. Some slightly lower elevated stations, placed further inwards on the ice sheet and thereby characterized by stable weather conditions, revealed comparable representativity. Stations in the ablation zone, primarily near the coast and in the Southern half of the island, were stronger affected by changing conditions during melt season. For weather stations at sites with varying elevations and different surfaces, a high representativity was not a given anymore. It mainly appeared during the shift between snow-covered and snow-free land as the area partly covered in snow showed differences in reflectance. Meltwater lakes close by influenced the albedo representativity markedly. Meltwater streams and crevasses revealed deviations as well but not as strong as lakes.

Acknowledgment

I would like to acknowledge and give my warmest thanks to my supervisor Baptiste Vandecrux who introduced me to the topic under the Geological Survey of Denmark and Greenland (GEUS) and guided me through all the stages of writing my project. I was given the chance to dig deeper into the field of remote sensing what has had my interest for so long.

Another special thanks I would like to give, is to my supervisor Aslak Grinsted. His advice and ideas shaped the realization of this project significantly.

Finally, a huge thanks goes to my family for supporting my decision to complete my studies in Denmark as well as to my friends for supporting me during the entire study time.

Table of Contents

1. Introduction

The Greenland ice sheet represents an important component in the Earth's climate system. It is a key indicator of the past, current and future progress of global climate. Not only is it an indispensable foundation for scientists to understand the changing conditions, but it also affects the Earth's energy balance with its highly reflecting surface and therefore the planet's climate. By reflecting a large proportion of incoming solar radiation, it enhances cooling of the earth. Albedo, representing the brightness of a surface and thereby its ability of reflecting incoming radiation, can be observed from space by satellites as well as in situ by automated weather stations. For the reason that both have individual footprints of investigating, it is challenging to directly compare their data. The weather station measures a very limited area while remote sensing observations examine way larger areas. Ryan et al. (2017) observed a significant difference in albedo results between in situ and satellite-retrieved data. Particularly heterogeneous surfaces, that occur in summer when the snow melts, influence the representativity. In this study, the local conditions of 40 weather stations were observed in order to determine their representativity of the surrounding area.

1.1. Background

Impacts of Climate Change on the Arctic

After Antarctica, the Greenland ice sheet is the second largest ice sheet in the world. Located in the polar region of the Northern Hemisphere, Greenland is part of the Arctic. In the Arctic, interconnected physical, chemical and biological systems are found that are directly and indirectly affected by climate change and interact in the global climate system. Ecosystems, weather conditions and human communities are impacted by the shifts. Researchers agree that the Arctic shows an undeniable warming. Each of the past years from 2014 to 2018 showed the highest annual surface air temperature that has been measured in the Arctic since the beginning of observational records in 1900, which has significant ice mass loss as a consequence. Between 1971 and 2017, the annual surface temperature in the Arctic rose by 2,7 °C; 3,1°C during the cold season and 1,8°C during the warm season. Evidence from lake sediments, tree rings and ice cores prove that Arctic summer temperatures have been higher in the past few decades than at any point in time in the past 2000 years. Projections as well as observations confirm that the annual warming in the Arctic is more than twice the global mean, especially in winter. From 1971 to 2017, the warming was 2,4 times faster than the mean of the Northern Hemisphere (AMAP, 2019).

Likewise, the temperature of the sea surface and ocean is increasing, too. Those rises in temperature result in an accelerated process of snow and ice melting. The sea ice is very vulnerable to atmospheric warming and the influx of warmer waters from the South (AMAP, 2017). Even if the world successfully maintains global warming near +2°C, the Arctic is expected to have a noticeably different environment by mid of the 21st century. Under current trends and projections, the melt season will start earlier and last longer. This will result in shorter snow and ice periods (Overland et al., 2019). The four most important cryospheric characteristics influenced by global warming are losses of sea ice, snow, permafrost and land ice. All of them are projected to occur over the next 50 years (AMAP, 2017).

Arctic sea ice indicates a shift from multiyear to seasonal sea ice with decreased extents and thickness. AMAP (2017) expects the Arctic to experience ice-free summers by the end of 2030 under the current warming conditions. Especially during spring, snow scope has reduced in recent decades. Projected impacts in Arctic snow cover involve a 10-20% decrease of the snow cover period in most of the Arctic by mid-century. This trend will remain as Arctic temperatures continue to rise even when the worldwide greenhouse gas emissions stop rising. Projections predict future precipitation to increase in the Arctic, however, with more of the precipitation falling as rain rather than snow (AMAP, 2017).

Models show a 20% decline in near-surface permafrost area in the Arctic by 2040, with minor dependence on the RCP scenario (Arzhanov, 2013). Land ice masses show a slow response time, especially the Greenland ice sheet. With atmospheric and oceanic warming over the century, independent of greenhouse gas reductions, projected mass loss from land ice does not stabilize before the end of the 21st century (AMAP, 2017). Furthermore, under current temperatures (1981–2010), Arctic glaciers should additionally lose about 35% of their volume (Mernild, 2013).

The individual seasons are affected differently by climate change: The greatest increase in surface air temperature is seen in autumn, in regions where the sea ice is gone by the end of summer. This indicates that the sea is absorbing more solar radiation during the summer as the ice cover decreases. The extra energy is being released as heat in autumn, further warming the Arctic's lower atmosphere. Over land, the number of days with snow cover has changed the most in spring. Early snow melt is enhanced by earlier and stronger warming of land that is no longer snow-covered (AMAP, 2011). Those intensifying seasonal changes have a large effect on the brightness of Greenland's surface and its reflectance of sunlight.

Climate influences on the Greenland ice sheet

Precipitation, sea ice loss and surface melt along with runoff are three main factors affecting the Greenland ice sheet development. Throughout the recent climate history, statistically, over 90% of the precipitation over the Greenland ice sheet has fallen as snow, working as the major source of ice sheet mass gain (Ettema et al., 2009). Ice masses form when snow that falls during winter does not melt entirely over the summer. Over thousands of years, the layers of snow pile up into thick masses of ice, growing thicker and denser with the mass of new snow and ice layers compressing the older layers. In order to remain stable, the ice sheet has to accumulate the same mass of snow as it loses to the sea. Areas where more mass is gained than lost are called accumulation zones. When the snow and ice ablation (melting) exceed the accumulation, the term ablation zone is used (NSIDCa).

Since the early 1990s, several observations and modelling findings have indicated strong warming and an increase in runoff in Greenland. High-altitude sites warmed by approximately 2,7°C over the past 30 years (Orsi et al., 2017). Satellite measurements showed statistically significant widespread surface warming over the Northern ice sheet from 2000 to 2012 (Hall et al., 2013). Ice core analysis found the 2000–2010 decade to be the warmest for around 2000 years. The precipitation frequency, intensity and distribution as well as humidity are increasing under the changing climate and affect the freshwater flow into the Arctic Ocean. This influences important components like ocean circulations, nutrient level, acidification or the biological pump, which again, interconnect globally. Additionally, a change in precipitation affects the soil moisture influencing vegetation growth, which has a major importance in the food chain for wildlife. Higher humidity can amplify warming and snowmelt (AMAP, 2019).

The Greenland ice sheet is the largest single source of barystatic sea-level rise (Hofer et al. , 2020). A geodetic reconstruction indicated an annual ice sheet mass change of -186,4 ± 18,9 Gt from 2003 to 2010, with the losses concentrated along the northwest and southeast coasts (Kjeldsen et al., 2015). The combination of an increase in dynamic thinning of the ice and a reduction in surface mass balance cause the ongoing mass loss of the ice sheet over recent years. The increase in surface melting and runoff are very dominating elements in the process (Andersen et al., 2015; van den Broeke et al., 2017).

The surface meltwater on the Greenland ice sheet, primarily caused by solar radiation, is part of a supraglacial hydrological system. Mainly located in the ablation area, the system includes supraglacial lakes, streams, crevasses, and moulins. Meltwater accumulates in the lakes and flows off through streams and crevasses. Some goes directly across the ice sheet surface to the ocean, while most is transported through vertical surface-to-bed hydrologic connections (moulins) and after all

reaches the subglacial area and then the sea. The supraglacial lakes add to the negative mass balance of the ice sheet because the melting rate of the ice sheet is affected by the low albedo of the lakes, which cause a decreased solar radiation reflectance (Yuan et al., 2020). The IPCC (2013) declares it as likely that the annual period of surface melt on Arctic persistent sea ice lengthened by 5,7 ± 0,9 days per decade over the period from 1979 to 2012.

An ice sheet is constantly in movement as of its large mass, slowly flowing downwards under its own weight's pressure. Near the coast, most of the ice moves through relatively fast-moving outlets: ice streams, glaciers and ice shelves. The higher temperatures in the past decades however have caused meltwater to trickle through beneath Valley glaciers that end up in the ocean, initiating them to flow faster and increasing the rate of ablation as well as ice loss from the continent. This results in Greenland's ice melting even faster than expected. The rate of melting could increase with further rising temperatures. Melting all of Greenland would increase the global sea level by approximately 7m (Kump et al., 2014).

Greenland's interconnection with Earth's climate

The cryosphere is an integral part of the climate system and affects climate regionally as well as globally. Greenland contributes essentially towards that impact (AMAP, 2017). There are several mechanisms of the cryosphere interacting with the climate system. Essential cryospheric feedback mechanisms involve the albedo (See chapter *Ice-Albedo-Feedback*) and heat storage changes from loss of glaciers, sea ice, and snow cover. The ocean surface stores thermal energy. Sea ice prevents a direct heat transfer from the ocean into the atmosphere. With increasing temperatures, the ice cover is thinning and decreasing which leads to a higher heat flux from the ocean to the atmosphere. This results in higher temperatures and therefore creates a feedback cycle. Other important feedback mechanisms include the increased carbon releases from permafrost; shifts in clouds and increases in water vapor; and atmospheric and ocean transport shifts. These phenomena are not fully understood yet but play an important role and can alter the rate or even direction of climate change and associated changes in the cryosphere (Overland et al., 2019).

The Greenland ice sheet is one of several potential tipping elements in the Earth's climate system, which means it is characterized by a threshold behaviour. Models suggest that there are only certain levels of the Greenland ice sheet volume that are stable, implying that once a tipping point is exceeded, a significant part of the ice sheet will melt, causing several meters of global sea level rise. The exact temperature of the tipping point is uncertain. IPCC (2013) estimates it to be a warming of somewhere between 1,9 and 4,6°C. There is also no real consensus on the timescales implicated. Estimates range from several hundred to a thousand years, making it a slow process.

However, if the Greenland ice sheet experiences further enhanced melting in the future, the cooler freshwater of nearby surface waters will have major effects on the ocean circulation. The likelihood of significant circulation changes is challenging to quantify, but climate models indicate that additional freshwater, similar to current rates of Greenland melting, are enough to have measurable impacts on ocean temperature and circulation (Steffen et al., 2018).

Another important aspect of the Greenland ice sheet is its role as a valuable source of insights for science. Extracted ice cores from ice sheets and ice caps help scientists to understand past variations in Earth's climate. The several layers of ice contain trapped gases, water molecules and dust that give information about the climate over the past millions of years (Kump et al., 2014).

Ice-Albedo-Feedback

Albedo is a non-dimensional, unitless quantity that indicates how well a surface reflects solar energy. The value varies between 0 and 1 (NSIDCb). With its bright white colour, snow has a very high albedo of 80 to 90%. The high reflectivity of snow means it can have a major effect on the regional energy balance. When solar radiation hits the snow crystals, a small amount is transmitted to heat the snowpack while most of the radiation is reflected back to space. The heat prevents the snow from instantly freezing into ice while the reflected sunlight keeps regional temperatures lower than they would otherwise be (Kump et al., 2014).

With the increasing temperatures Earth and especially the Arctic is experiencing, the snow cover of Greenland is decreasing. Hence, darker surfaces like ice, water or tundra appear, which have a much lower albedo rate. Warmer conditions encourage snow crystal metamorphosis that, like the presence of liquid water, reduce snow albedo to below 65%. This effect increases the absorbed solar energy by roughly a factor of two. Impurities such as dust, black carbon or microbes can lower glacier ice albedo beneath 30%, meaning that, when snow ablates, the impurity rich bare ice increases absorbed sunlight by a factor greater than three (PROMICE, 2019). Surface albedo has been labelled as an Essential Climate Variable and a Target Requirement for climate monitoring (WMO, 2011). A reduced albedo results in a temperature rise of the surface and the air nearby. According to IPCC (2013), in the decade previous to 2013, the surface albedo of the Greenland ice sheet has reduced by up to 18% in coastal regions, resulting in more solar energy being absorbed with an enhanced surface melting as consequence.

Monitoring of the ice sheet

A major aspect in identifying the Arctic's interaction with the climate is monitoring. Two important monitoring concepts are remote sensing measurements by satellites from space and in situ measurements by automated weather stations (AWS).

Satellite Observations

Observing and monitoring the enormous, remote Greenlandic ice sheet is a challenge and often only feasible globally from space. Commonly used are the remote sensing products of Landsat 8 and MODIS. The satellite Landsat 8 was launched in February 2013. Its cargo consists of two sensors - the Operational Land Imager (OLI) and the Thermal Infrared Sensor (TIRS). These provide seasonal reporting of the global landmass at a spatial resolution of 30 meters (visible, NIR, SWIR), 100 meters (thermal), and 15 meters (panchromatic) (NASAa). MODIS (Moderate Resolution Imaging Spectroradiometer) is an important instrument aboard the Terra and Aqua satellites. They launched in 1999 and 2002. Terra's orbit around the Earth is scheduled so that it moves from north to south across the equator in the morning, while Aqua passes south to north over the equator in the afternoon. They are viewing the entire surface of the Earth every 1 to 2 days, acquiring data in 36 spectral bands with a resolution of 250 meters (bands 1-2), 500 meters (bands 3-7) and 1000 meters (bands 8-36) (NASAb)

Automated Weather Stations

Automated weather stations (AWS) measure a large spectrum of different weather parameters on a local scale. Under changing conditions, the measured data can vary a lot over time. Especially in Greenland, major variations occur during a year due to melt season. AWS are an important tool to give scientists ground truth of what remote sensing instruments observe. Particularly in respect of the seasonal changes, the albedo in Greenland is expected to fluctuate significantly due to melting snow and ice. As a result, darker areas like darken ice, lakes, crevasses or land appear. Depending on the location of the AWS, the reflectivity can change significantly within a small area because of elevations differences. This can conclude in wrong assumptions about an area. Alongside of that, when measuring albedo, it is challenging to directly compare ground and satellite-retrieved values. Only when the measured surface is homogeneous at the length-scale of both satellite pixel and in situ footprint, it is justified (Ryan et al., 2017).

1.2. Aim of the study

As *1.1.* states, the Greenland ice sheet is directly affected by climate change. At the same time, the ice sheet creates a crucial trigger point that can have a massive effect on global climate if it is experiencing further melting. Researchers rely on automated weather stations to observe the changes since they have the advantage towards satellite products of reporting ground truth.

Albedo plays a significant role in the interconnection of the ice sheet and the global energy balance. The albedo of a surface can drastically change within a small range, which results in a limited representativity of an AWS site. With that in mind, the primary objective of this study is to assess the representativity of 40 automated weather stations for their local conditions in terms of albedo. The main information is retrieved from high resolution Landsat 8 data through the application of Google Earth Engine. The key analysis contains the comparison of the reflectance of the pixel in which the station is located, to the surrounding pixels within a $1km^2$ area, on a 15m-resolution-scale. A second additional analysis introduces data of the AWS as well as of a MODIS product to put the key findings into context.

After reviewing former research papers on this topic, it is expected to see a higher representativity on albedo further inwards on the ice sheet, increasing with more consistent weather and the therefore smaller seasonal fluctuations. This explanation also justifies the hypothesis about stations in the North having a higher chance of representativity. Ryan et al. (2017) gives information on how comparable albedo data retrieved by satellite-imagery and in situ are, especially during the melt season that occurs in summer. Their results revealed, that compared to satellite-retrieved values, the in situ measurements overestimate albedo by up to 0,10 at the end of the melt season. These disagreements are caused by the individual footprints capturing the spatial heterogeneity of the ice insufficiently. The occurrence of these differences was discovered for almost half of the 21 observed weather stations in the study.

This study is expected to give further valuation on how representative the individual weather stations are for their surrounding area. Connected prospects to this main research question include which local conditions occur when being representative or not representative and how it is connected to the melt season. It can bring information on whether a point-to-pixel comparison between MODIS and AWS data seem reasonable as well as indicate on how valuable satellite and AWS data occur when addressing albedo observations.

2. Methodology

2.1. Study area and time span

Covering an area of over 2,1 million km^2, Greenland is the world's largest non-continent island, located between the Arctic and Atlantic oceans, very close to the geographically north pole. About 75% of the island is covered in ice. It is situated between the latitudes 59°N and 83°N and the longitudes 11°W and 74°W (Rasmussen, 2021). It is therefore placed within the Arctic circle. A consequence of that is the missing sunlight during winter. For that reason, most stations' locations do not have data available in winter. All available months have been included as it is an individual analysis for each station's representativity. With Landsat 8 having launched in February 2013, the study's timespan was chosen to start just then and run until December 2020, which creates a time span of 8 years. For a clearer understanding of the results, a familiarity with the individual year's climate is of advantage:

All in all, *2013* demonstrated a large melting from both the Greenland ice sheet and the Arctic sea ice. The surface mass balance was lower than normal with a gain of 166 Gt (average since 1990: 368 Gt) The sea ice extent was 21% lower than the 1981-2009 average. Record temperature in late July triggered strong ice sheet surface melting (Polar Portal, 2013).

2014 showed a melting of the ice sheet above the average (since 2002). Nevertheless, was the Arctic sea ice strengthened that year. The surface mass balance of the Greenland ice sheet was lower than normal. The increased melting concluded in a below average reflectance of sunlight. A new warmth record was established in west Greenland in June 2014 (Polar Portal, 2014).

In *2015*, the melt season in Greenland ended with a surface melting larger than usual, even though the beginning of the summer was cold and snowy, and the melting season began late. Overall, the summer was relatively cold but featured a heat wave in July in the north and northwest (Polar Portal, 2015).

2016 revealed early melting due to record high temperatures in Greenland and the largest loss of glacier area since 2012. The extend of the melt season was high but not record-high. The albedo of the ice sheet was the fifth lowest in 17 years (Polar Portal, 2016).

2017 was characterized by a mild summer: fairly cool with a weak and short melt season. The surface mass balance in 2017 was above the average of 1981-2010, mostly resulting from high amounts of snow during winter. The reflectance however was not higher than the long-term average (Polar Portal, 2017).

2018 had an extremely cold summer. The surface mass balance aligned with the average from 1981-2010 up until summer, when it started to increase as a result of the lowest recorded average melting degree since the observations have started in 2008. The unusually cold and snowy summer caused the albedo of the ice sheet to reach the historical high in May, June, and the beginning of August since the reflectance of sunlight has been observed from 2000 (Polar Portal, 2018).
2019 was characterized by a warm, dry, and long summer. It forced the surface mass balance to a level well below the average of the period 1981-2010. It was lower than the all-time low year in 2010 throughout the period from February until mid-June. The enormous melting event decreased the ice sheet albedo to an extraordinary low level, marking a record minimal value in late summer 2019 (Polar Portal, 2019). The average surface broadband albedo over the Greenland ice sheet was 77.7% in summer 2019, classified as the second lowest value in the period of 2000-2019. Spring was generally above average at all sites (PROMICE, 2019).
2020 was once again a warm year in the Arctic. However, there were huge regional differences. In Greenland, the temperatures were close to normal. The extent of the Arctic sea ice was very low, concluding in new monthly records for low coverage of sea ice in July and October (Polar Portal, 2020).

2.2. Data

Landsat 8 TOA reflectance

The processed Landsat 8 data is a calibrated top-of-atmosphere (TOA) reflectance collection (Tier 1), provided by Google Earth Engine (Gorelick et al., 2017), with a TOA computation according to Chander et al. (2009). TOA radiance represents every light that is reflected off the planet as seen from space, including the impact of the atmosphere. It has the advantages of removing the cosine effect of different solar zenith angles due to the time difference between data acquisitions; compensating for different values of the exoatmospheric solar irradiance caused by spectral band differences and lastly, the correcting for the variation in the Earth–Sun distance between different data acquisition dates. These variations can be significant geographically and temporally (Chander & et al., 2009).
This study used the data of the panchromatic band (Band 8) in order to receive high resolution data and to collect the full reflectivity. Instead of capturing visible colours separately, the panchromatic band combines them into one channel. Therefore, the sensor can see more light at once. The covered wavelengths extend from 0,52 to 0,90µm (NASAa).

To rank the representativity of a locally measuring AWS, it was assumed that it corresponds to the ratio between the B8 reflectance at the AWS location ρ_{AWS} and the mean reflectance of the surrounding pixels $\bar{\rho}$ within a 1km² area just as the albedo ratio between those two is expected to occur (equation 1). For that reason, this study used the panchromatic band as a proxy for albedo.

Equation 1: Ratio proxy panchromatic band and albedo

$$\frac{B8_{\bar{\rho}}}{B8_{(\rho_{AWS})}} = \frac{\alpha_{\bar{\rho}}}{\alpha_{(\rho_{AWS})}}$$

With a resolution of 15 meters, it is double as sharp as the other bands which is very valuable for a local analysis of the AWS location.

Investigation area and MODIS Daily Albedo

Around each AWS, a polygon corresponding to a 1km² pixel of the actual MODIS grid was cut out as the investigation area A_{MODIS}. It was determined manually but since the resolution of the replicated MODIS is 1km and GEE allows to zoom in onto a small scale, the rate of deviation to the actual grid as a consequence of this manually proceeded step is very limited.

In a second analysis, MCD43A3 V6 Albedo Model dataset, also provided by GEE, was used. It is a daily 16-day product that delivers both directional hemispherical reflectance (black sky albedo) and bihemispherical reflectance (white sky albedo) for each of the MODIS surface reflectance bands (B1 - B7) as well as 3 broad spectrum bands (visible, near infrared, and shortwave) (Schaaf & Wang). The actual albedo is a value which is interpolated between black sky and white sky albedo. Since this research focused on the reflectance ratio between a certain pixel and the mean of the area (see *Landsat 8 TOA reflectance*) and its course in a year rather than the value itself, the selection was simplified. The white-sky albedo for the shortwave broadband was processed. White-sky albedo is defined as the albedo in the absence of a direct component and is independent of solar zenith angle (Lucht et al., 2000). The variable representing the MODIS Daily Albedo product in this study is α_{MODIS}.

It is important to remember that other than the weather station, which calculates a daily mean value, the MODIS and Landsat products are centred variables using snapshots (Schaaf & Wang, 2015). This also means that images on different days are taken to different times of the day.

Automated Weather Stations

Located across the Greenlandic continent, a network of automated weather stations track temperature, atmospheric pressure, humidity, wind speed, and the downward and upward components of solar (shortwave) and terrestrial (longwave) radiation among other parameters. The automated weather stations in Greenland are handled by PROMICE (Program for Monitoring of the Greenland Ice Sheet), GC-Net (Greenland Climate Network) and IMAU (Institute for Marine and Atmospheric Research, Utrecht University). The AWS locations are displayed in figure 1. Their exact location as well as later assigned representativity category (see *3.1.*) are shown in table 1. The majority of the stations is located on the ice sheet. The stations are primarily spread over eight melt regions of the Greenland ice sheet. In most regions, one station is situated in the lower ablation zone close to the edge of the sheet, while one or two are found in the middle and/or upper ablation zone. That way, comparable values of different altitudes are received. Exceptions are the weather stations KAN U (located in the lower accumulation area), MIT and NUK K (on independent glaciers), and KAN B (on tundra, one kilometre from the ice sheet margin).

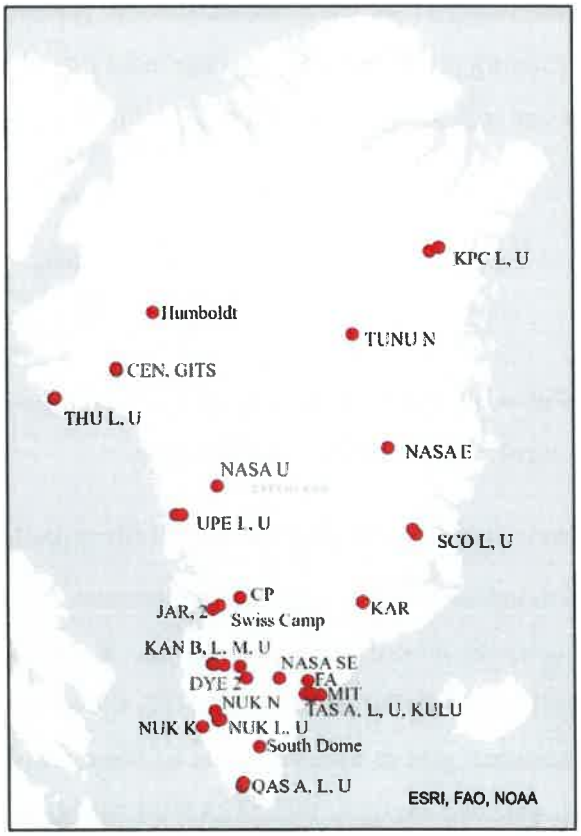

Figure 1. The locations of the investigated automated weather stations in Greenland

The albedo generated by the automated weather stations is calculated from the tilt-corrected up- and downwards shortwave radiation using values obtained for solar zenith angles below 70°. The AWS stores all parameters locally at a ten-minute time interval (PROMICE, 2019). The variable used in analysis *3.2.* is the daily mean product and termed as α_{AWS}.

Table 1. Automated weather stations in Greenland, their location and the in *3.1.* assigned representativity category (GC-Net, PROMICE, IMAU)

Station Name	**Location**			**Representativity**
	Latitude	Longitude	Elevation [m]	**Category**
CEN	77,1826	-61,1127	1886	A1
CP1	69,87975	-46,98667	2022	A1
CP2	69,87968	-46,98692	1990	A1
DYE 2	66,48001	-46,27889	2165	(A1)
FA	66,3618	-39,3086	1661	A1
GITS	77,13781	-61,04113	1887	A1
Humboldt	78,5266	-56,8305	1995	(A1)
JAR	694,98358	-49,68156	962	A2
JAR 2	69,42	-50,0575	568	A2
KAN B	67,1252	-50,1832	350	B
KAN L	67,0957	-49,9485	680	A2
KAN M	67,0667	-48,8327	1270	A2
KAN U	67,0003	-47,0243	1840	A1
KAR	69,69942	-33,00058	2579	A1
KPC L	79,9108	-24,0832	370	A1
KPC U	79,8345	-25,1665	870	A1
KULU	65,75845	-39,60177	878	A2
MIT	65,6923	-37,8277	450	B
NASA E	75	-29,99972	2631	A1
NASA SE	66,4797	-42,5002	2425	A1
NASA U	73,84189	-49,49831	2369	A1
NUK K	64,1623	-51,3587	710	B
NUK L	64,4822	-49,5325	540	A2
NUK N	64,9452	-49,885	920	A2
NUK U	64,511	-49,2663	1130	A2
QAS A	61,243	-46,7328	1000	A2
QAS L	61,0308	-46,8488	280	A2
QAS U	61,1758	-46,819	900	A2
SCO L	72,224	-26,818	470	A2

SCO U	72,3937	-27,2383	980	A2
South Dome	63,14889	-44,81717	2922	(A1)
Swiss Camp	69,56833	-49,31582	1149	A2
TAS A	65,7797	-38,9008	890	A2
TAS L	65,6403	-38,8987	260	B
TAS U	65,6978	-38,8668	570	A2
THU L	76,3998	-68,2662	570	A2
THU U	76,4197	-68,146	770	A2
TUNU N	78,01677	-33,99387	2113	A1
UPE L	72,8932	-54,2953	220	A1
UPE U	72,8883	-53,5715	940	A1

() Stations did not show a sufficient amount of data

2.3. Data processing

The data was processed using Google Earth Engine (Gorelick et al., 2017). GEE is a platform to geospatially analyse Earth's surface. It contains several satellite imagery data as well as geospatial datasets with planetary-scale analysis capabilities and is available for scientists of all kinds. The used datasets of Landsat 8 and MODIS imagery was provided in GEE.

Analysis 1

To evaluate the environment around an AWS location, the area within a 1km² MODIS pixel (A_{MODIS}) was observed, corresponding to four 500m-resolution MODIS pixels. By using the panchromatic band of Landsat 8, a resolution of 15m was given. Therefore, the Landsat pixel representing the station's value ρ_{AWS} in this analysis captured an area of 225m². The 1km² large area of A_{MODIS} around ρ_{AWS} was taken as a reference area to compare the variability and therefore the representativity of AWS monitoring to MODIS products, that provide one value for the entire area. A corresponding approach is realised in *Analysis 2*.

By applying a cloud mask (bit 4), images declaring the station's location as cloudy were not generated. Furthermore, images of data points with an extraordinarily deviation compared to its neighbouring values have been manually observed and excluded when clouds missed by the cloud mask were detected. To avoid night images with strongly differing values, the Worldwide Reference System row has been set to less than or equal to 122. The output of this process was cloud-free data of daylight images for each AWS location between 2013 and 2020, including the B8 reflectance at the station ρ_{AWS}, the mean $\bar{\rho}$ and standard deviation σ_ρ of the B8 data within the MODIS

polygon A_{MODIS} and information about the cloud cover rate for each image for further alignments. Figure 2 demonstrates this study's case. The individual Landsat 8 pixels are displayed within the A_{MODIS} polygon and show a variability of reflectance. The red point represents the location of an AWS.

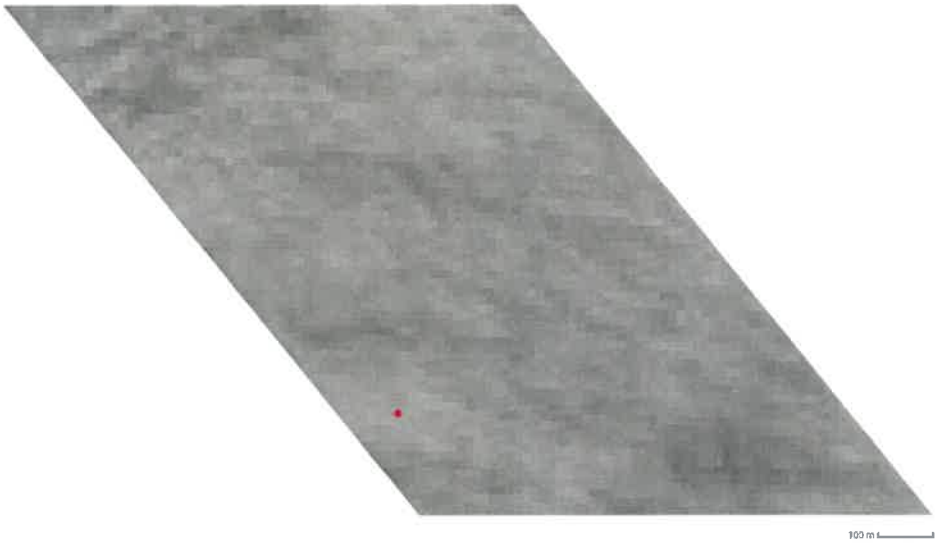

Figure 2. Inspection of high-resolution Landsat 8 pixels (panchromatic band, resolution of 15 m) within a polygon corresponding to the shape of a 1km² MODIS pixel

To classify the representativity into categories, the Root Mean Square Deviation (RMSD) (equation 2) between ρ_{AWS} and $\bar{\rho}$ was calculated over the entire time span for each location. The parameter d_i represents the difference between ρ_{AWS} and $\bar{\rho}$ over time. The variable n represents the number of dates showing useful data.

Equation 2. Root Mean Square Deviation

$$\sqrt{\frac{\sum {d_i}^2}{n}}$$

It describes the overall differences between the values. Based on the RMSD result, the automated weather stations were classified into three different categories. Figure 3 in the third chapter of this paper, *Results,* displays the RMSD value of each station. Three major clusters in the chart determined the three categorization groups. Category A1 captures all AWS that were surely representative for their close surrounding area (RMSD <0,001). Category A2 covers AWS that showed representativity with some deviations (RMSD 0,001-0,005). The stations that clearly indicated large deviations were grouped into category B (RMSD >0,005). To analyse the differences within the

area, plots showing the station's value ρ_{AWS} and the mean $\bar{\rho}$ as well as the standard deviation σ_{ρ} were created to display the results.

Analysis 2

For two stations, one showing minimal and one showing a rather large variability within the polygon, the MODIS Daily Albedo data (α_{MODIS}) and the Albedo data of the weather station (α_{AWS}) were generated. MODIS Daily Albedo is using a resolution of 500m. The pixel in which the AWS is located was evaluated. For each day when accessible Landsat 8 data was generated, the daily product of MODIS Daily Albedo was extracted. This comparison shows more about the accordance of the MODIS Daily Albedo to the AWS albedo product, even though they measure different footprints. Furthermore, it can support the previous analysis of high-resolution data. The stations NUK K (high variability) and CEN (small variability) were chosen for this analysis.

3. Results

The following figure shows the outcome of the Root Mean Square Deviation categorizing. The RMSD for each station can be found in *Appendix A*. The figure reveals that all automated weather stations located at a level above 1500m, were grouped into category A1. A few lower located stations reached the same category but most <1500m situated stations resulted to be grouped in A2. Four stations that showed a rather high deviation, were placed into category B.

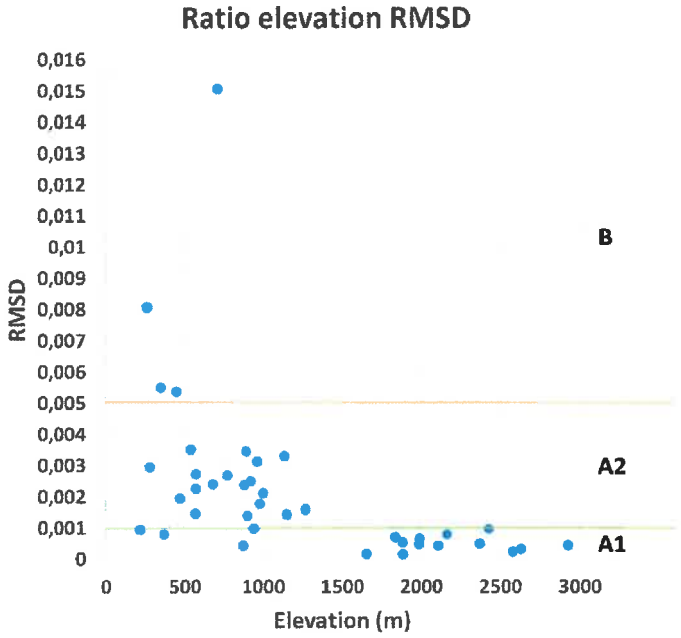

Figure 3. The ratio between elevation and RMSD of AWS

3.1. Landsat 8 Analysis

The amount of data varied extremely between the stations depending on their location. While some provided several hundreds of data points for the observed time span, a few stations presented less than a handful of dates per year. If the latter was the case, it is stated in the station's results description. Furthermore, it was detected that the year 2013 generally had a very limited number of images available, which results in missing information for that year's summer. It is still displayed to represent the available dates of the year.

To represent each category, one station's analysis is exhibited in detail with the corresponding generated diagrams. The charts of the remaining stations can be found in *Appendix B* of this paper.

Category A1 – always representative

AWS grouped in this category barely exhibited any deviations and therefore were representative for their location all throughout the year. Their RMSD summarizing all years stayed below 0,001.

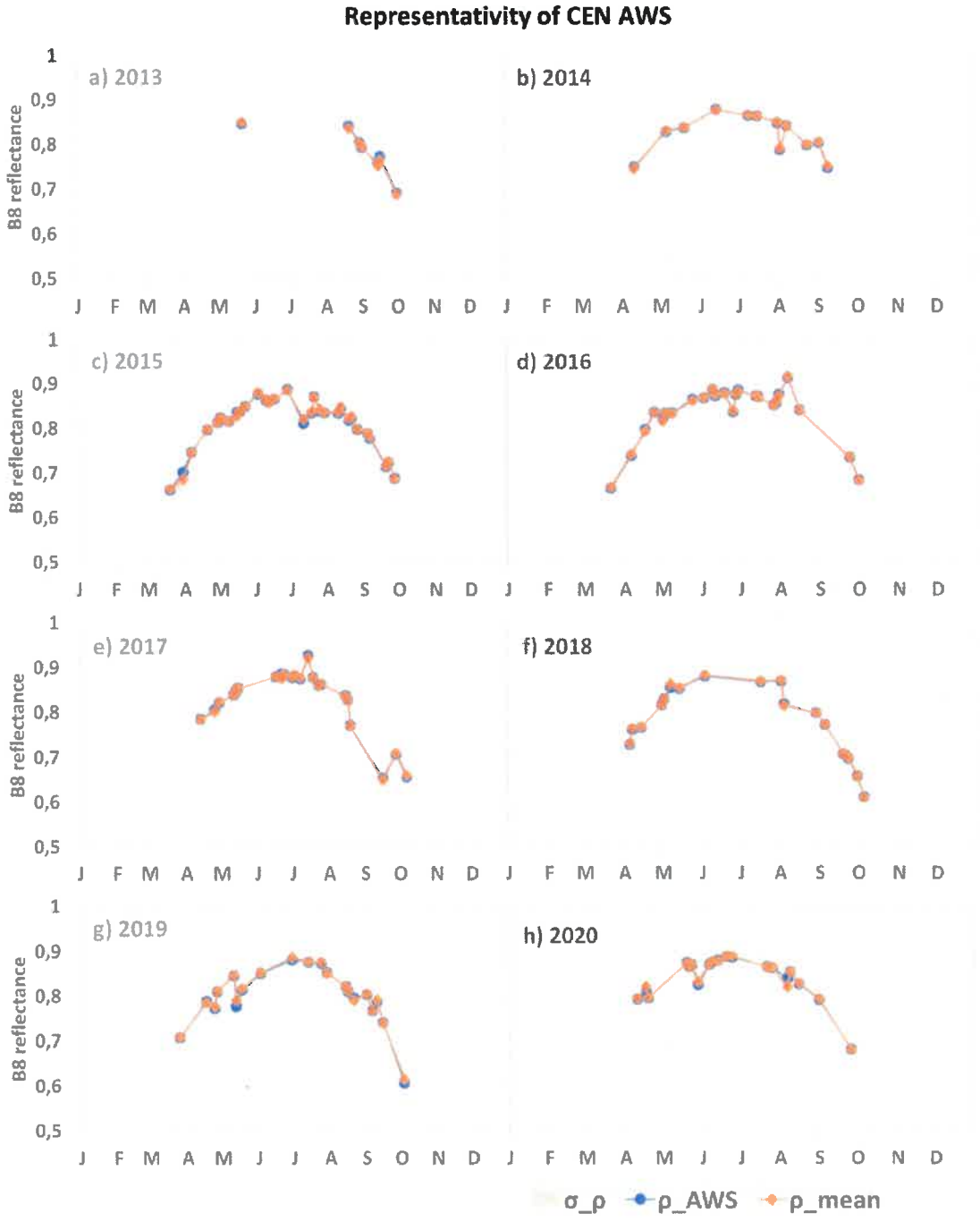

Figure 4. Panchromatic reflectance at CEN weather station for the years 2013-2020

Figure 2 illustrates the ratio of the value at the station ρ_{AWS} in blue, the mean of the area $\bar{\rho}$ in orange and its shaded, here minimal, standard deviation σ_ρ within A_{MODIS} for the years 2013-2020

for *CEN* weather station. CEN is located further inwards on the ice sheet at an elevation of 1886m which concludes in it being snow-covered throughout the year.
The accordance of ρ_{AWS} and $\overline{\rho}$ was very high. Throughout the year the rate of reflectance varied but the difference between the two values was continuously low. The changes in reflectance were probably caused by images taken at different times during the day. Especially towards the beginning and end of the year, the reflectance showed a lower rate than for the rest of the year. The change in solar illumination influences the rate of reflectance. Small deviations that can be found in the graphs (April 2015 for instance) were caused by small atmospheric disturbances, like a veil of clouds or small variations in the snowpack. The observation of the images confirmed that the site was always coated by a homogenous bright snow cover, which is why it rarely showed any fluctuations.

Other automated weather stations grouped in this category:
CP1 and CP2 are only a few meters apart from each other. This concluded in the same outcome of this study for both stations. They are located at a very consistent site that was covered in snow all year and therefore any remaining fluctuations in the data ratio or deviation were produced by thin cloud layers or other external disturbance.

FA is another station on the ice sheet that presented a snow cover all year around. It is not excessively far from the margin of the ice sheet which might conclude on more intensely reflectance changes when observing it on a bigger scale. On the local scale that was observed, the AWS was very representative.

GITS is in the north of the Greenlandic West-Coast. Because of the high latitude, the station was on snow-covered ice throughout the year. It was very representative for the region and barely showed any fluctuations within the MODIS footprint area.

KAR weather station can be found in the Southern half of the Greenlandic East Coast. The observations showed that the site is very unchanging. The disparity between ρ_{AWS} and $\overline{\rho}$ was constantly low while the rate of reflectance was relatively stable.

KAN U presented very steady conditions due to an evenly snow-covered site throughout the year. Very occasionally, minor deviations were found that are likely caused by snowstorms or other external short-term influences.

Statistically, *KPC L* station was representative for the location but near the boundary value to category A2. It is located right at the edge of the ice sheet with an area of tundra nearby. This, however, makes it a site that constantly showed slight variations between ρ_{AWS} and $\bar{\rho}$ as the surface changes drastically within a small area. Most years showed a similar pattern: compared to the mean, ρ_{AWS} was slightly larger throughout the year with the exception in summer when it turned into being smaller, especially noticeable for 2016, 2017 and 2018. 2019 showed the same pattern, just not as clear and intense. When exactly the ratio turned, varied from year to year. 2013, 2014 and 2015 shared the higher trend of ρ_{AWS} outside the melt season but in summer, 2014 showed a relatively alignment of the two variables. During melt season in 2015, it switched between an over- and underestimation as the pixel's representativity several times. With a mean of 0,029 and a median of 0,027 for all years, the standard deviation during the year was relatively steady. This seemed to be due to its position at a slightly elevated location which was snow-covered for longer than other areas close by. A great quantity of data was available for this location which resulted in a higher number of fluctuations. Nevertheless, a pattern is recognizable and overall, a high representativity is provided. Outside of A_{MODIS}, however very close, accumulations of meltwater on the ice sheet as well as on tundra were located (figure 4).

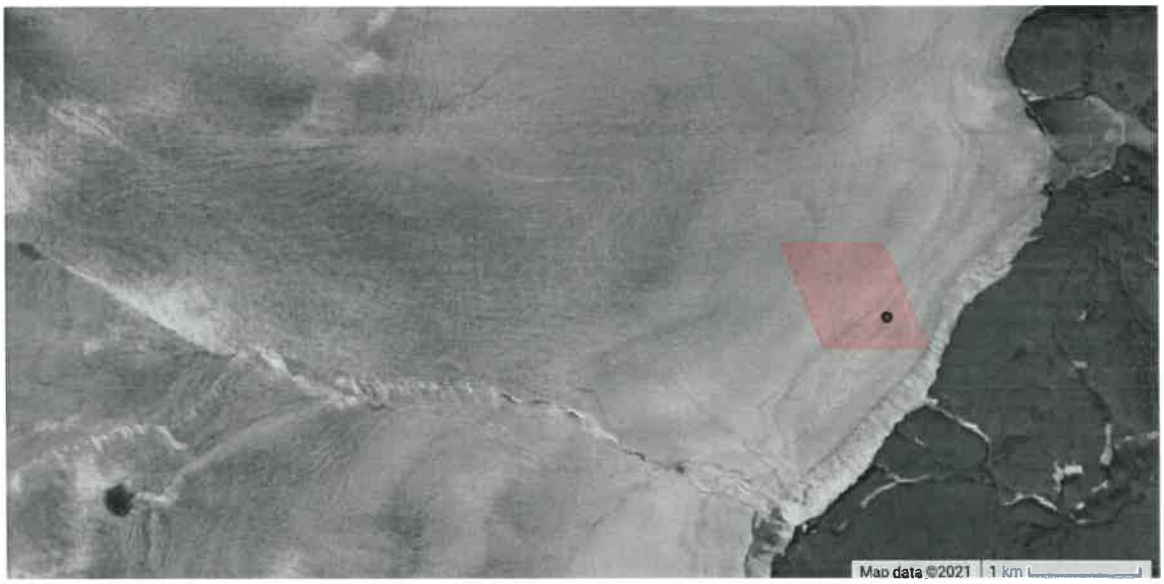

Figure 5. KPC L on July 14th, 2017 (Landsat 8 TOA, USGS/Google)

UPE U indicated a representative pattern, especially outside of the melt season. With 940m, it is located at a higher elevation than UPE L and about 20km further inwards on the ice sheet. The increasing temperatures in summer resulted in the ablation of snow, causing deviation in the data. The AWS is situated in an area with changing elevations. It was noticed that in summer, some areas had a thinner snow cover than others which raised changes in the reflectance. Considering

the A_{MODIS} area, the values were relatively stable. 2020 demonstrated the highest deviations. 2014 and 2018 showed one outlier value each. The other years showed minor differences in the ratio. Some images revealed small meltwater lakes in the larger surroundings outside of A_{MODIS}.

The automated weather stations *DYE 2, Humboldt, South Dome and TUNU N* were covered with a very limited number of images which concluded in a small data range for the sites. The available data showed very consistent values without any deviation because of a homogenous snow cover all year. For the location of *NASA U* and *NASA SE* the number of cloud-free Landsat images was even smaller. The available values showed a $\rho_{AWS}/\overline{\rho}$ ratio very close to 1 because it was a homogenous ice ground. However, the amount of data was not sufficient to make a confident statement about the station's representativity.

Category A2 – representative with limited deviations

Stations in this category demonstrated an overall representative performance. However, some years or months differed from that behaviour which distinguished them from the stations classified in category A1. Their RMSD lay between 0,001 and 0,005. QAS U is one of the stations that met those conditions. Figure 6 illustrates the B8 reflectance from 2013-2020 for QAS U. Before July, sometimes August, of each year, the reflectance was very consistent due to the snow-covered surface. A clear decrease in the rate was noticed in summer when the melt season occurred. Some years, like 2019, showed a higher decrease in reflectivity while others, like 2015 or 2018, displayed a very small amplitude in summer. The change of reflectance comes along with slightly increasing deviations. Overall, QAS U indicated a relatively high representativity of the area. As can be seen in the figure, in 2015 the weather station was accurately representative for the area without any exceptions. Other years showed a high representativity in the winter month while the summer ratio within A_{MODIS} was not completely balanced. The local conditions of the site are shown in figure 7a.

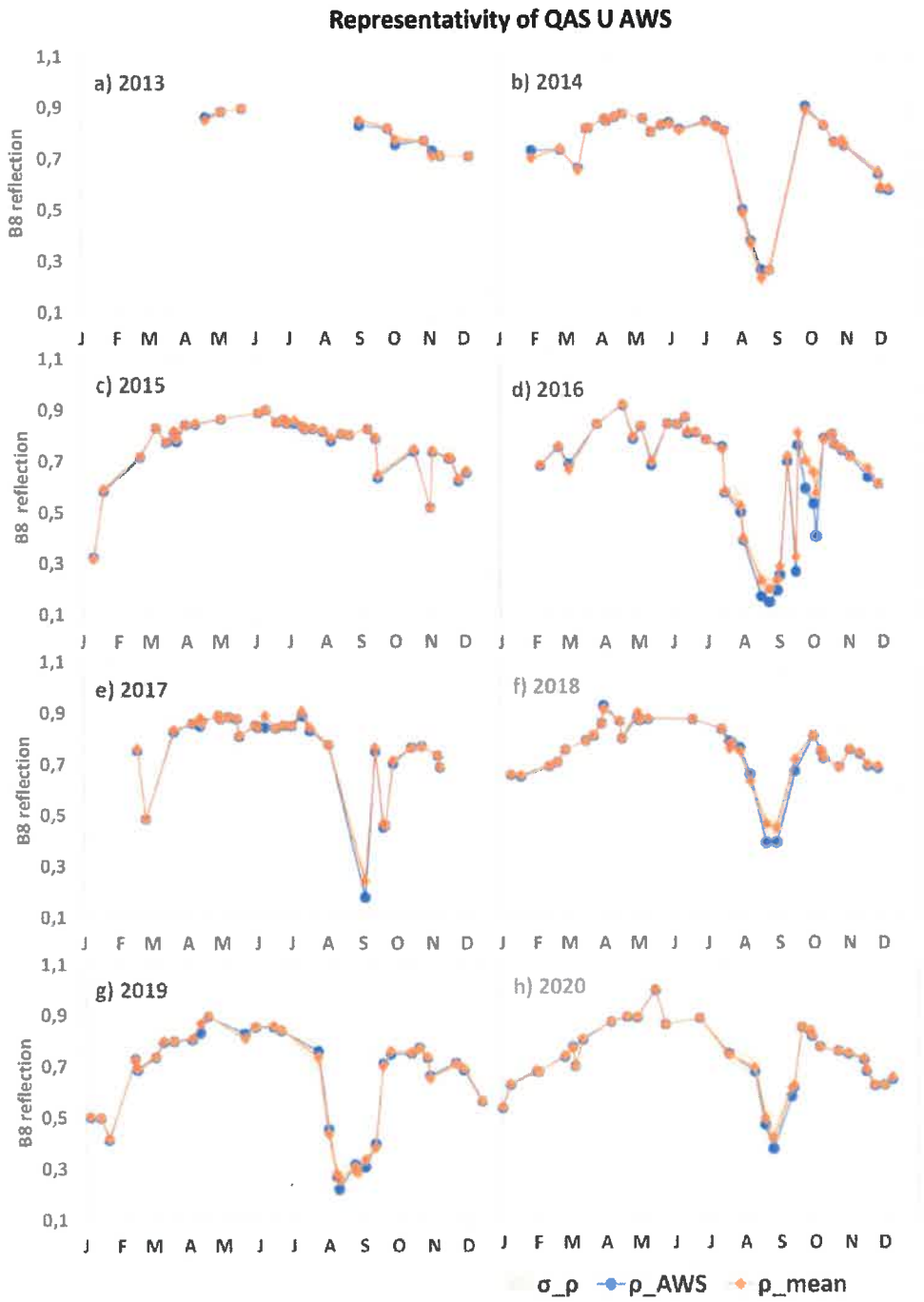

Figure 6: Panchromatic reflectance at QAS U weather station for the years 2013-2020

Other automated weather stations grouped in this category:

The site of *JAR* was characterized by snow-covered winters and appearing meltwater streams in summer (7b) along with varying elevations. In general, the AWS and the mean were relatively in synchrony, but it changed with the seasons. Mostly in spring as well as in autumn, the mean was slightly higher than the AWS. This ratio switched to the opposite in summer when the station's location showed a slightly higher value. Until June, the disparity between the AWS location and

the mean was mostly between 0,2 and 0,3 with 2014 and 2019 differing (latter around 0,5). The standard deviation in spring occurred to be the lowest compared to the rest of the year. The rate of ρ_{AWS} agreed with the course of the maximal negative standard deviation of the mean. The highest standard deviation was seen when the melt season started. ρ_{AWS} and $\bar{\rho}$ slightly drifted apart and showed disagreements of up to 1,2 (summer 2019). The images showed meltwater streams, that initially were covered by a layer of snow, followed by the revelation of the darker ice underneath. The ice might contain impurities like dust or algae which could be an explanation for the pattern shown in figure 7b. When more of the snow was melted, the disparity became smaller again. In contrast, summer 2017 showed a surprisingly high deviation for that time of the year. In September, when the colder temperatures returned, the mean showed a higher value than the AWS pixel's reflectance for all years but 2018. The standard deviation increased again. 2020 showed an overall stable course throughout the year, with barely any large differences but it must be considered that there were less useful images, due to clouds, especially in summer.

JAR 2 showed a general pattern of a slightly higher reflectance at the AWS' pixel in spring, that turned into a lower reflectance when the snow melt started, before returning to its previous state. The individual years demonstrated different performances of that pattern, some stronger while others revealed the disparity barely. The higher value in spring remained in a scope of maximum +0,02 while the differences in summer were spotted to be not larger than -0,05. In some summers, ponds of meltwater were seen close to A_{MODIS} (figure 7c).

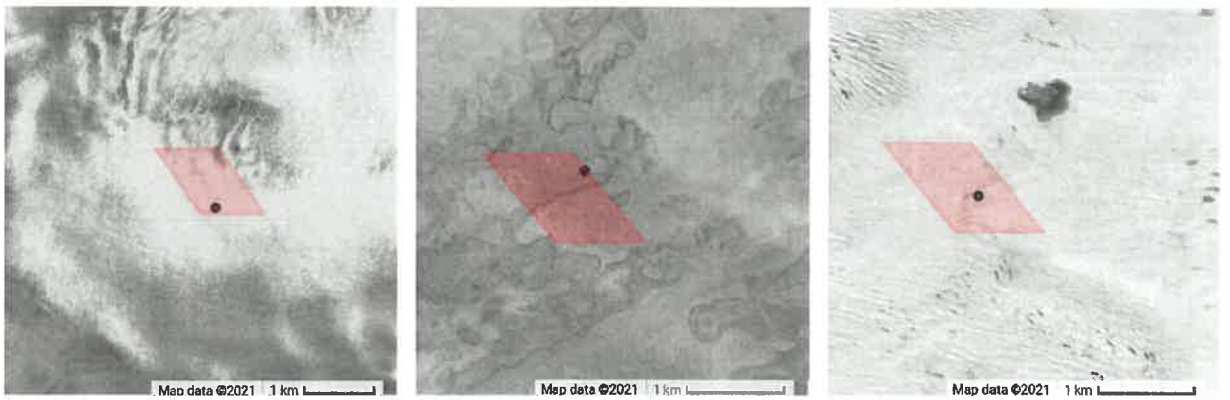

a) QAS U, July 23rd 2019	b) JAR, August 27th 2014	c) JAR 2, June 7th 2017

Figure 7. Seasonal occurrences at the sites of QAS U, JAR and JAR 2 (Landsat 8 TOA, USGS/Google)

KAN L is the one out of the three KAN weather stations that is the closest to the coast. This was represented in the variability of the results. In general, a slightly larger standard deviation in comparison to the other two stations was seen, especially in autumn and early spring. A possible reason might be differences in elevations, as a result some areas took longer to be snow-free. The station did not show any extraordinary occurrences nearby but the surface it is placed on is very heterogeneous ice. When some spots were covered in snow in autumn, the contrast between circumstances at the different altitudes was even larger. It resulted in a high standard deviation. In general, it was doubtful to say the location showed a certain pattern. 2014 and 2019 showed the AWS having a higher value than the mean in summer, while 2015 and 2017 showed a lower value. 2016 and 2018 revealed the AWS to be very representative and accurate in summer.

KAN M showed a relative representativity of the surface reflectance throughout the year. In the years 2013, 2019 and 2020, ρ_{AWS} and $\bar{\rho}$ corresponded almost perfectly with a few exceptions. The other years showed larger differences between the two variables, especially 2014 and 2018, latter with a standard deviation of up to 0,07 in August. When considering the station's location, shown in figure 8, the representativity of the surface reflectance can be identified as restricted to the $1km^2$ polygon in this analysis because a larger scale would result in a significantly change of surface and reflectance. Lakes that appeared a few kilometres away from the station in summer would influence the analysis.

Figure 8. The location of KAN M weather station on June 17th 2019 (Landsat 8 TOA, USGS/Google)

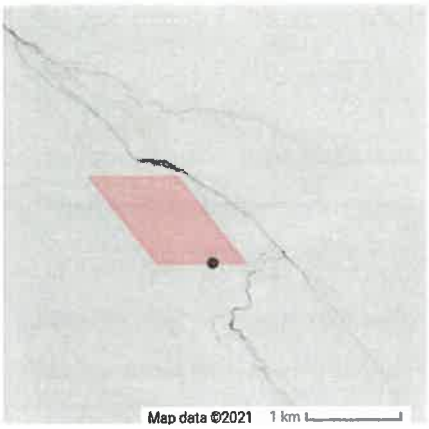

Figure 9. Crevasses showing up close to KAN M station in August 2019

Furthermore, in late August 2019 and late July 2020, crevasses were spotted close to the weather station (figure 9), however outside of the observed polygon. Therefore, they are not included in this analysis.

The automated weather station *KPC U* is generally a stable weather station site. It is situated in Northern Greenland, on a slope on ice, close to the edge of the ice sheet. In winter, the representativity was high in all years because of a homogenous snow cover. With rising temperatures in summer, the snow melted and the images revealed multiple meltwater streams (figure 10). Those, as well as areas of snow saturated with water brought fluctuations in the ratio and standard deviation throughout summer. 2015 and 2019 were affected the most by these occurrences and showed the highest deviations.

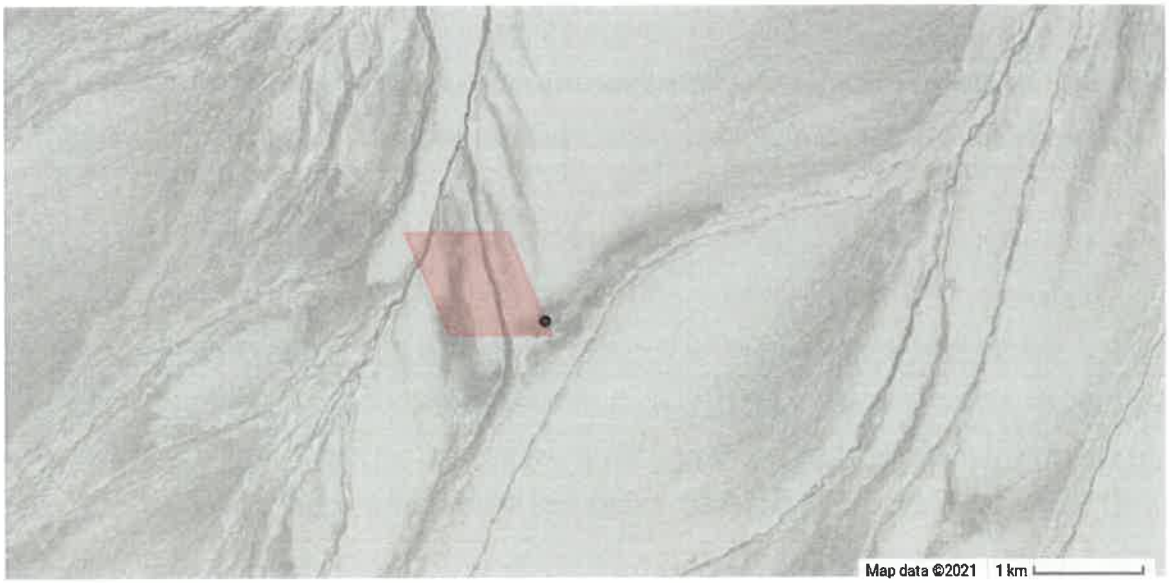

Figure 10. Meltwater streams at KPC U weather station on July 20th 2019 (Landsat 8 TOA, USGS/Google)

KULU is only a few kilometres away from the ice sheet margin. In the analysis, it demonstrated a very stable state of representativity at the AWS' location throughout the year with small deviations in the summer months. It showed the pattern to slightly overestimate the mean at the station's location in early summer, what then changed into a slight underestimation in late summer when the snow was melted. This was a result of topographically height differences and snow accumulating at the lower parts (figure 11a). At the start of the melt season, the station's location was covered in snow before it became snow-free as well, while small parts within the polygon still

showed snow-cover. Some years demonstrated this pattern stronger than others. 2015 did not show the ρ_{AWS} lying below $\bar{\rho}$, while 2020 showed the opposite.

NUK L is located on a glacier tongue (figure 11b). The observations showed a constant small standard deviation from the mean for all years with a median of 0,046. Most often, ρ_{AWS} dealt with slightly smaller rates than $\bar{\rho}$ in spring and autumn. In summer, the exact period depending on the year's climate circumstances, the two rates happened to be very close to each other stating a higher representativity. 2018 was an exception with ρ_{AWS} being at a lower rate in summer as well. 2015 also showed a disagreement with the pattern: in spring the AWS' location was reflecting more than the mean. In February and November, an increased standard deviation was noticed, caused by shadows of the mountains situated next to the station.

NUK N showed a varying surface reflectance in the course of a year. During melt season, the reflectance decreased enormously. Being located at the edge of the ice sheet, the station is highly affected by the changing seasons. Located on a heterogenous surface with different elevation, as can be seen in figure 11c, the surface had changing local conditions and therefore displayed a constant slight standard deviation within the polygon. In most years, the value at the AWS met the mean of A_{MODIS} during winter seasons which resulted in a high representativity of the station. 2018 showed slight variances. When melt season started, all years indicated the same systematic change. The melt season mostly started in the beginning of July and ended in September or October. In 2018 it was significantly shorter, whereas in 2019 it started earlier. The snow started melting and the underneath appearing ice revealed a much smaller reflectance. The station seems to be located on an elevation that was snow-free ahead of its close surrounding. The standard deviation within A_{MODIS} increased during that time compared to the colder months. Snow events brought individual peaks during the melting season. Also, right next to the ice sheet, lakes of meltwater formed (Figure 11c).

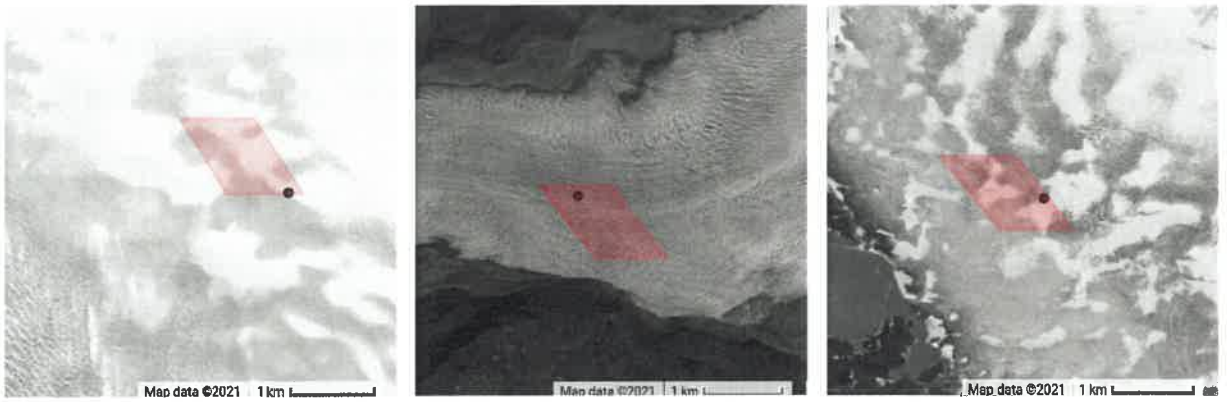

a) KULU, August 6th 2017	b) NUK L, July 18th 2018	c) NUK N, June 21st 2014

Figure 11. Seasonal occurrences at the sites of KAN L, KULU and NUK L (Landsat 8 TOA, USGS/Google)

NUK U resulted in a high representativity during the colder month with a synchrony of the AWS location and the mean, only showing small deviations within the MODIS area. However, in the summer months, the deviation within A_{MODIS} increased for the reason that the first snow melted, and lakes appeared (figure 13a). These have a lower reflectance due to a darker surface. Especially 2014, 2015, 2016 and 2019 revealed large distinctions between ρ_{AWS} to $\bar{\rho}$ as well as within A_{MODIS}, the standard deviation reaching from 0,09 to 0,17. 2018 as a cold year showed its maximum deviation in summer with 0,06. Individual snow events displayed in form of onetime peaks in the graph.

QAS A did not show a recurring pattern over the years. It is located on the ice sheet in the South of Greenland. All years showed a representative trend for spring and autumn when the ice sheet was snow-covered. In summer, the individual graphs differed in their behaviour. In 2015 for example, ρ_{AWS} was constantly representative for A_{MODIS}. The reflectance barely decreased during year. When examining the satellite images, it was noticed that the area was still covered in snow in August 2018 (figure 12a). It did not melt completely like it did in other years. In 2016, a larger deviation was noticed when the melt period started. The reflectance decreased and variations in the ratio between ρ_{AWS} and $\bar{\rho}$ appeared. Figure 12b explains that it was caused by the snow being partly ablated. At that point, the location of the AWS was snow-covered and showed a higher reflectance than the mean, which included dark areas as well. Shortly afterwards, it shifted to ρ_{AWS} being below the mean. The same phenomenon was spotted in 2019 (figure 12c). When the snow melt was further in progress, most of the snow was melted, resulting in the appearance of bare ice with a limited number of snow spots. The ice underneath showed a darker ground at the AWS' location. This could be caused by a depression with impurities like dust or soot.

The station showed a pattern of a differing summer, nevertheless, could not be resulted in a clear recurring pattern because the individual years showed overestimations, underestimations as well as a representativity at the AWS's location compared to the mean of the polygon, depending on how much of the snow-cover melted.

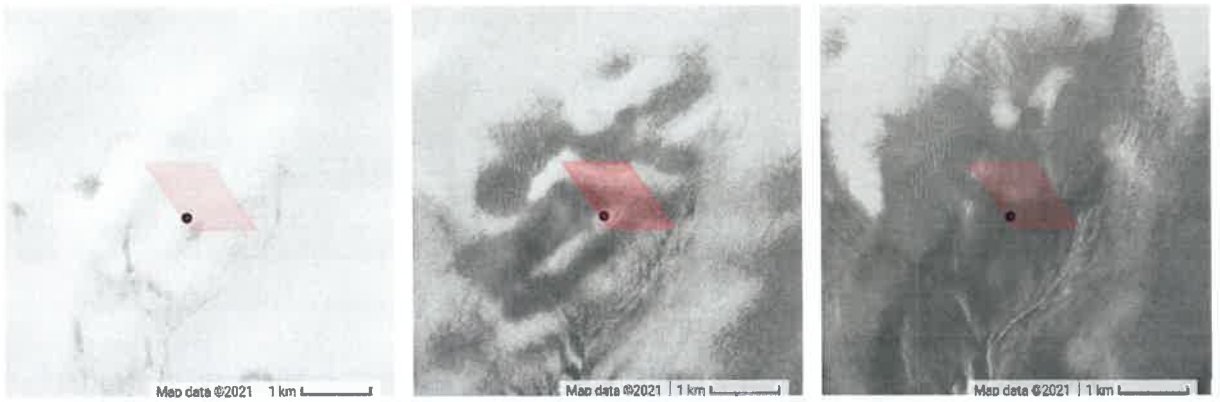

a) August 15th 2015	b) July 30th 2016	c) August 10th 2019

Figure 12. Differences in melt season at QAS A station for 2015, 2016 and 2019 (Landsat 8 TOA, USGS/Google)

At *QAS L*, the value of the AWS pixel often lay below the mean of the polygon but represented it well during the summertime when the snow had already melted. Larger differences were found outside of the melting season because of a varying combination of snow, ice and rock surface (figure 13b). The station site seemed to be situated at a topographically low, close to a slope which contained a thicker snowpack that formed the end of the ice range before it switches to coastal rocks. This explained the lower rate of ρ_{AWS}. Because of the location so close to the coast as well as in the South of the country, the melting season started rather early. 2014 revealed a relatively good representativity throughout the whole year.

The representativity of *SCO L* was relatively accurate. With small deviations, the graphs of ρ_{AWS} and $\bar{\rho}$ were found to run very close to each other. In spring, ρ_{AWS} showed a slightly higher rate in most years, followed by a lower rate in summer. The years 2015 and 2019 made exceptions. 2015 constantly showcased ρ_{AWS} below the mean while 2019 displayed an accordance of the values in spring. The variations throughout the year were caused by the uneven surface of the glacier the AWS is sitting on. Shadows increased the standard deviation in the beginning and ending of the year. With the location being on a glacier tongue (figure 13c), the representativity is very local and not for a broader area since it is bordered by mountains.

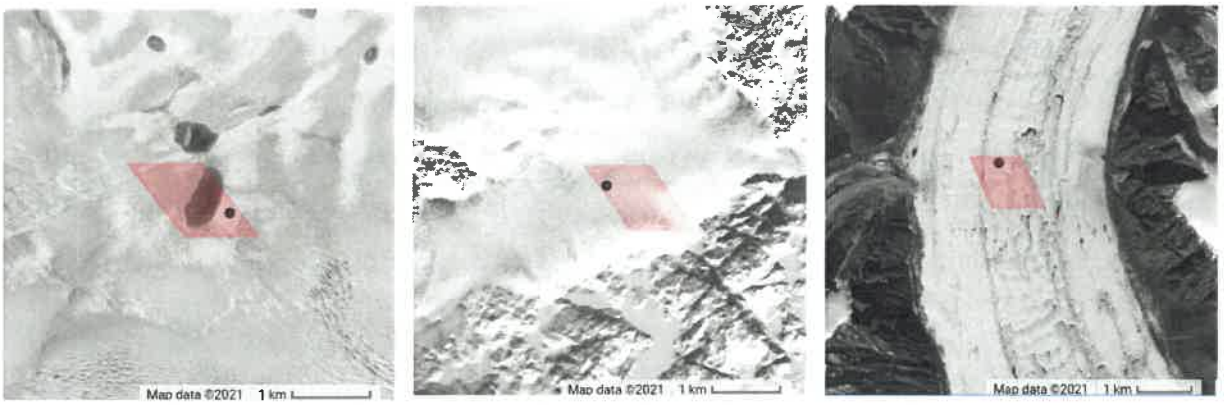

a) NUK U, May 16th 2016	b) QAS L, February 25th 2020	c) SCO L, May 24th 2019

Figure 13. Seasonal occurrences at the sites of NUK U, QAS L and SCO L (Landsat 8 TOA, USGS/Google)

Generally, the analysis of *SCO U* showed the AWS pixel being slightly under the mean most of the time. When analysing the images, the station was found in the middle of a glacier tongue (figure 14a) just like SCO U, characterized by rills due to melting and refreezing in the different seasons. Topographically, those grooves are lower and therefore reflect less. The AWS is seemed to be located in one of those. Sometimes, the station was covered by the shadow of the mountains nearby, which displays an important consideration when measuring the reflectance. It showed in the beginning and end of the graphs by displaying sudden lower values, or a high deviation when only part of the polygon was shadowed. Just like SCO L, the AWS sitting on a glacier tongue limits the representativity, so it is not accurate for a broader area.

The site at *Swiss Camp* appeared to be characterized by lakes showing in summer, which are covered by snow in winter. For all years, the reflectance varied a lot in the course of a year. The lakes appeared in summer when the snow started melting, however, right outside of A_{MODIS} (figure 14b). Therefore, the decreasing standard deviation during the melt season as well as ρ_{AWS} and $\bar{\rho}$ drifting apart is caused by differences in surface elevation and not by the lakes. Further into the melt season, the accordance of ρ_{AWS} and $\bar{\rho}$ decreased. The analysis showed a very representative result for the rest of the year. When the lakes occurred, they were encircled by the still snow-covered ice. An analysis on a larger scale would therefore result in significantly higher deviations.

TAS A was representative for its surrounding area in some years while in other years, the summer indicated a slight deviation when the ice sheet is partly covered in snow and partly snow-free (figure 14c). Most of the time, the AWS was in a darker snow-free spot and therefore measured a slightly smaller reflectance compared to the mean, reaching from a difference of 0,14 in 2019 to

over 0,2 in 2018. Some years showed this effect stronger than others, while 2014, 2015 and 2020 barely had any deviation within A_{MODIS}. ρ_{AWS} and $\bar{\rho}$ aligned almost perfectly. The AWS is located at the edge of the ice sheet on a surface with small height variations. When analysing the images, the differences in the behaviour were always caused by the snow distribution within the polygon. The years without noticeable deviations did not show any images where A_{MODIS} was half covered in snow. Either the snow cover or the ice dominated.

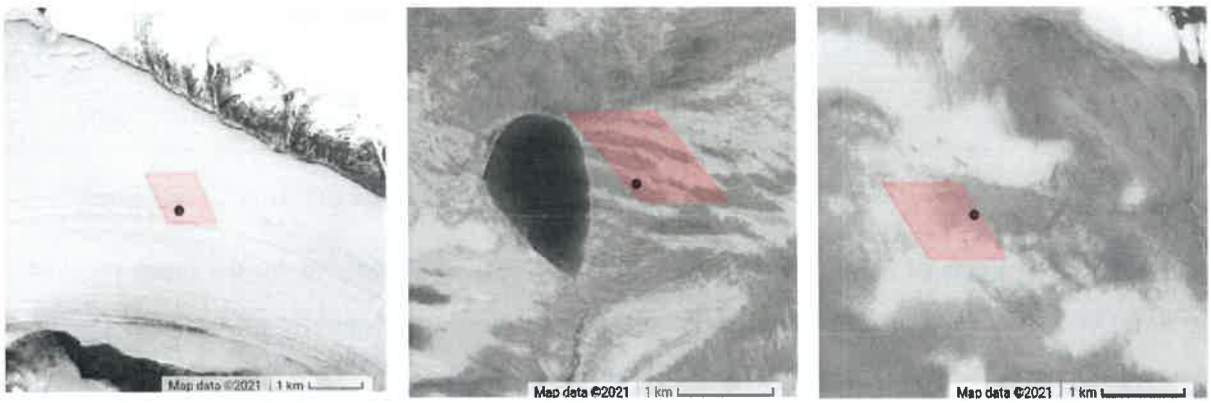

a) SCO U, June 4th 2014	b) Swiss C., July 10th 2019	c) TAS A, August 13th 2017

Figure 14. Seasonal occurrences at the sites of SCO U, Swiss Camp and TAS A (Landsat 8 TOA, USGS/Google)

TAS U barely showed any deviations. The years (2013), 2016, 2018 and 2020 proved a significant representativity. In some years however, especially in 2017 and 2019, ρ_{AWS} demonstrated a slightly higher rate than the mean $\bar{\rho}$ caused by the snow melt. The maximum variation between the two was 0,07 in June 2019. Mostly however, it was a homogenous surface and all values within the polygon were very similar.

THU L is situated close to the Western end of the ice sheet. Apart from summer, the representativity of the station was quite accurate for all years. During that time, it was snow-covered and therefore presented a homogenous surface. The location seemed to be influenced by topographically altitude differences and gradients. Over the seasons, certain areas were conspicuous because they constantly were the first to be snow-free (see figure 15b). This occurred in several images, causing higher deviations. On the images, those areas showed a certain pattern on the ice surface. It might indicate sub-surface meltwater streams or a band of either flatter and smoother ice where less snow accumulates in winter due to winds, or a band of darker ice that, when the snowpack becomes thin enough, decreases the albedo and causes the snow to melt faster. It caused large shifts in the summer month because of the varying surface brightness. Each pixel exhibited a different reflectance. Especially in the beginning of summer, the disagreements of ρ_{AWS} and $\bar{\rho}$ was

high, when only part of the area's snow was melted. Therefore, some sections had a high reflectivity while others presented a darker surface of ice underneath. Darker parts of the ice could also include impurities like mineral or dust that were moved into depressions by meltwater. At the start of the melt season, some years exhibited a slight overestimation at the station's pixel compared to the mean because other parts within the polygon were snow-free before the station's location. However, some years demonstrated this occurrence while others did not. Because THU L is located right at the edge of the ice sheet, the representativity only speaks for the local area within A_{MODIS}. A wider radius would include darker reflecting tundra.

THU U showed to be representative for the area in spring and autumn. The standard deviation was minor while ρ_{AWS} and $\bar{\rho}$ ran very accurate. From June, the latest July, on, summer rates decreased while showing a separation of the values because snow ablation began. The AWS is right at the margin of the ice sheet, not far from the coast. Influenced by that, many images revealed A_{MODIS} partly covered in snow while a large part was already snow-free. This resulted in deviant values in several years, especially 2014, 2016, 2017, 2019 and 2020. The location of the AWS was covered in snow for longer than its surroundings in most years and therefore ρ_{AWS} was at a higher rate than the mean. 2018 was a rather cold year, a large deviation was not seen. Another reason for that might be that images in the beginning of August, when other years indicated a lower representativity, were too cloudy to process. For that reason, it cannot confidently be said that 2018 did not show the same pattern as the other years. 2015 also did not show the large deviation in summer. The analysis of the images revealed a very fast melting. It therefore shifted from one representative state (fully covered in snow) to another (snow-free darker ice). As can be seen in figure 15c, THU U is covered in snow for longer than THU L.

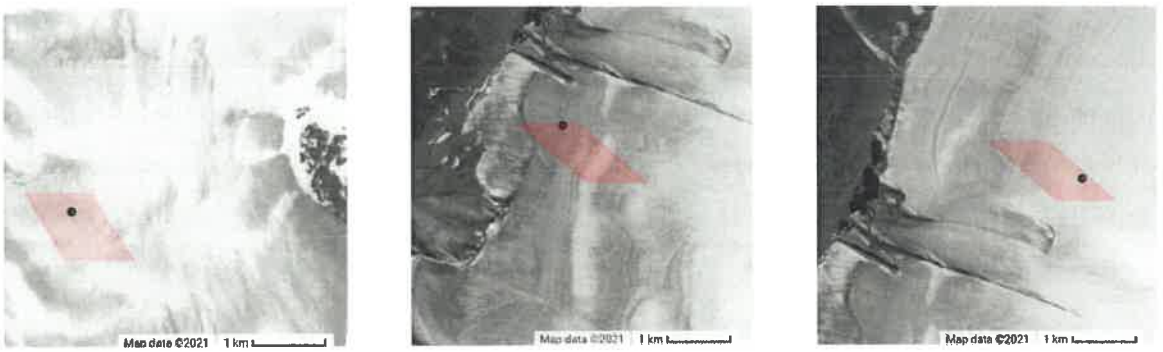

a) TAS U, June 16th 2019	b) THU L, August 9th 2020	c) THU U, August 9th 2020

Figure 15. Seasonal occurrences at the sites of TAS U, THU L and THU L (Landsat 8 TOA, USGS/Google)

Category B – large deviations

This category represents weather stations with a RMSD > 0,005. They are characterized by large deviations between ρ_{AWS} and $\overline{\rho}$. An example for it is *NUK K*. Figure 16 illustrates the processed surface reflectance for NUK K weather station from the years 2013 to 2020. The year 2013 only had a very limited number of images which is why no significant connections between the different dates were made and the standard deviation is displayed differently. NUK K has a unique location on a small glacier on top of a mountain in the coastal area surrounded by fjords (figure 17a). Because of this varying region, the reflectance fluctuated a lot. In early spring and late autumn, the mountain was covered in snow which brought a more homogenous surface. However, because of the low solar altitude, shadows of surrounding mountains fell onto the station's position, which caused a high deviation in contrast to the snow-covered surroundings. It resulted in ρ_{AWS} lying below $\overline{\rho}$ in winter. In spring, most values did not show the reflectance of the surface but a cloud that was located on top of the mountain but nowhere around it. This was a repeatedly occurring event in several images. In late spring and early summer, the snow started melting and increased the difference between the two components enormously. The glacial ice has a colder surface than rocks, which caused the snow around to melt earlier than on the ice. Therefore, ρ_{AWS} was much higher reflecting than the mean when the melt season started. Once the snow was melted, the differences decreased as ice surface is much darker than snow, however, still brighter than rock. All years showed the same pattern over the year. 2019, which was a very warm year, showed the smallest standard deviation within A_{MODIS}.

MIT station is located on a surface of ice on top of a mountain on an island, separated from the ice sheet. It is surrounded by tundra (figure 17b) on a smaller scale and certainly by water on a bigger scale. In the analysis, it displayed a similar pattern within the years, depending on if it was a rather warm or cold year. In summer, when the snow melted, the deviation was increasing. The AWS pixel constantly displayed a higher value than the mean because the AWS is located at a point that is steadily covered in snow when the season is changing from spring to summer. As exceptions, in 2014 and 2017, ρ_{AWS} were representative for the MODIS area in summer, while 2016 had a slight underestimation at the station's spot when comparing ρ_{AWS} to $\overline{\rho}$. In late summer, when the AWS location was snow-free as well, the difference decreased again.

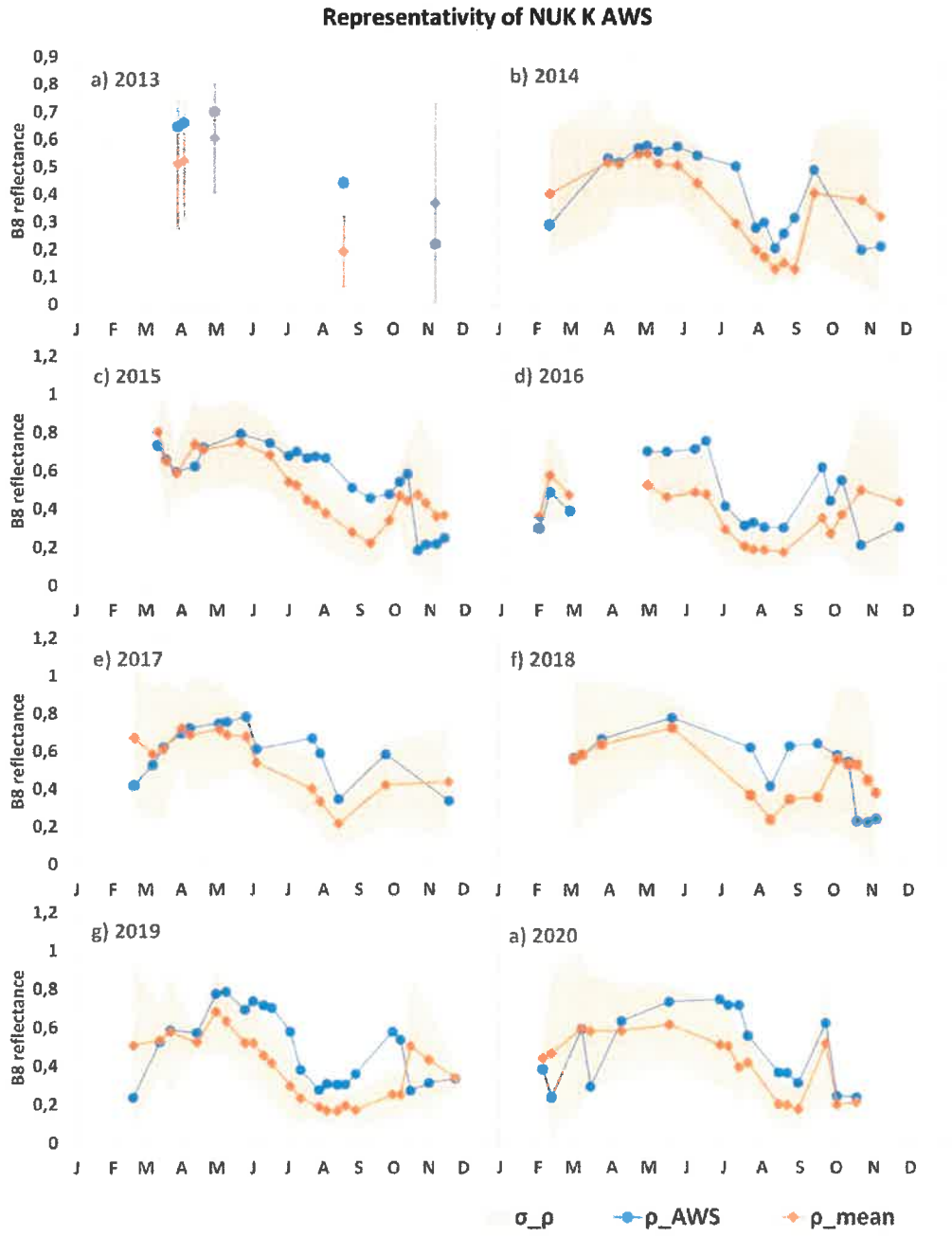

Figure 16. Panchromatic reflectance at NUK K weather station for the years 2013-2020

The individual years all behaved similar at *TAS L* site. In spring, ρ_{AWS} was slightly below $\bar{\rho}$ with only small deviation, resulting in being relatively representative. With the start of the melt season, the two values drifted apart. The deviation increased significantly with $\bar{\rho}$ repeatedly laying outside of the standard deviation range because it was reflecting much less. The reason for this behaviour was the surface partly being covered in snow while other parts were already melted and the bare ice appeared (figure 17c). Around August, slightly differing between the individual years, ρ_{AWS}

and $\bar{\rho}$ settled down at a lower rate now that the ice was snow-free. The representativity was given again, just before the surface reflectance increased towards winter.

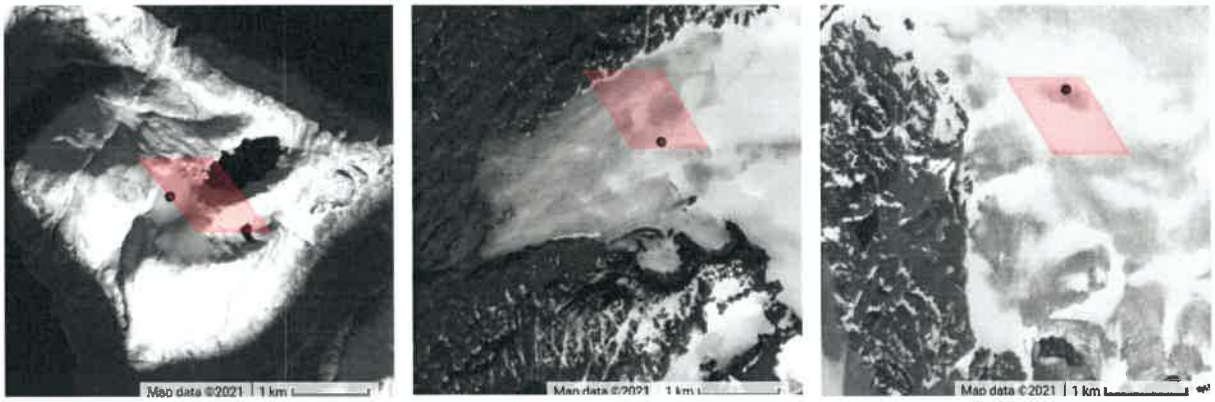

a) NUK K, Sep. 16th 2014	b) MIT, July 20th 2020	c) TAS L, June 12th 2017

Figure 17. Seasonal occurrences at the sites of NUK K, MIT and TAS L (Landsat 8 TOA, USGS/Google)

3.2. Accuracy of albedo proxy

This analysis was done to support the assertions from the previous analysis as well as compare the automates weather station data to a MODIS albedo product. The following results represent one representative site (CEN) and one site showing a recurring pattern with large deviations (NUK K).

Representative site

For CEN weather station, data was available from mid-2017 on. The station's albedo α_{AWS} is represented by dark yellow triangles in the graph (figure 18). The albedo data of MODIS α_{MODIS} is represented by green star-symbols. The data was available for all observed years. The comparison showed α_{MODIS} to be very stable throughout the years, just like expected. It was the same behaviour as the Landsat 8 analysis in *3.1.* revealed for CEN. α_{MODIS} showed less fluctuations than the band 8 reflectance values, probably caused by MODIS' larger footprint. That the different parameters do not match in values was to be expected because they are different products. They should however show the same trend as they all depend on the surface reflectance. The weather station did not run as accurate, but also had less data to compare. Still, especially in 2020 and 2019, expect for the two outliers in the beginning, α_{AWS} demonstrated the same trend as the satellite data. 2017 and 2018 did not have many records but the ones available supported the assumption. The values of α_{MODIS} and α_{AWS} lay close to each other, always below the Landsat data.

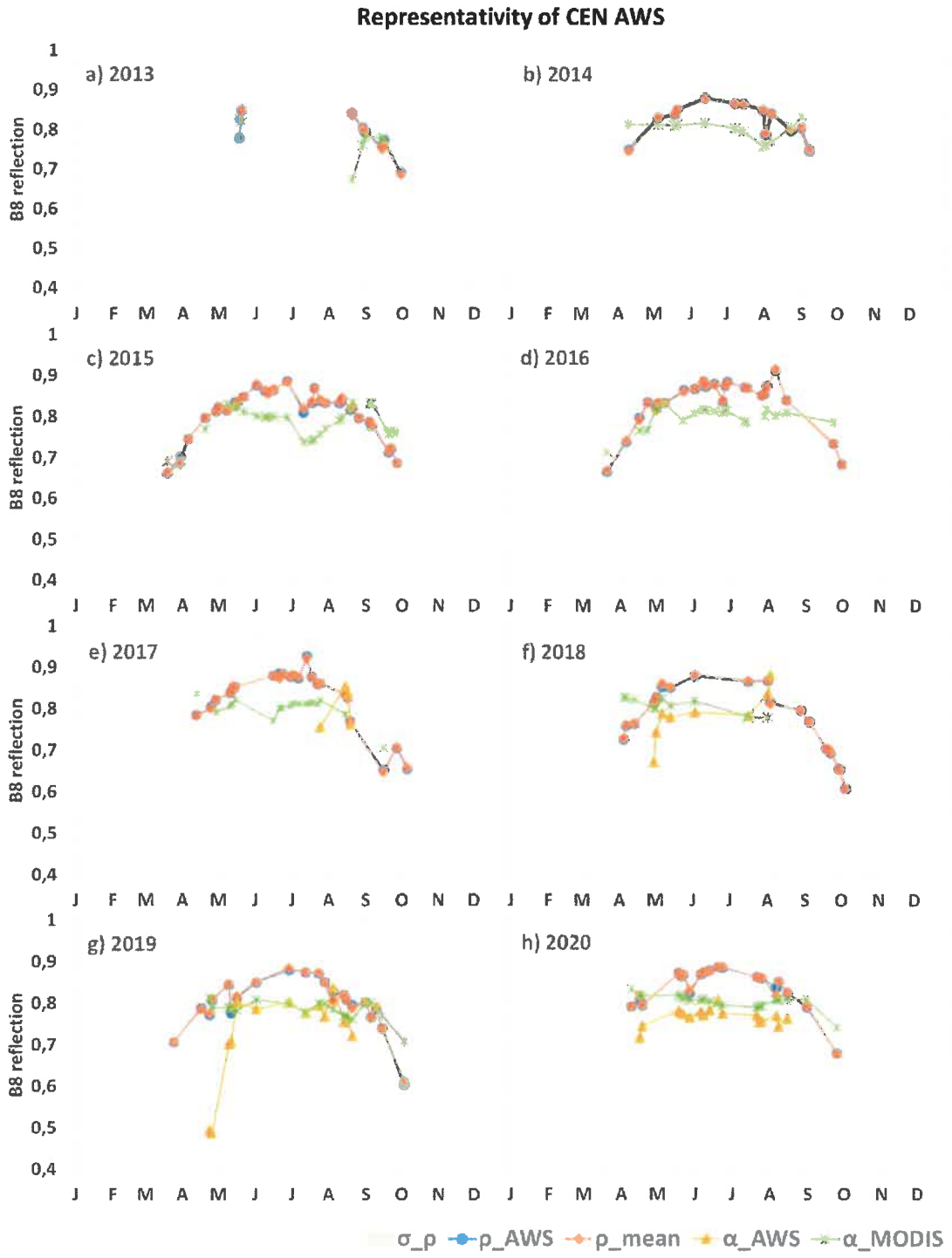

Figure 18. Comparison of Landsat 8 analysis, AWS data and MODIS albedo product for CEN

Varying site

Figure 19 shows the comparison of different albedo data products of NUK K. Except for 2013, each year can be compared. AWS data was available from mid-2014 and MODIS albedo data for all years. 2013 only had very few data points but the available records agreed immensely to the

course of α_{MODIS} and $\bar{\rho}$. α_{MODIS} followed the trend of the decreasing values during the melt season for all years. Some individual data points, like June 2017, were slightly off but that was rarely seen. As displayed in figure 19, α_{MODIS} followed the movement of $\bar{\rho}$, while the weather station data followed ρ_{AWS} very well. Especially 2014, 2016, 2018, and with a few exceptions 2019, displayed a high agreement between the two variables. In 2020, they demonstrated the same trend, but the weather station data was smaller in value than ρ_{AWS}. 2017 showed a few outliers in August, so did 2015 in April.

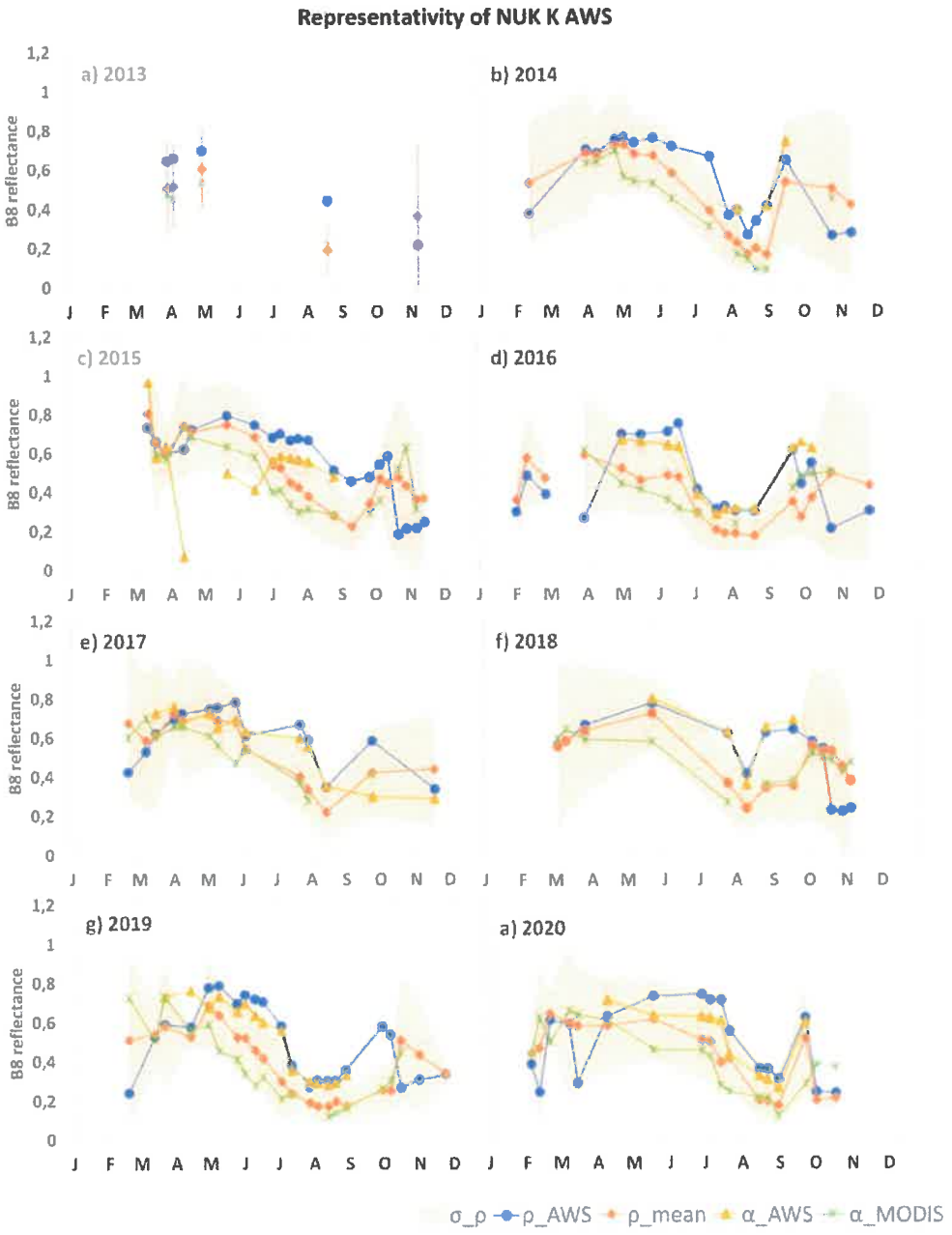

Figure 19. Comparison of Landsat 8 analysis, AWS data and MODIS albedo product for NUK K

4. Discussion

Several papers have discussed the albedo variability of the Greenland ice sheet, especially with regard to the melt season (Bøggild et al., 2010; Moustafa et al., 2017). For homogenous surfaces, studies declare remote sensing products to operate well (Ryan et al., 2017). It also implies that in situ and MODIS albedo data perform similar under those conditions (Moustafa et al., 2017). For non-homogenous surfaces, this is not the case. To compare automated weather station data and remote sensing products, single 'point-to-pixel' methods alone can be insufficient in characterizing and validating the variation of surface albedo. As Moustafa (2017) stresses, high-resolution imagery is needed to resolve high sub-pixel variability in the ablation zone, and therefore, further improve the characterization of Greenland's surface albedo. This is what this study aimed for. By examining the spatial differences around each weather station over time, using high-resolution imagery, local variability was revealed that gave important prospect for the representativity of an AWS location compared to the nearby area, which then again can be adjusted for 'point-to-pixel' comparisons.

When evaluating the previous presented results, 40% of the automated weather stations proved to be significantly representative for their location with a RMSD below 0,001. Meaning that not only the AWS data provided a decent description of the site but also that MODIS products will assess a similar albedo for the area. When considering the location of the representative stations (figure 20), the hypothesis that locations further inwards on the ice sheet are more stable as well as the ones further North can be confirmed. It is caused by the more stable climate in the accumulation zone compared to the ablation zone. The inner ice sheet presents higher elevations, is less influenced by the marine climate and therefore offers colder and steadier temperatures. Furthermore, the ice sheet's high reflectance of solar radiation brings additional cooling (Kump et al., 2014). Each station at an altitude above 1500m showed to be highly representative. This report supports the statement by Ryan et al. (2017) that homogenous surfaces bring a higher spatial as well as temporal representativity at the AWS location, especially with the respect to seasonal variability.

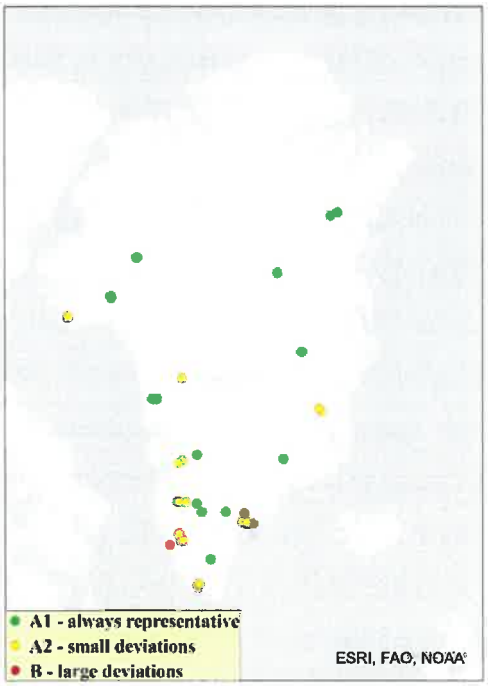

Figure 20. The location of AWS grouped into representativity categories

As mentioned, predominantly stations further inwards on the ice sheet, that do not experience strong melting in summer, showed the highest representativity. But also stations located at the margin like UPE L indicated a high representativity in the analysis when they shift from snow-covered to snow-free surface was relatively rapid. UPE L, located at a height of 220m, is situated in the ablation zone but the representativity over the year dominated over the small variations during melt season. The albedo data of A1 weather stations can confidently be used without adjustments.

The ice underneath is darker than fresh or old snow which concludes in a lower albedo. However, AWS can still be representative when the surface is homogenous. This assumes that there is a consistent surface underneath and no unregular pattern of less reflecting impurities like mineral dust, soot or ice algae within the ice. Ice darkens with increasing impurities. When the location demonstrates a varying surface and experiences snow melt on a degree that at least parts of the surface become snow-free, a deviation can be expected. It is caused by the darker reflecting ice, tundra or other phenomena that occur once the snow melts. Potentially some patches of old snow survive that show brighter reflectance in analysed images.

Depending on the location of the AWS, higher or lower rates, compared to the mean, arose for the period of the melt season due to those occurrences. The positions where snow melts first, and where the snow may survive longer, depend on the exposure to sunlight and snow depth. In topographic lows, the snow is usually thick because of an accumulation by wind and its potential location in the shade for part of the day. On hills, the thin snowpack is exposed to more sun and melts faster. Previous mentioned impurities are moved by the meltwater, which rinses off ice bumps and accumulates impurities in depressions. In these cases, the location's reflectance has a strong seasonal dependence. The stations are mainly representative during the winter months while in summer, variations must be considered when working with the albedo data.

In the case of an automated weather station positioned right next to tundra or on a mountain peak, like it is the case at NUK K, it is difficult to get an impression of the surrounding's albedo. It should be seen as a limited albedo representing a very restricted area. In this case, dominantly arising for category B, it needs to be considered whether the AWS albedo product proves as useful for planned investigations. The ratio between ρ_{AWS} and $\bar{\rho}$ must be observed when working with the station. The four largely varying stations in category B are all situated in Southern Greenland, which supports the assumption about a generally higher chance of representativity when moving northward.

Considering the outcomes of this study, they correspond to the findings observed in Ryan et al. (2017). A comparison of three weather stations in the K transect (KAN L, KAN M and KAN U) showed an annual bias between MODIS and in situ observations in their study. The deviation decreased with moving towards the centre of the ice sheet. This paper's results observed the same variability, with KAN L showing the highest annual deviation out of the three, placed in category A2. Ryan et al. proved that variability is changing during summertime, melting of the snow increasing the deviation between the location of the AWS and the surroundings. Their paper concluding similar results for these three stations, obtained with other methods and data, supports the confidence of this study. Ryan's comparison of AWS and MODIS data performed similar to the approach of a high-resolution imagery method used in this study.

With an evaluation of each individual weather station, showing the exact seasonal course for each of the past 8 years, a lot of valuable information about the location's local conditions is given. The images help to understand why we see these variations and what the occurrence of certain events means for albedo reflectance.

It is important to be cautious that the results of this study might be affected by the manually determined MODIS pixels, where subsequently manual sorting had to be performed, as well as by the simplicity of the applied cloud mask. Future development may include the exact coordinates of the MODIS grid and a more precise cloud mask. The comparison between high resolution, AWS and MODIS data can be continued in further research to build up confidence in the results and discover further outcomes. Additional data, with regards to the stations that were poorly covered by the processed Landsat 8 data, can be included. This study revealed a few locations showing occurrences, lakes for instance, just next to the examined A_{MODIS}, which therefore were not included in the analysis. With that in mind, a study with an extended investigating area could find great interest. Furthermore, each season can be observed individually to discover more details about recurring patterns. Establishing corresponding adjustment coefficients for weather stations form additional potential benefit for the future.

Albedo measurements carried out by weather stations are often considered as ground truth. This report's analysis discovered whether an automated weather station's albedo can confidently be used because it is representative for the area, or whether it has to be adjusted. The study proposes a simple derivation for a representativity analysis. In a defined area of the surrounding region, representing a $1km^2$ resolution MODIS pixel, the stations can now be classified on their representativity in terms of albedo reflectance. Furthermore, it eases comparisons between different albedo products, whether they are satellite-retrieved or stationary origin. The analysis in *3.2.* supports the confidence of the study. The MODIS albedo showed a behaviour similar to the mean of

the Landsat 8 data ($\overline{\rho}$) while the AWS' albedo ran close to Landsat's ρ_{AWS}. It helped to understand that the in *3.1.* received ratio was truthful and functioning as a proxy. However, when a precise representation of the area is wanted, the standard deviation needs to be considered to know if the mean is simply the average of the area or a representative of what is seen in the region. The standard deviation explains whether ρ_{AWS} and $\overline{\rho}$ are truly corresponding or only accidently happen to meet. The strength of this report is the broad application on 40 weather stations situated in Greenland, which helps future research studies to justify a weather station's performance in terms of albedo and better classify their approaches into context.

5. Conclusion

The albedo representativity of automated weather stations in Greenland is strongly dependent on the characteristics of its surroundings. Particularly during the melt season, large shifts can occur. To confidently use the AWS data in scientific research, an evaluation of the albedo data is necessary to know if it is sufficient to represent the area. It is an important advantage for research on the Greenlandic ice sheet, as the investigation is mainly realized by remote sensing. Remote sensing products cannot simply be compared to AWS data when inconvenient circumstances are given. While homogenous surfaces create a high representativity, AWS locations featuring lakes, crevasses or ice impurities, as well as those situated close to tundra or rock, demonstrate a heterogenous surface and therefore variations in albedo. For those stations, the data is to be used with caution. The increasing global warming causes longer melting periods and therefore an extended time of darker incidents being revealed instead of being covered under a homogenous snowpack. Generally, it is concluded that weather stations on high elevations (>1500m) are very likely to represent the albedo of the region well. Stations at a lower altitude and closer to the coast must be treated individually depending on local occurrences.

The graphs created within this research help to precisely detect variations throughout the year while the satellite imagery reveals which events occur in the environment of a station. Based on this report, future studies can rely on individual adjustment information for each of the 40 weather stations. This research leads to a more secured evaluation of AWS albedo data to improve further examinations of the Greenland ice sheet. To have all stations confidently covered without gaps, further research is firmly encouraged.

References

AMAP (2011). Snow, Water, Ice and Permafrost in the Arctic (SWIPA): Climate Change and the Cryosphere. Arctic Monitoring and Assessment Programme (AMAP), Oslo, Norway. xii + 538 pp.

AMAP (2017). Snow, Water, Ice and Permafrost in the Arctic (SWIPA) 2017. Arctic Monitoring and Assessment Programme (AMAP), Oslo, Norway. xiv + 269 pp

AMAP (2019). *Artic Climate Change Update 2019.* Arctic Monitoring and Assessment Programme (AMAP), Oslo, Norway

Andersen, M.L. , L. Stenseng, H. Skourup, W. Colgan, S.A. Khan, S.S. Kristensen, S.B. Andersen, J.E. Box, A.P. Ahlstrøm, X. Fettweis, R. Forsberg (2015). *Basin-scale partitioning of Greenland ice sheet mass balance components (2007–2011)*, Earth and Planetary Science Letters, Volume 409

Arzhanov, M. & Eliseev, A. & Mokhov, I.. (2013). *Impact of climate changes over the extratropical land on permafrost dynamics under RCP scenarios in the 21st century as simulated by the IAP RAS climate model.* Russian Meteorology and Hydrology. 38. 456-464. 10.3103/S1068373913070030.

Bøggild, Carl Egede, Richard E. Brandt, Kendrick J. Brown, Stephen G. Warren (2010). *The ablation zone in northeast Greenland: ice types, albedos and impurities.*

Chander, Gyanesh & Markham, Brian. (2009). *Summary of current radiometric calibration coefficients for Landsat MSS, TM, ETM+, and EO-1 ALI sensors. Remote Sensing of Environment.* 113. 893-903. 10.1016/j.rse.2009.01.007.

ESRI. (n.d.). Landsat 8 Imagery Available for Online Users. Retrieved April 19th, 2021, from https://www.esri.com/about/newsroom/arcnews/landsat-8-imagery-available-for-online-users/

ESRI. Greenland Maps in this paper were created using ArcGIS® software by Esri. ArcGIS® and ArcMap™ are the intellectual property of Esri and are used herein under license. Copyright © Esri. All rights reserved. For more information about Esri® software, please visit www.esri.com.'

Ettema, Janneke, Michiel R. van den Broeke, Erik van Meijgaard, Willem Jan van de Berg, Jonathan L. Bamber, Jason E. Box, and Roger C. Bales (2009). *Higher surface mass balance of the Greenland ice sheet revealed by high-resolution climate modeling.*

Gorelick, N., Hancher, M., Dixon, M., & Ilyushchenko. (2017). *Google Earth Engine: Planetary-scale geospatial analysis for everyone. Remote Sensing of Environment.*

Greenland Climate Network GC-Net (http://cires1.colorado.edu/steffen/gcnet/)

Hall, Dorothy K., Josefino C. Comiso, Nicolo E. DiGirolamo, Christopher A. Shuman, Jason E. Box, Lora S. Koenig (2013). *Variability in the surface temperature and melt extent of the Greenland ice sheet from MODIS.*

Hofer, S., Lang, C., Amory, C. et al. Greater Greenland Ice Sheet contribution to global sea level rise in CMIP6. Nat Commun 11, 6289 (2020). https://doi.org/10.1038/s41467-020-20011-8

Institute for Marine and Atmospheric research Utrecht (https://www.projects.science.uu.nl/icecl mate/aws/greenland.php)

IPCC (2013).Vaughan, D.G., J.C. Comiso, I. Allison, J. Carrasco, G. Kaser, R. Kwok, P. Mote, T. Murray, F. Paul, J. Ren, E. Rignot, O. Solomina, K. Steffen and T. Zhang, 2013: Observations: Cryosphere. In: Climate Change 2013: The Physical Science Basis. Contribution of Working Group I to the Fifth Assessment Report of the Intergovernmental Panel on Climate Change [Stocker, T.F., D. Qin, G.-K. Plattner, M. Tignor, S.K. Allen, J. Boschung, A. Nauels, Y. Xia, V. Bex and P.M. Midgley (eds.)]. Cambridge University Press, Cambridge, United Kingdom and New York, NY, USA.

Kjeldsen, K., Korsgaard, N., Bjørk, A. et al. *Spatial and temporal distribution of mass loss from the Greenland Ice Sheet since AD 1900*. Nature 528, 396–400 (2015). https://doi.org/10.1038/nature16183

Kump, Lee R., Kasting, James F., Crane, Robert G. (2014). *The Earth System.*

Lucht, Wolfgang, Crystal Barker Schaaf, Member, IEEE, and Alan H. Strahler, Member, IEEE (2000). *An Algorithm for the Retrieval of Albedo from Space Using Semiempirical BRDF Models.*

Mernild, S. H., Lipscomb, W. H., Bahr, D. B., Radić, V., and Zemp, M.: *Global glacier changes: a revised assessment of committed mass losses and sampling uncertainties*, The Cryosphere, 7, 1565–1577, https://doi.org/10.5194/tc-7-1565-2013, 2013

Moustafa, Samiah E., Asa K. Rennermalm, Miguel O. Román, Zhuosen Wang, Crystal B. Schaaf, Laurence C. Smith, Lora S. Koenig, Angela Erb (2017). *Evaluation of satellite remote sensing albedo retrievals over the ablation area of the southwestern Greenland ice sheet.*

NASAa. *Landsat 8 Bands*. Retrieved April 20th, 2021, from https://landsat.gsfc.nasa.gov/landsat-8/landsat-8-bands

NASAb. *About MODIS*. Retrieved April 19th, 2021, from https://modis.gsfc.nasa.gov/about/

NSIDCa. *Cryosphere Glossary*. Retrieved May 20th, 2021, from https://nsidc.org/cryosphere/glossary

NSIDCb. *Thermodynamics: Albedo*. Retrieved May 20th, 2021, from https://nsidc.org/cryosphere/seaice/processes/albedo.html

Orsi, Anais J., Kenji Kawamura, Valerie Masson-Delmotte, Xavier Fettweis, Jason E. Box, Dorthe Dahl-Jensen, Gary D. Clow, Amaelle Landais, Jeffrey P. Severinghaus (2017). *The recent warming trend in North Greenland.*

Overland, James, Edward Dunle, Jason E. Box, Robert Corell, Martin Forsius, Vladimir Kattsov, Morten Skovgård Olsen, Janet Pawlak, Lars-Otto Reiersenh, Muyin Wanga (2019). *The urgency of Arctic change*. Polar Science.

Polar Portal. (2013). *Polar Portal Season Report 2013.* Retrieved from http://polarportal.dk/fileadmin/user_upload/PolarPortal/season_report/Polar-portal-2013_EN_20150121Add.pdf

Polar Portal. (2014). *Polar Portal Season Report 2014.* Retrieved from http://polarportal.dk/fileadmin/user_upload/PolarPortal/season_report/Polar_Portal_2014_EN_20150121Add.pdf

Polar Portal. (2015). *Polar Portal Season Report 2015.* Retrieved from http://polarportal.dk/fileadmin/user_upload/PolarPortal/season_report/Polar-portal-EN-2015.pdf

Polar Portal. (2016). *Polar Portal Season Report 2016.* Retrieved from http://polarportal.dk/fileadmin/polarportal/Polar-portal-saeson-rapport-UK.pdf

Polar Portal. (2017). *Polar Portal Season Report 2017.* Retrieved from http://polarportal.dk/fileadmin/polarportal/Polar-portal-saeson-rapport-2017-UK.pdf

Polar Portal. (2018). *Polar Portal Season Report 2018.* Retrieved from http://polarportal.dk/fileadmin/user_upload/polarportal-saesonrapport-2018-EN.pdf

Polar Portal. (2019). *Polar Portal Season Report 2019.* Retrieved from http://polarportal.dk/fileadmin/user_upload/polarportal-saesonrapport-2019-EN.pdf

Polar Portal. (2020). *Polar Portal Season Report 2020.* Retrieved from http://polarportal.dk/fileadmin/user_upload/PolarPortal/season_report/polarportal_saeson rapport_2020_EN.pdf

PROMICE (https://www.promice.dk)

PROMICE. (2019). The Programme for Monitoring of the Greenland Ice Sheet: *PROMICE annual report 2019.*

Rasmussen, Rasmus Ole. *Greenland*. Encyclopedia Britannica, 10 Mar. 2021, https://www.britannica.com/place/Greenland. Accessed 29 April 2021.

Ryan, J. C., A. Hubbard, T. D. Irvine-Fynn, S. H. Doyle, J. M. Cook, M. Stibal, and J. E. Box (2017), *How robust are in situ observations for validating satellitederived albedo over the dark zone of the Greenland Ice Sheet?*, Geophys. Res. Lett., 44, 6218–6225, doi:10.1002/ 2017GL073661. Steffen et al. (2018). Trajectories of the Earth System inthe Anthropocene.

USGS. *MCD43A3 v006*. Retrieved May 19th, 2021, from https://lpdaac.usgs.gov/products/mcd43a3v006/

van den Broeke, M., Box, J., Fettweis, X. et al. *Greenland Ice Sheet Surface Mass Loss: Recent Developments in Observation and Modeling*. Curr Clim Change Rep 3, 345–356 (2017). https://doi.org/10.1007/s40641-017-0084-8

Yuan, J., Chi, Z., Cheng, X., Zhang, T., Li, T., & Chen, Z. (2020). *Automatic extraction of supraglacial lakes in southwest greenland during the 2014–2018 melt seasons based on convolutional neural network.* Water, 12(3), 891. doi:http://dx.doi.org.ep.fjernadgang.kb.dk/10.3390/w12030891.

Appendices

Appendix A

The table below displays the Root Mean Square Deviation between ρ_{AWS} and $\overline{\rho}$ for the 40 investigated automated weather stations in Greenland.

AWS	RMSD	AWS	RMSD
CEN	0,00055	*NUK K*	0,0151
CP1/CP2	0,0005	*NUK L*	0,00348
DYE 2	0,00079	*NUK N*	0,0025
FA	0,0002	*NUK U*	0,00329
GITS	0,00018	*QAS A*	0,00212
Humboldt	0,00066	*QAS L*	0,003
JAR	0,00313	*QAS U*	0,00146
JAR 2	0,00148	*SCO L*	0,00196
KAN B	0,00549	*SCO U*	0,0018
KAN L	0,00241	*South Dome*	0,00046
KAN M	0,0016	*Swiss Camp*	0,00145
KAN U	0,00071	*TAS A*	0,00344
KAR	0,00027	*TAS L*	0,0081
KPC L	0,00081	*TAS U*	0,00227
KPC U	0,00044	*THU L*	0,00273
KULU	0,00238	*THU U*	0,00269
MIT	0,0054	*TUNU N*	0,00044
NASA E	0,00034	*UPE L*	0,00097
NASA SE	0,00097	*UPE U*	0,00099
NASA U	0,00051		

Appendix B

Appendix B contains graphs for the representativity of the weather stations that were not illustrated in the main report. It displays data of the panchromatic band of Landsat 8. The reflectance at the weather station's location (ρ_{AWS}) is shown in blue, the mean of the surrounding pixel's data ($\bar{\rho}$) is illustrated in orange. The standard deviation within the area is demonstrated by the orange-shaded section.

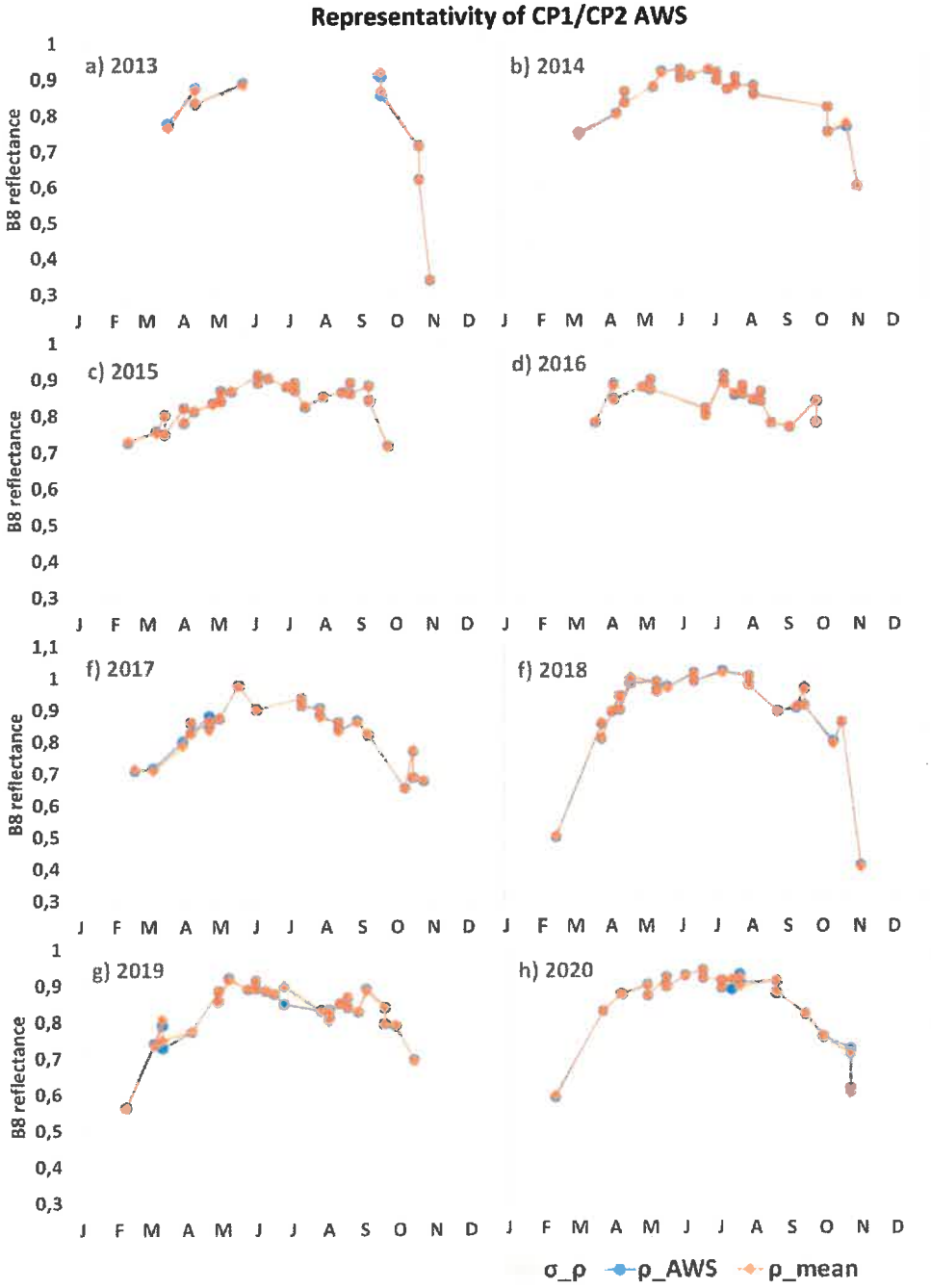

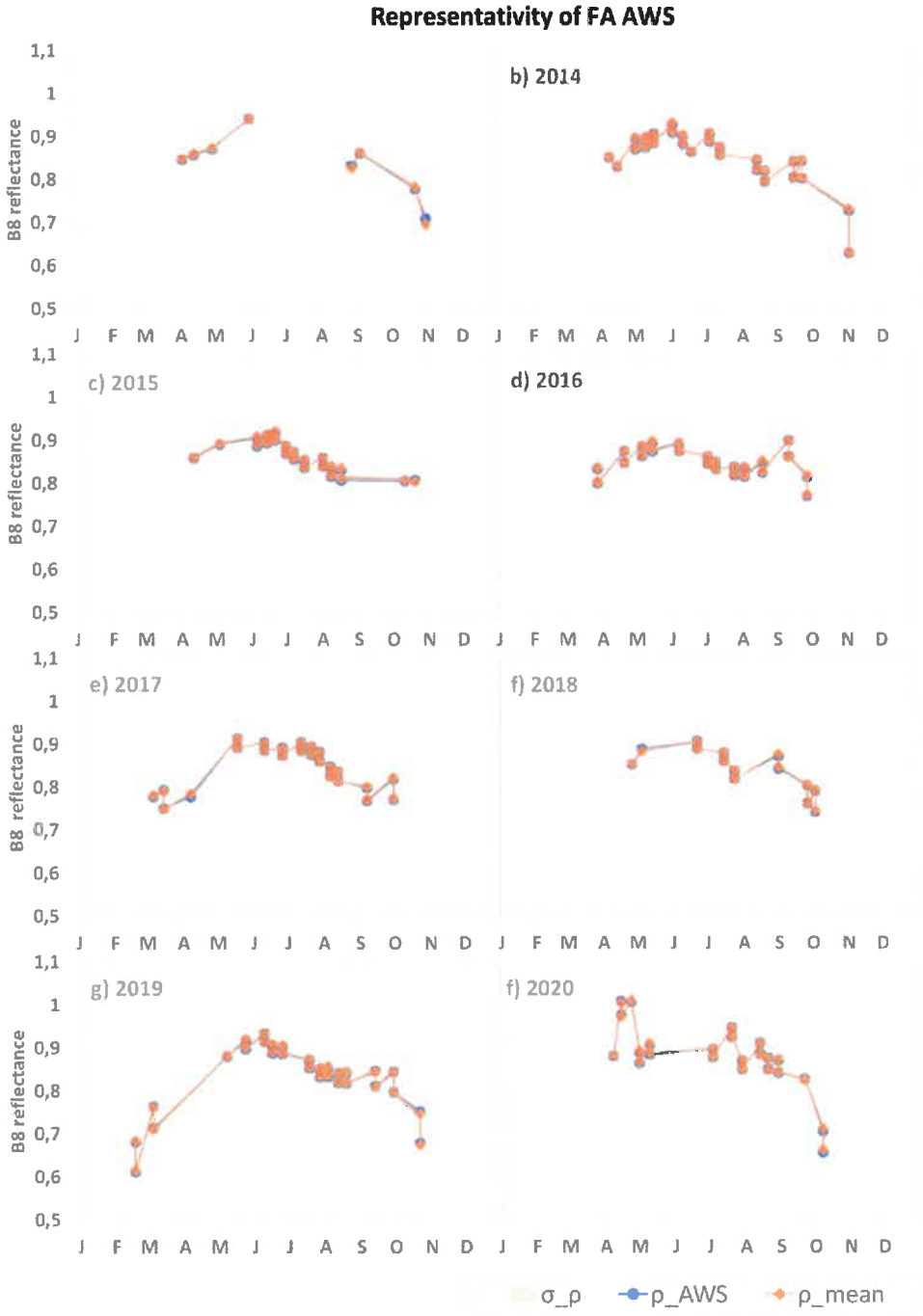
Representativity of FA AWS
b) 2014
c) 2015
d) 2016
e) 2017
f) 2018
g) 2019
f) 2020
B8 reflectance
1,1
1
0,9
0,8
0,7
0,6
0,5
J F M A M J J A S O N D
σ_ρ
ρ_AWS
ρ_mean

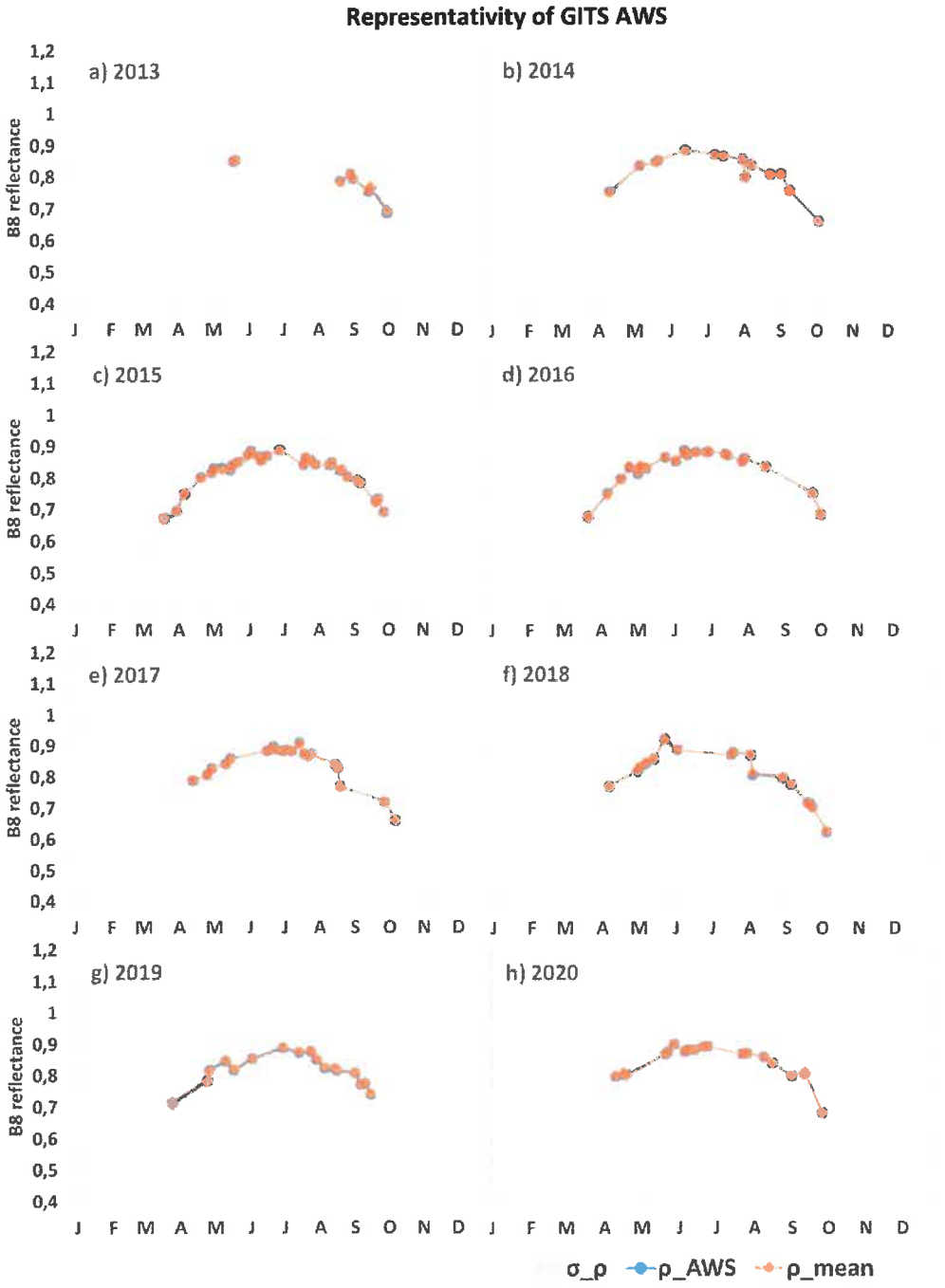
Representativity of GITS AWS
a) 2013
b) 2014
c) 2015
d) 2016
e) 2017
f) 2018
g) 2019
h) 2020
B8 reflectance
1,2
1,1
1
0,9
0,8
0,7
0,6
0,5
0,4
J F M A M J J A S O N D
σ_ρ
ρ_AWS
ρ_mean

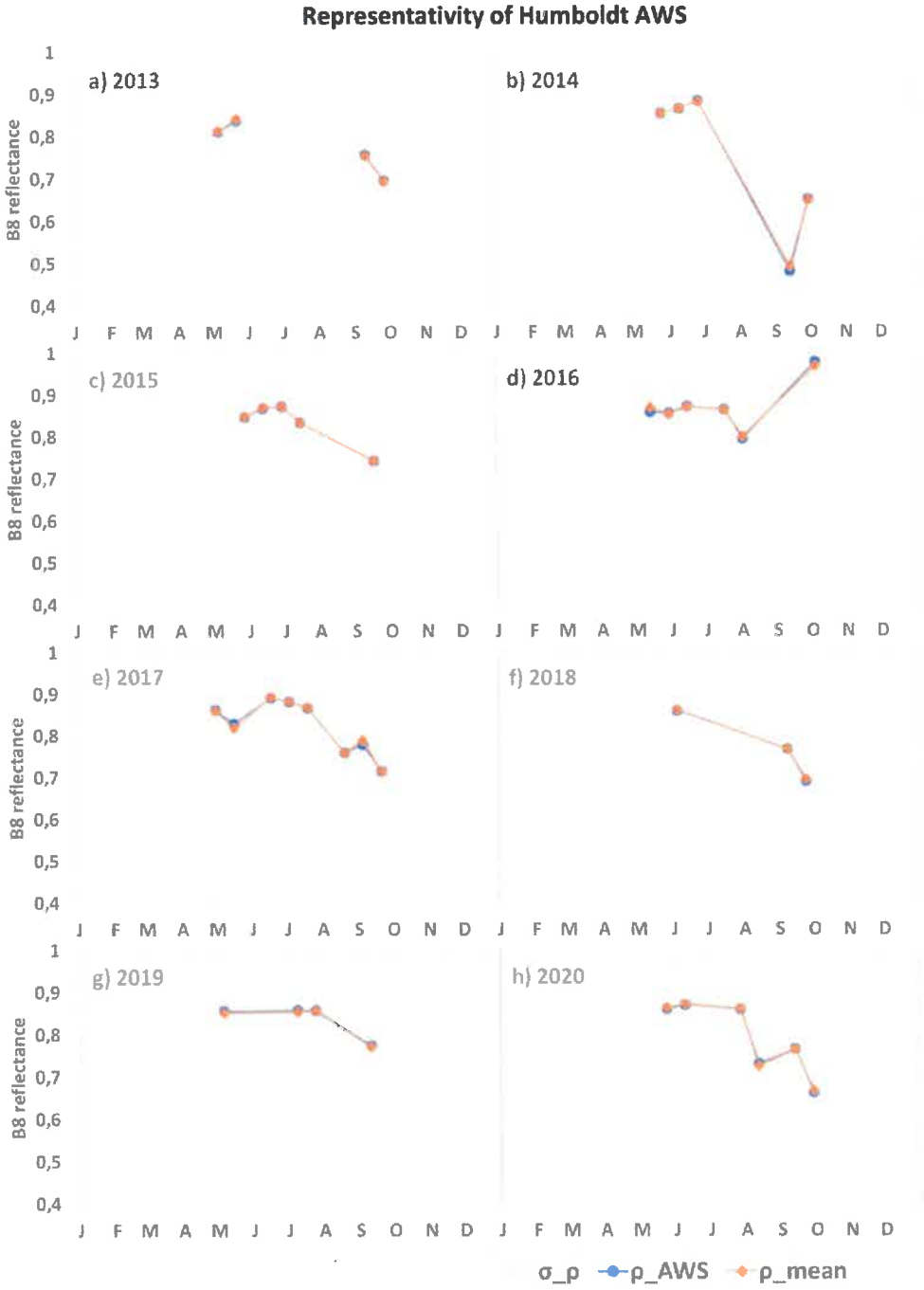
Representativity of Humboldt AWS
a) 2013
b) 2014
c) 2015
d) 2016
e) 2017
f) 2018
g) 2019
h) 2020
B8 reflectance
1
0,9
0,8
0,7
0,6
0,5
0,4
J F M A M J J A S O N D
σ_ρ
ρ_AWS
ρ_mean

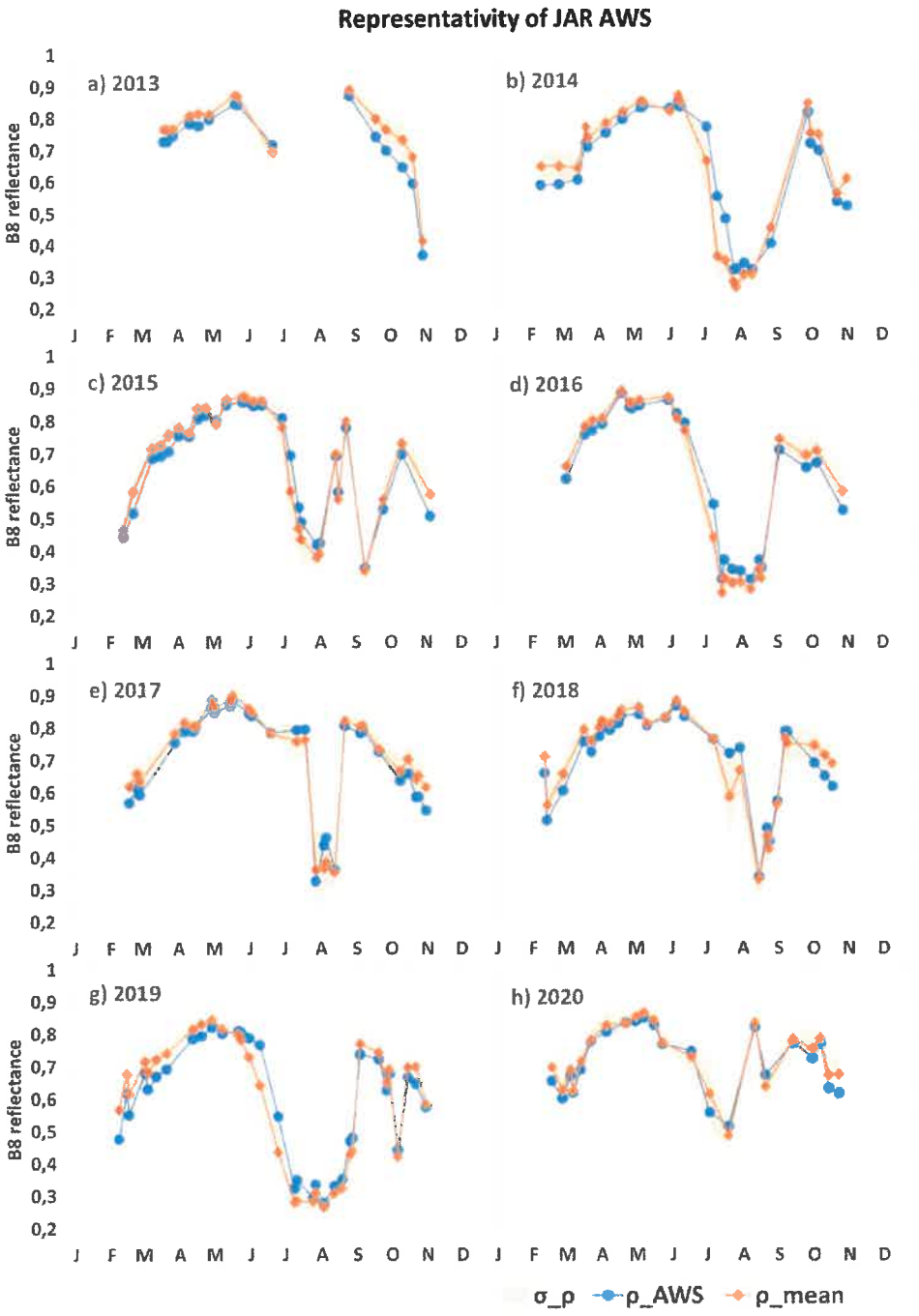
Representativity of JAR AWS
a) 2013
b) 2014
c) 2015
d) 2016
e) 2017
f) 2018
g) 2019
h) 2020
B8 reflectance
1
0,9
0,8
0,7
0,6
0,5
0,4
0,3
0,2
J F M A M J J A S O N D
σ_ρ
ρ_AWS
ρ_mean

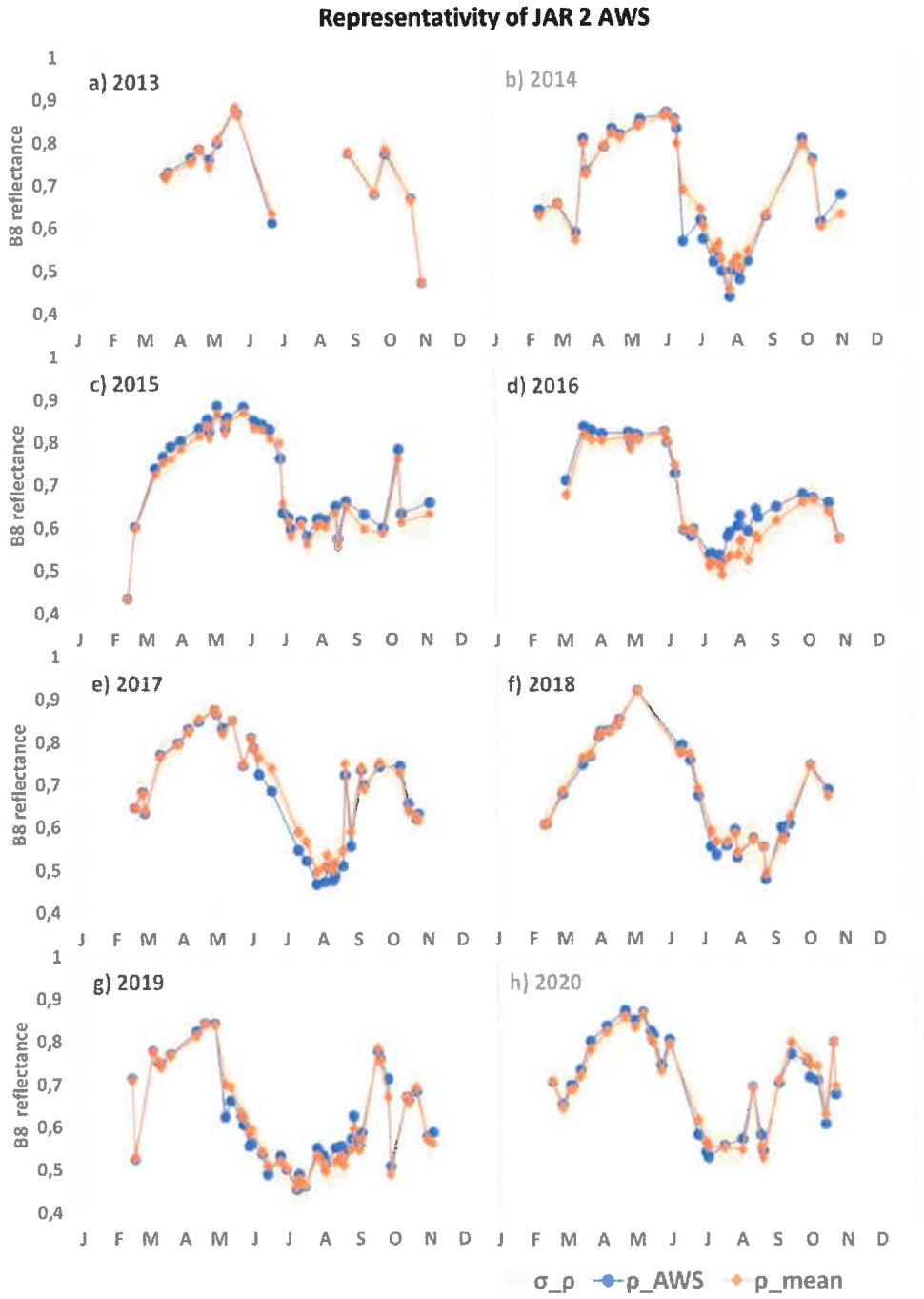
Representativity of JAR 2 AWS
a) 2013
b) 2014
c) 2015
d) 2016
e) 2017
f) 2018
g) 2019
h) 2020
B8 reflectance
1
0,9
0,8
0,7
0,6
0,5
0,4
J F M A M J J A S O N D
σ_ρ
ρ_AWS
ρ_mean

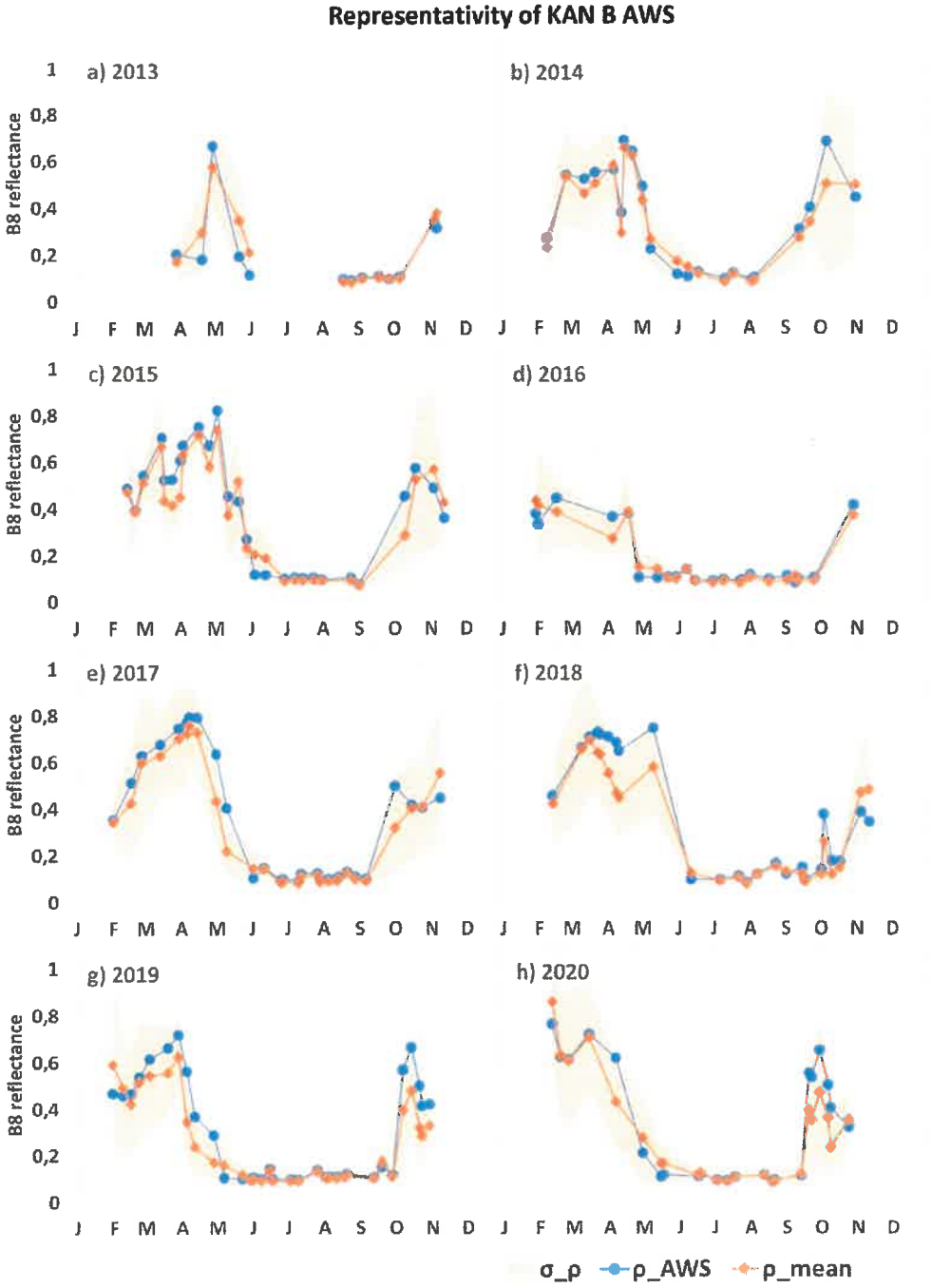
Representativity of KAN B AWS
a) 2013
b) 2014
c) 2015
d) 2016
e) 2017
f) 2018
g) 2019
h) 2020
B8 reflectance
1
0,8
0,6
0,4
0,2
0
J F M A M J J A S O N D
σ_ρ
ρ_AWS
ρ_mean

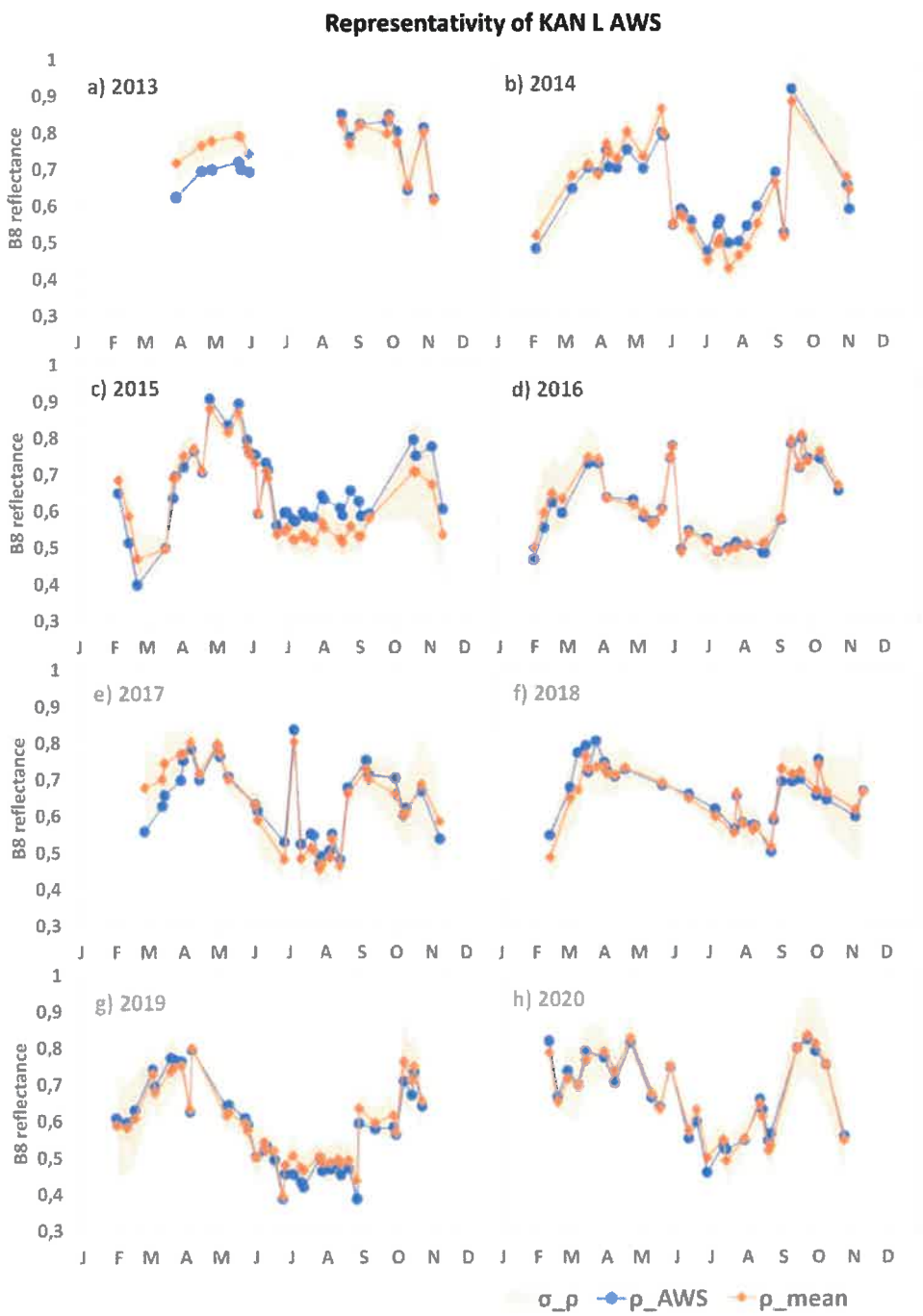
Representativity of KAN L AWS
a) 2013
b) 2014
c) 2015
d) 2016
e) 2017
f) 2018
g) 2019
h) 2020
B8 reflectance
1
0,9
0,8
0,7
0,6
0,5
0,4
0,3
J F M A M J J A S O N D
σ_ρ
ρ_AWS
ρ_mean

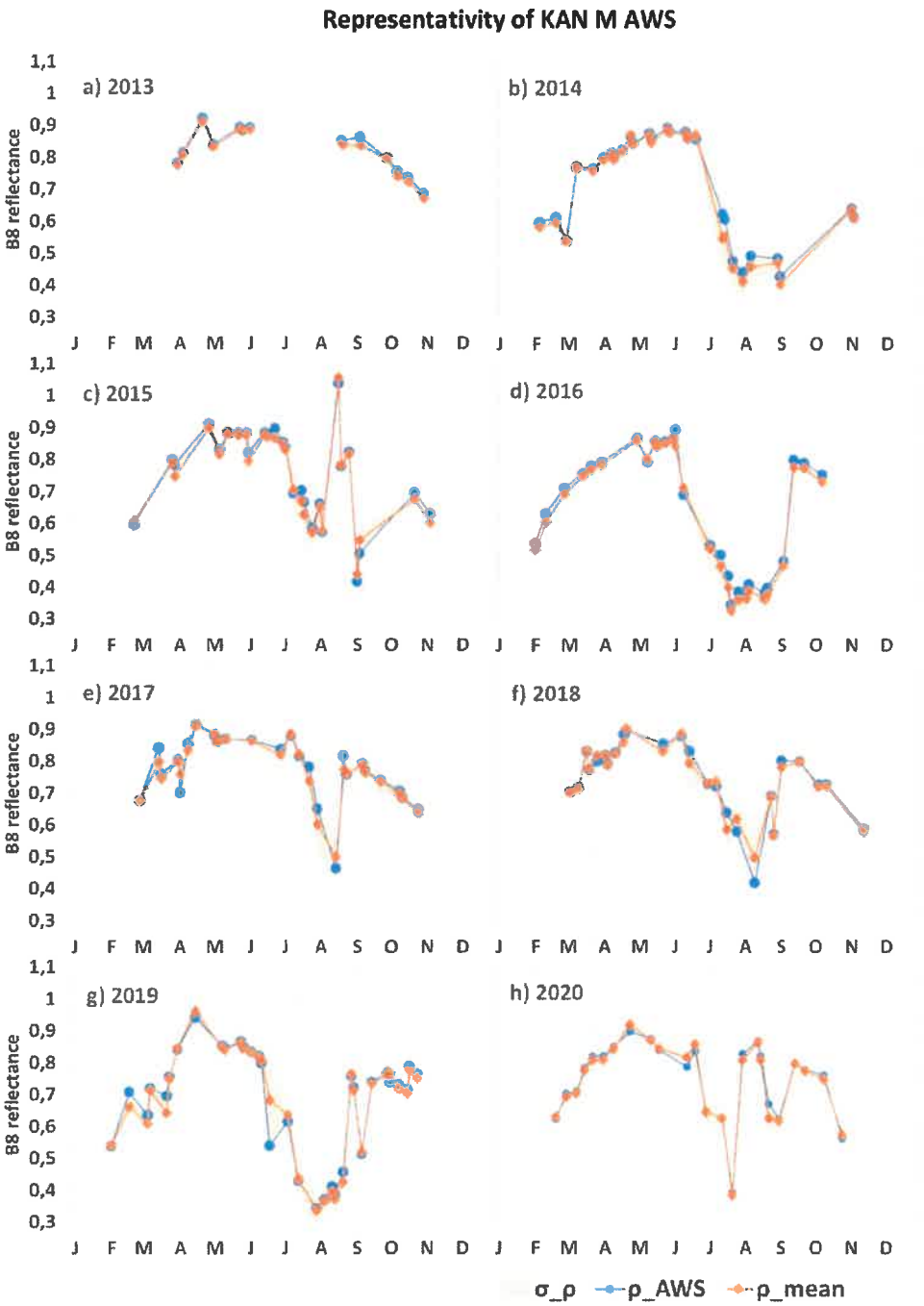
Representativity of KAN M AWS
a) 2013
b) 2014
c) 2015
d) 2016
e) 2017
f) 2018
g) 2019
h) 2020
B8 reflectance
1,1
1
0,9
0,8
0,7
0,6
0,5
0,4
0,3
J F M A M J J A S O N D
σ_ρ
ρ_AWS
ρ_mean

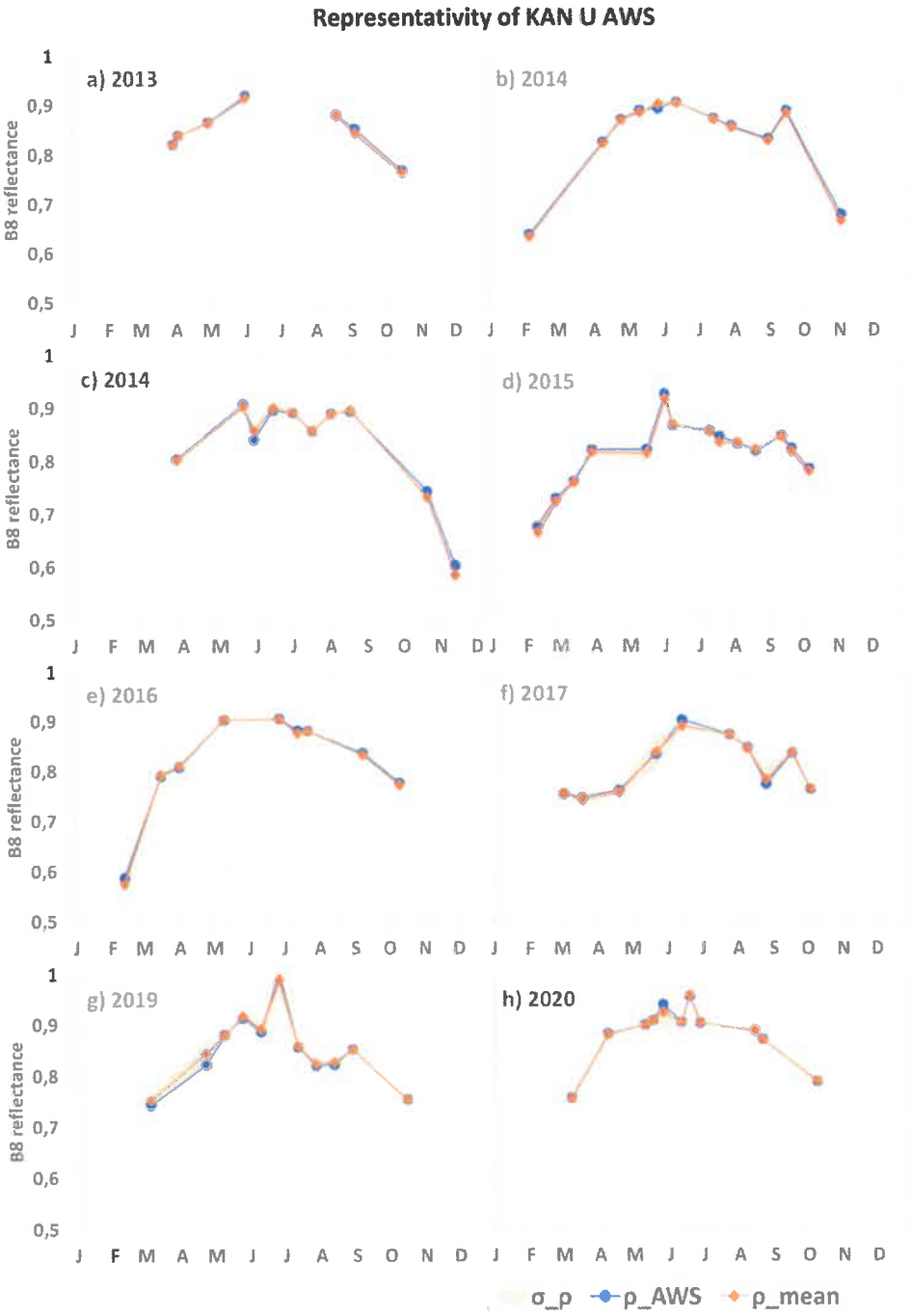
Representativity of KAN U AWS
a) 2013
b) 2014
c) 2014
d) 2015
e) 2016
f) 2017
g) 2019
h) 2020
B8 reflectance
1
0,9
0,8
0,7
0,6
0,5
J F M A M J J A S O N D
σ_ρ
ρ_AWS
ρ_mean

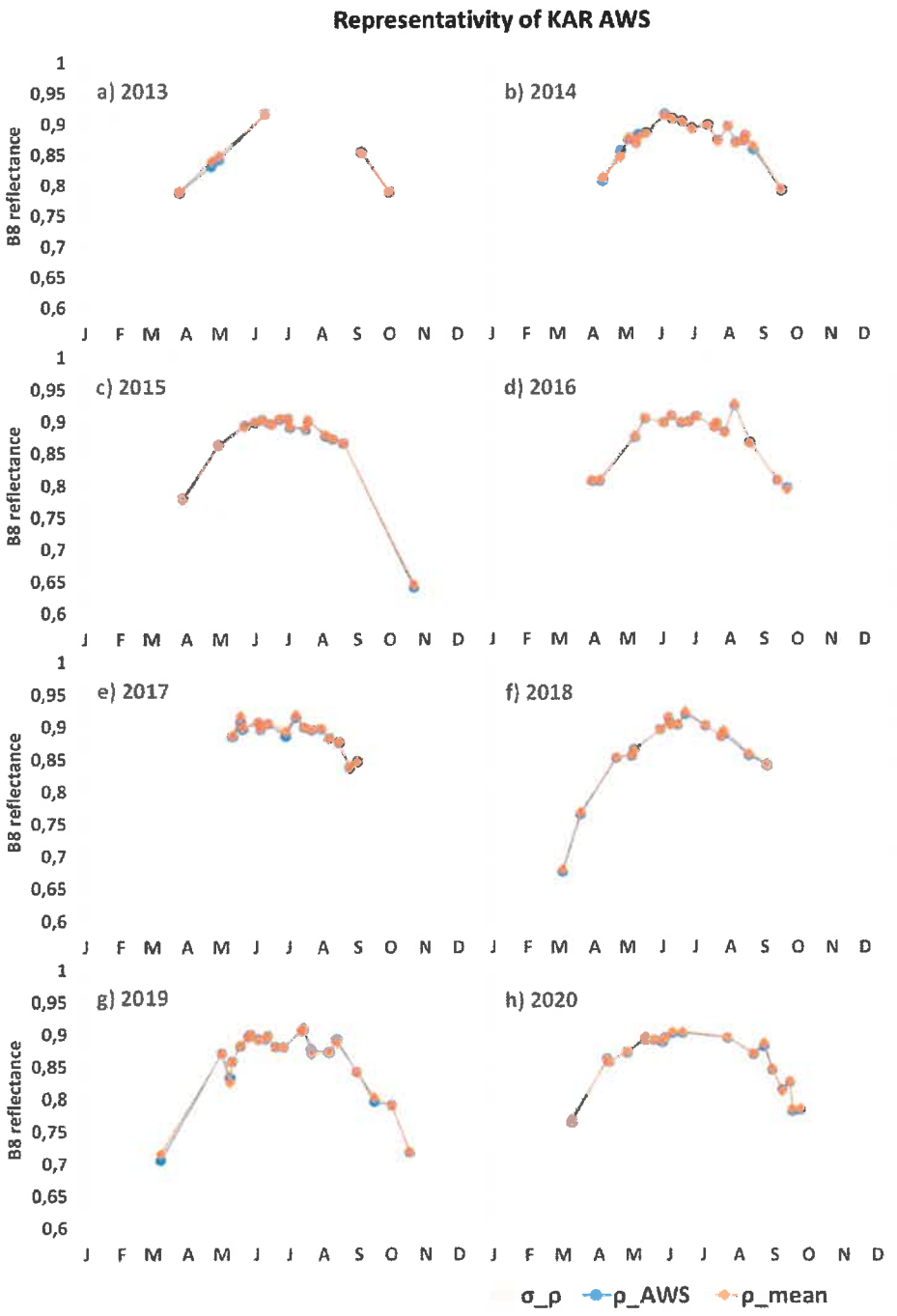
Representativity of KAR AWS
a) 2013
b) 2014
c) 2015
d) 2016
e) 2017
f) 2018
g) 2019
h) 2020
B8 reflectance
1
0,95
0,9
0,85
0,8
0,75
0,7
0,65
0,6
J F M A M J J A S O N D J F M A M J J A S O N D
σ_ρ
ρ_AWS
ρ_mean

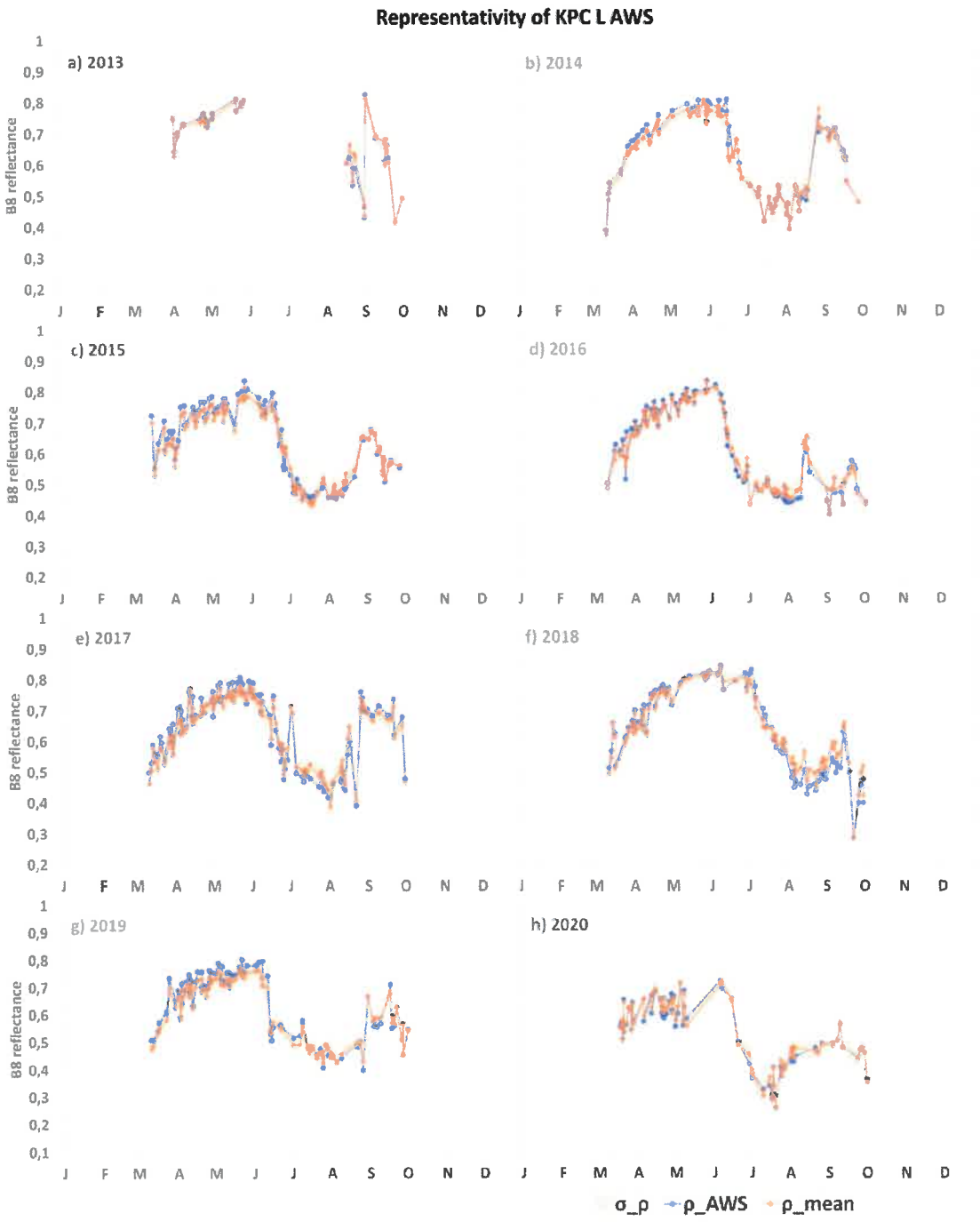
Representativity of KPC L AWS
a) 2013
b) 2014
c) 2015
d) 2016
e) 2017
f) 2018
g) 2019
h) 2020
B8 reflectance
J F M A M J J A S O N D
σ_ρ
ρ_AWS
ρ_mean

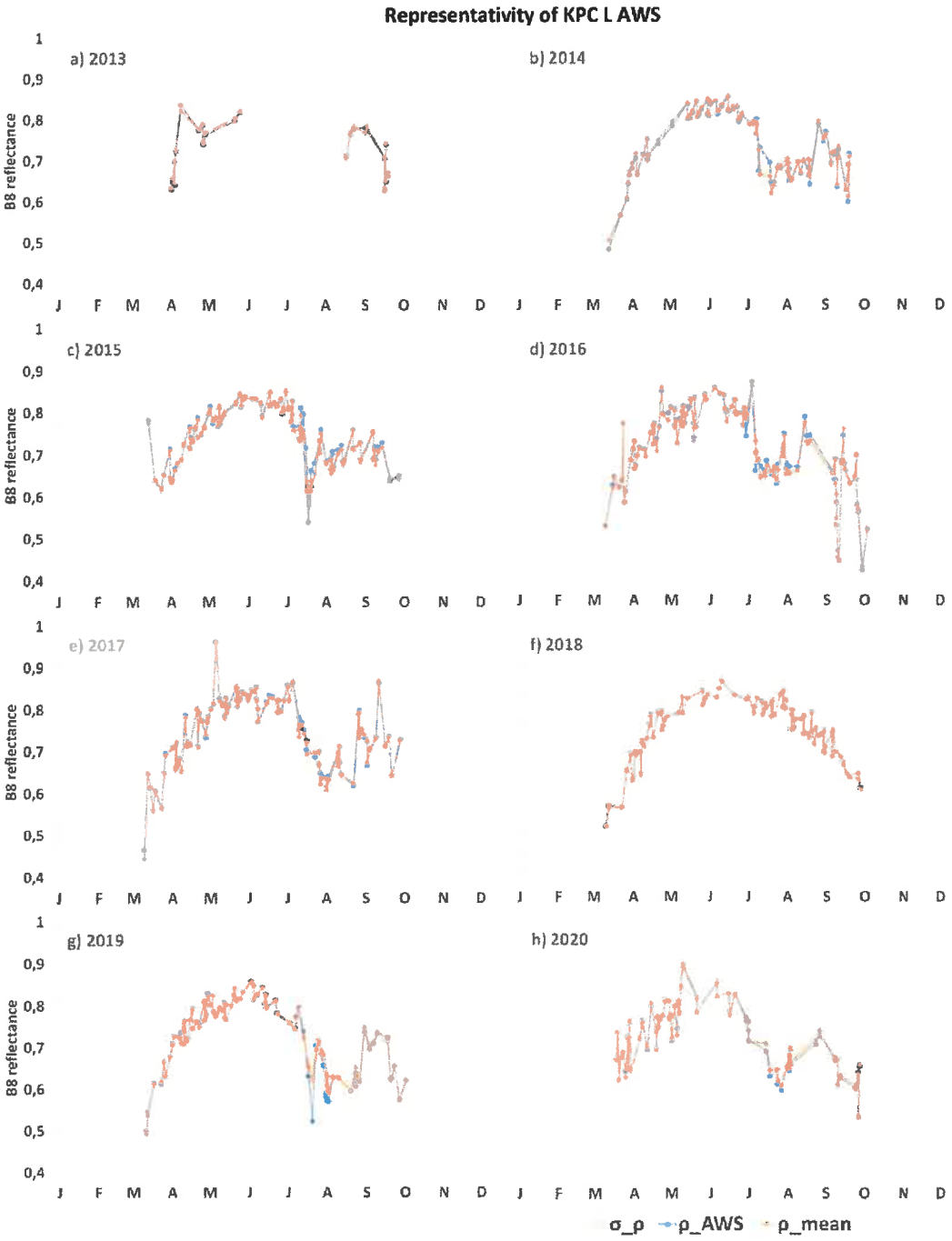
Representativity of KPC L AWS
a) 2013
b) 2014
c) 2015
d) 2016
e) 2017
f) 2018
g) 2019
h) 2020
B8 reflectance
1
0,9
0,8
0,7
0,6
0,5
0,4
J F M A M J J A S O N D
σ_ρ
ρ_AWS
ρ_mean

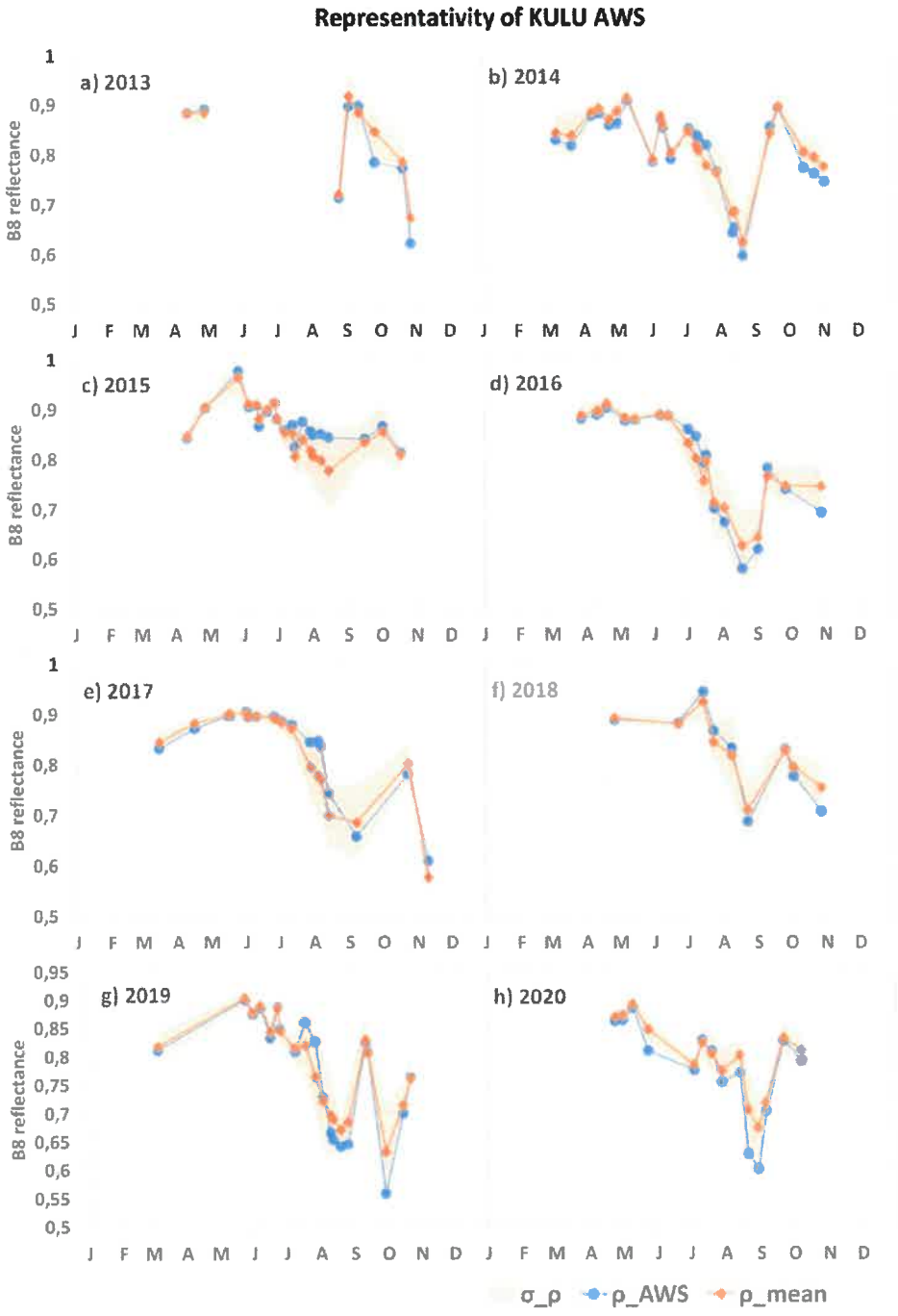
Representativity of KULU AWS
a) 2013
b) 2014
c) 2015
d) 2016
e) 2017
f) 2018
g) 2019
h) 2020
B8 reflectance
J F M A M J J A S O N D
σ_ρ
ρ_AWS
ρ_mean

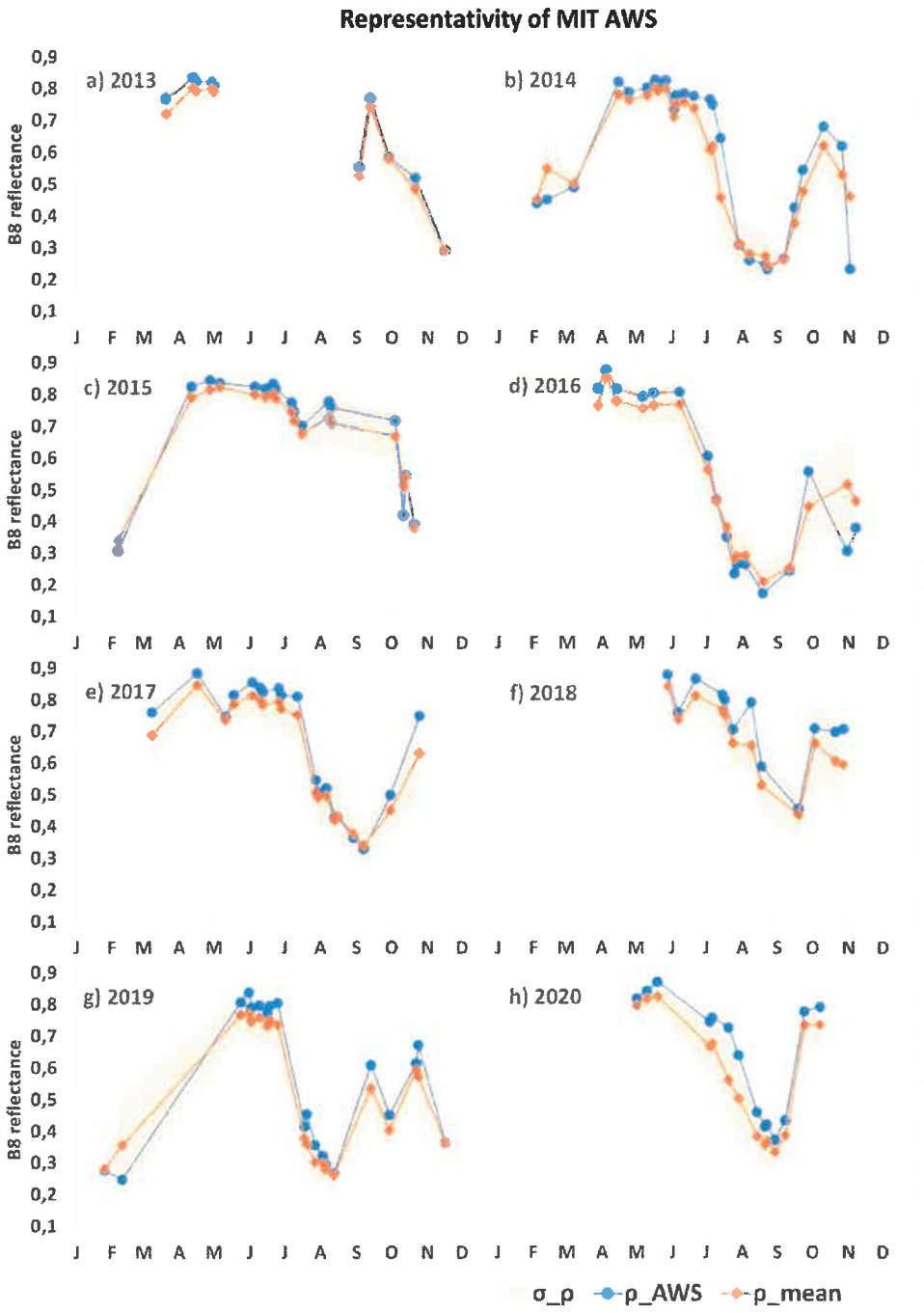
Representativity of MIT AWS
a) 2013
b) 2014
c) 2015
d) 2016
e) 2017
f) 2018
g) 2019
h) 2020
B8 reflectance
0,9
0,8
0,7
0,6
0,5
0,4
0,3
0,2
0,1
J F M A M J J A S O N D
σ_ρ
ρ_AWS
ρ_mean

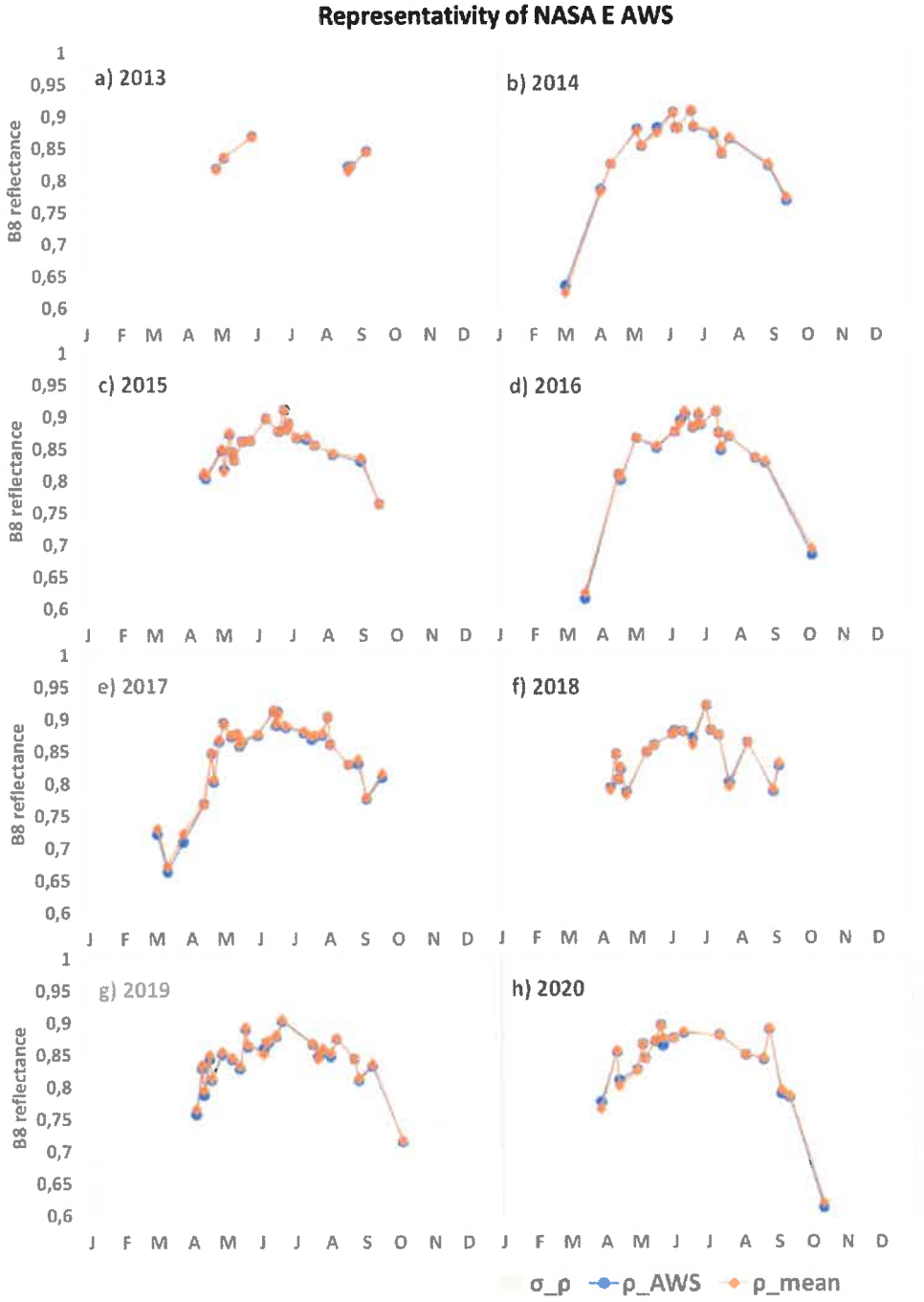
Representativity of NASA E AWS
a) 2013
b) 2014
c) 2015
d) 2016
e) 2017
f) 2018
g) 2019
h) 2020
B8 reflectance
1
0,95
0,9
0,85
0,8
0,75
0,7
0,65
0,6
J F M A M J J A S O N D
σ_ρ
ρ_AWS
ρ_mean

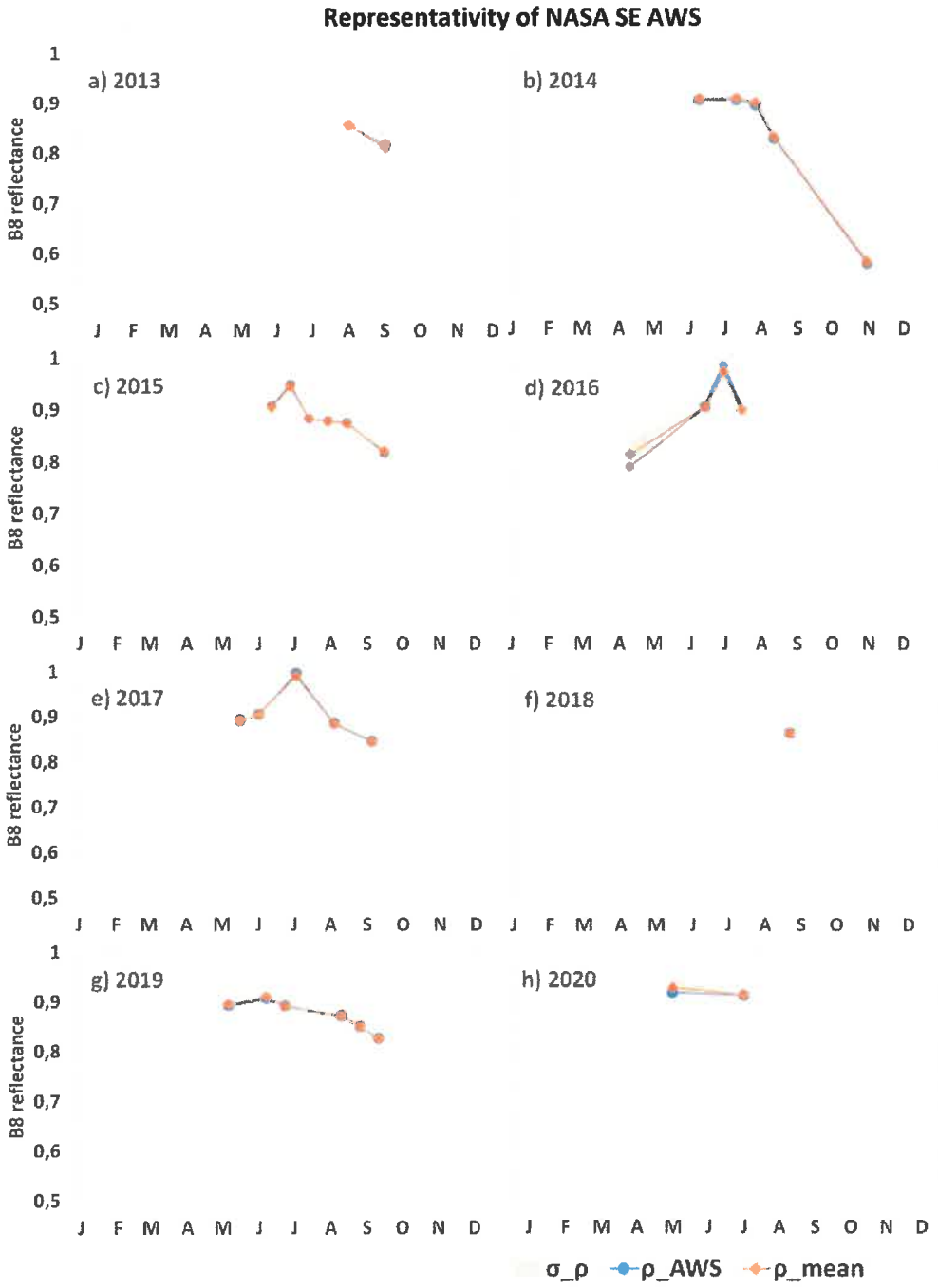
Representativity of NASA SE AWS
a) 2013
b) 2014
c) 2015
d) 2016
e) 2017
f) 2018
g) 2019
h) 2020
B8 reflectance
1
0,9
0,8
0,7
0,6
0,5
J F M A M J J A S O N D
σ_ρ
ρ_AWS
ρ_mean

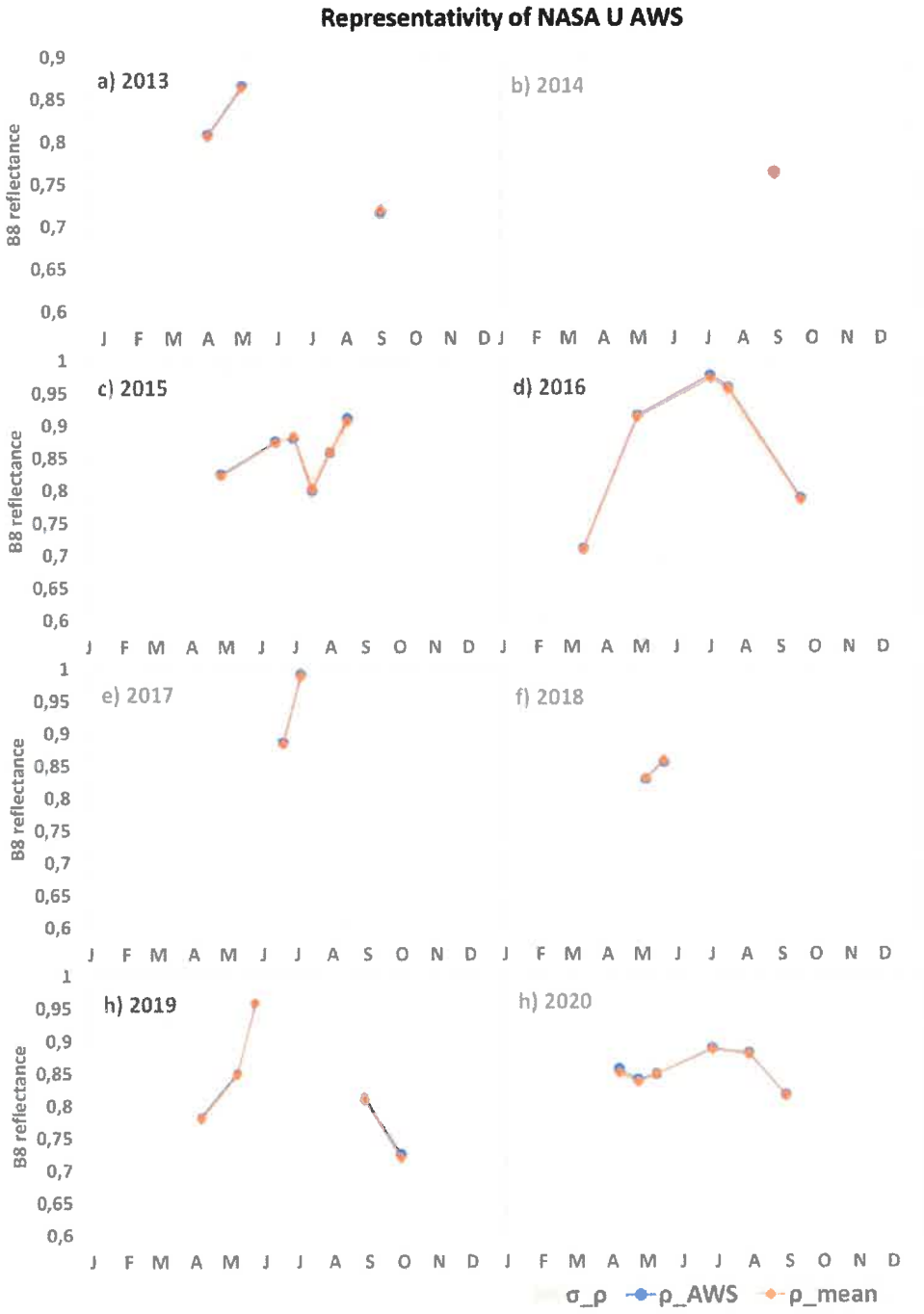
Representativity of NASA U AWS
a) 2013
b) 2014
c) 2015
d) 2016
e) 2017
f) 2018
h) 2019
h) 2020
B8 reflectance
J F M A M J J A S O N D
σ_ρ
ρ_AWS
ρ_mean

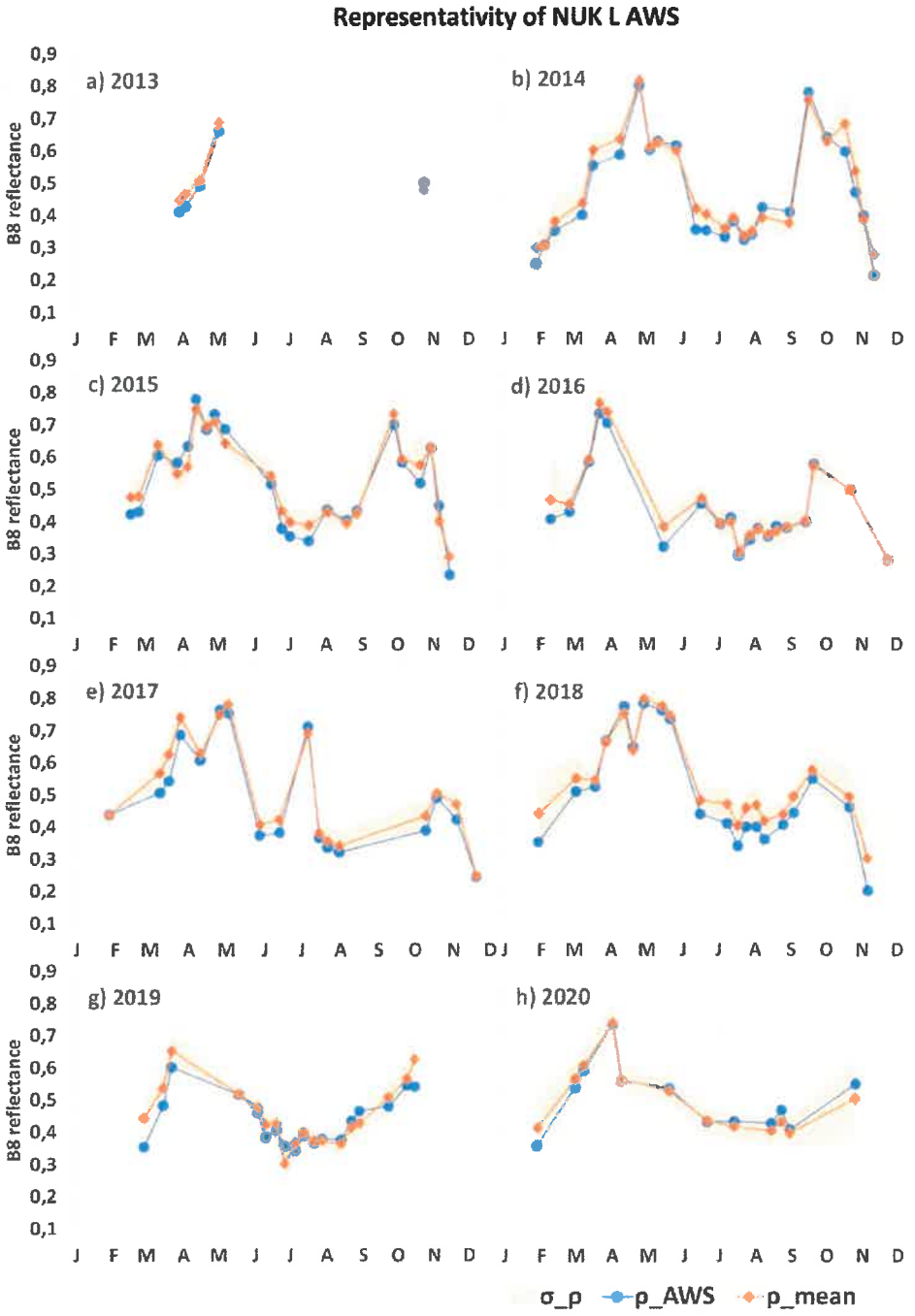
Representativity of NUK L AWS
a) 2013
b) 2014
c) 2015
d) 2016
e) 2017
f) 2018
g) 2019
h) 2020
B8 reflectance
0,9
0,8
0,7
0,6
0,5
0,4
0,3
0,2
0,1
J F M A M J J A S O N D
σ_ρ
ρ_AWS
ρ_mean

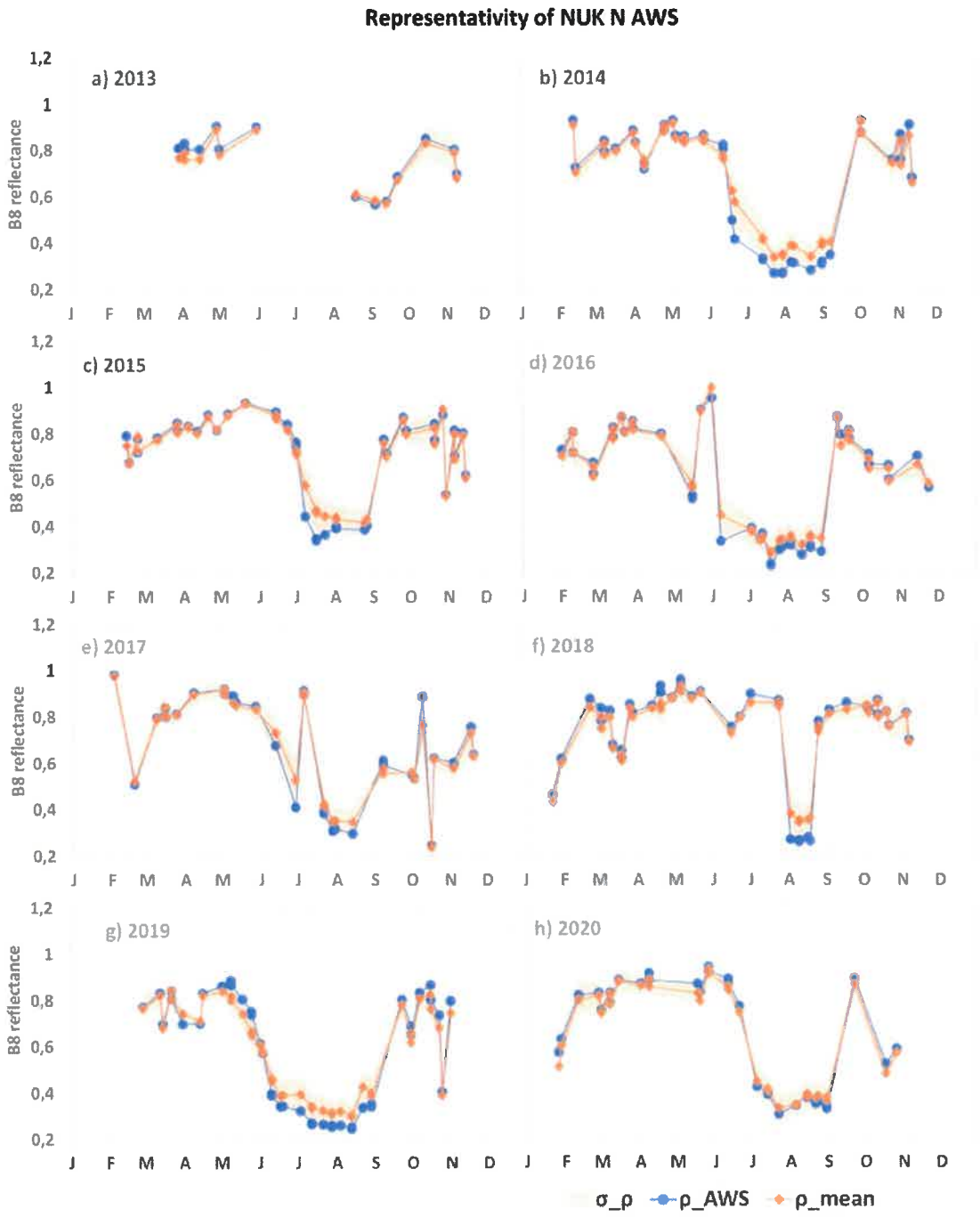
Representativity of NUK N AWS
a) 2013
b) 2014
c) 2015
d) 2016
e) 2017
f) 2018
g) 2019
h) 2020
B8 reflectance
1,2
1
0,8
0,6
0,4
0,2
J F M A M J J A S O N D
σ_ρ
ρ_AWS
ρ_mean

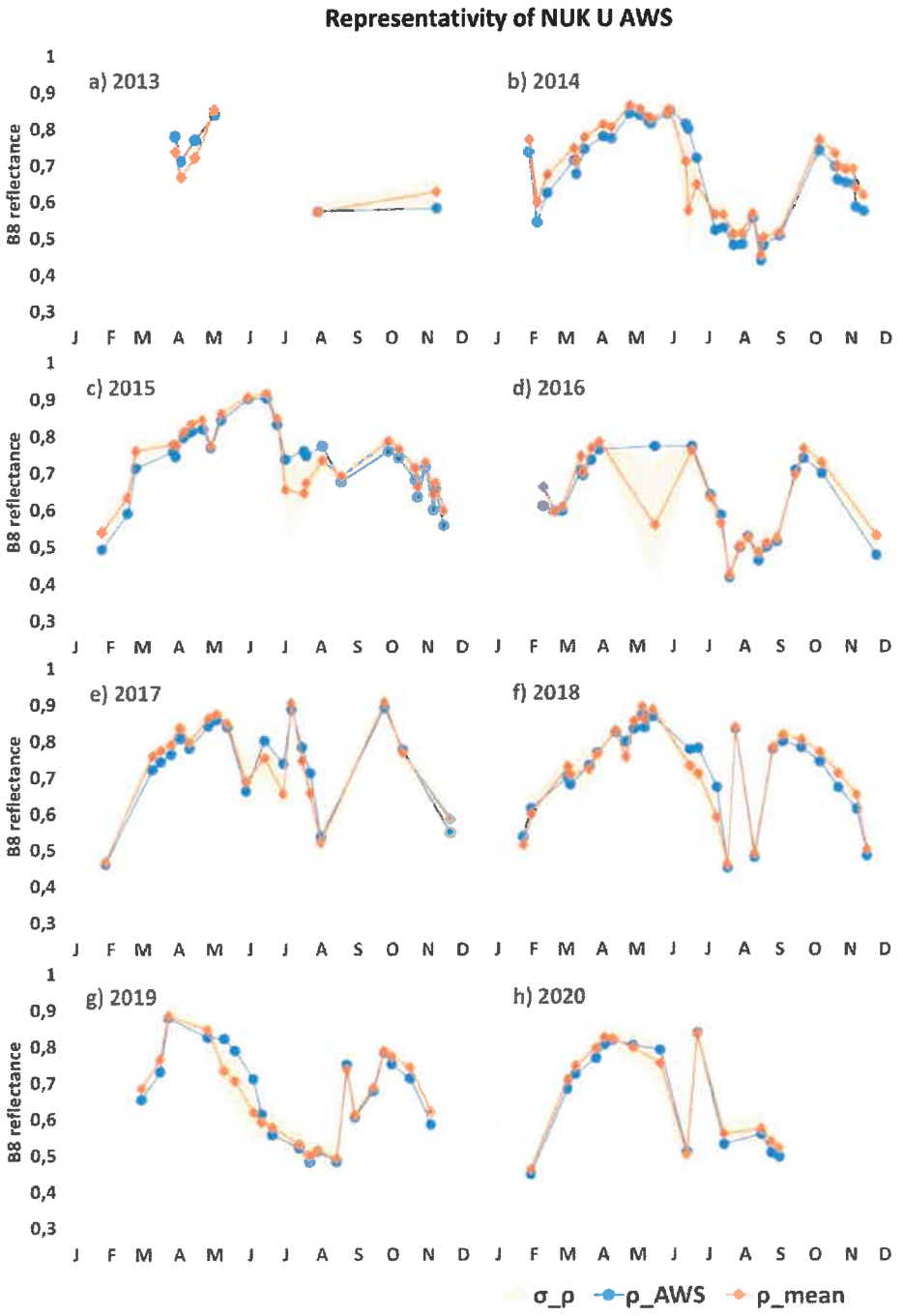
Representativity of NUK U AWS
a) 2013
b) 2014
c) 2015
d) 2016
e) 2017
f) 2018
g) 2019
h) 2020
B8 reflectance
1
0,9
0,8
0,7
0,6
0,5
0,4
0,3
J F M A M J J A S O N D J F M A M J J A S O N D
σ_ρ
ρ_AWS
ρ_mean

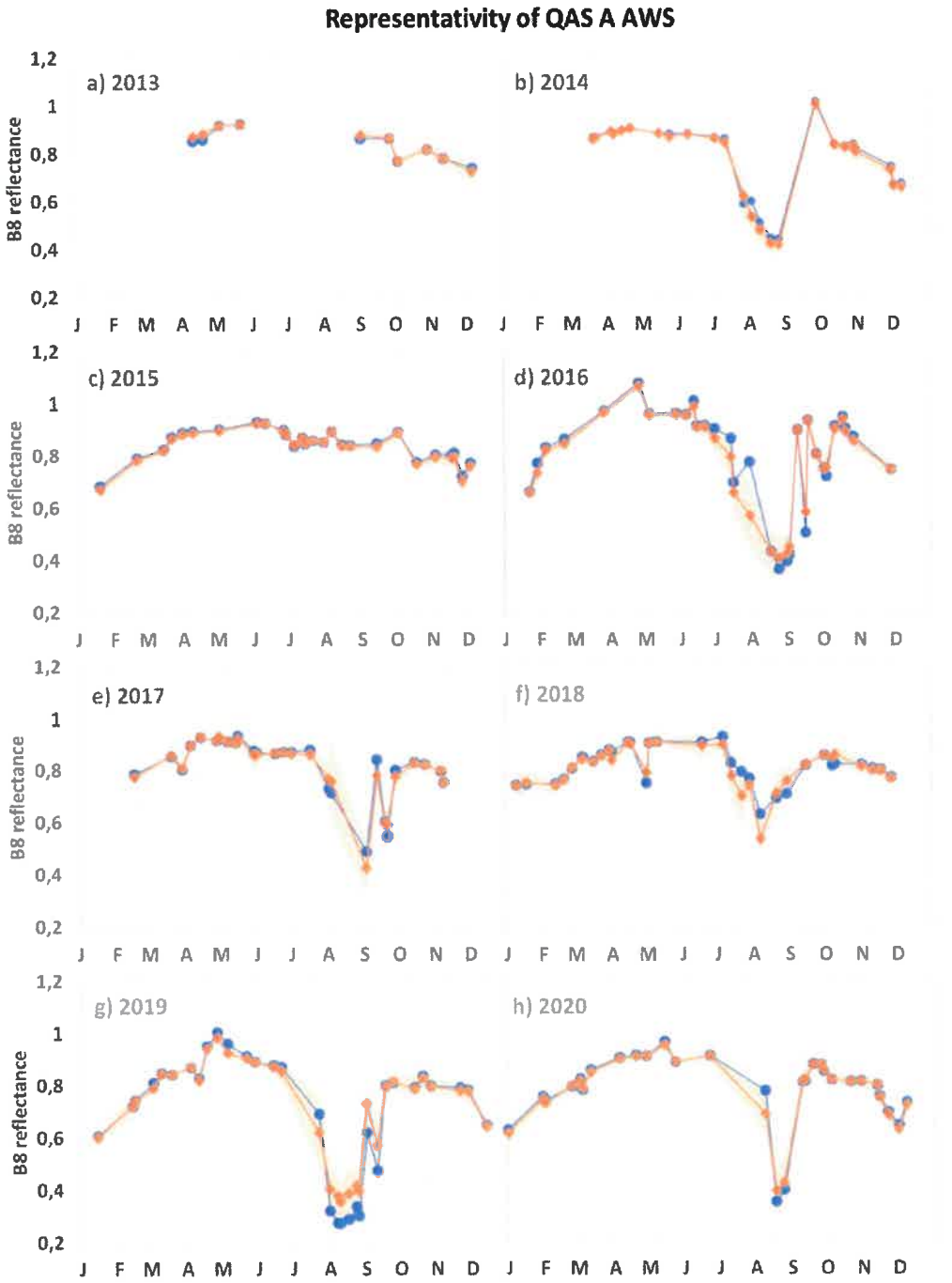
Representativity of QAS A AWS
a) 2013
b) 2014
c) 2015
d) 2016
e) 2017
f) 2018
g) 2019
h) 2020
B8 reflectance
1,2
1
0,8
0,6
0,4
0,2
J F M A M J J A S O N D

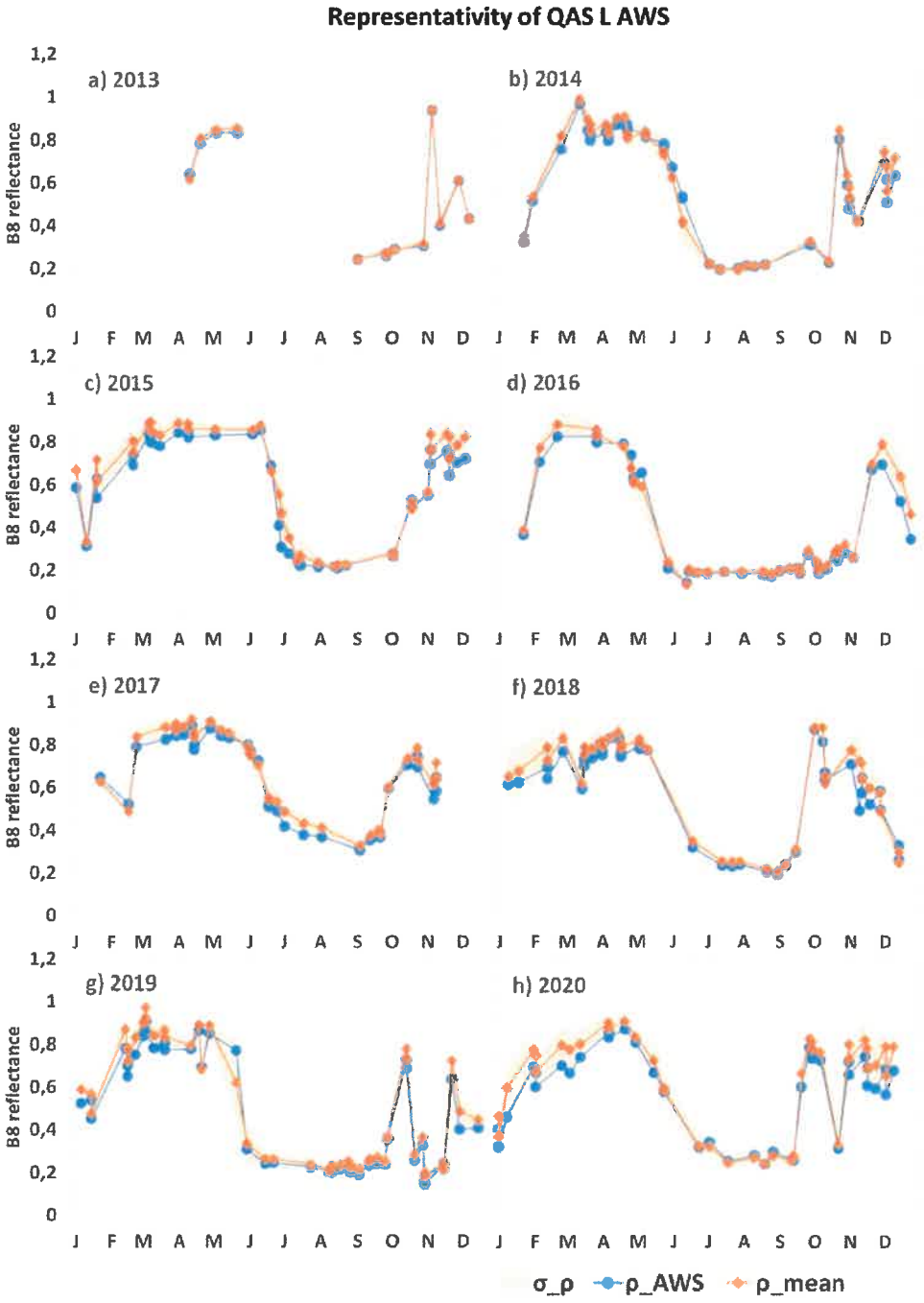
Representativity of QAS L AWS
a) 2013
b) 2014
c) 2015
d) 2016
e) 2017
f) 2018
g) 2019
h) 2020
B8 reflectance
1,2
1
0,8
0,6
0,4
0,2
0
J F M A M J J A S O N D
σ_ρ
ρ_AWS
ρ_mean

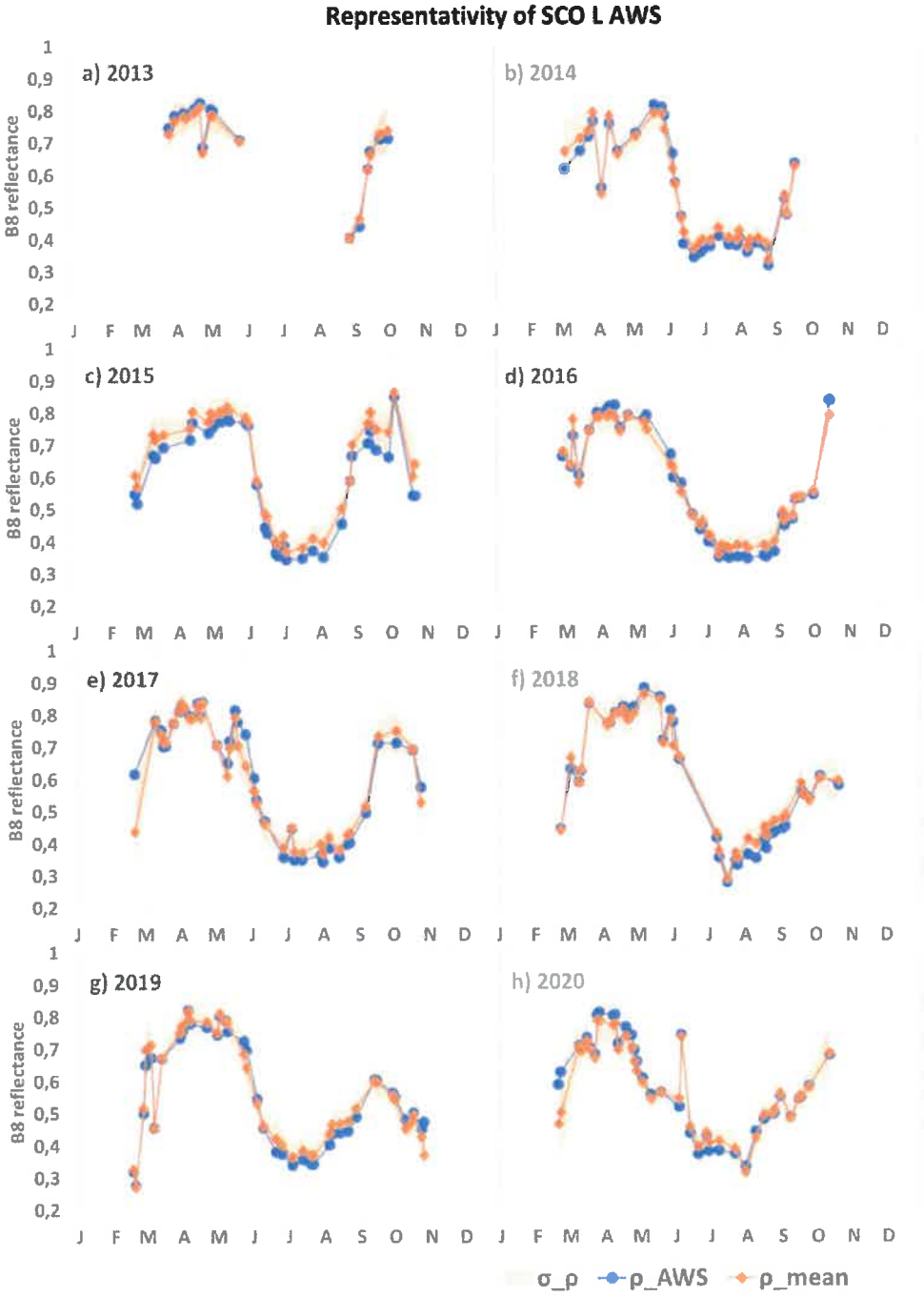
Representativity of SCO L AWS
a) 2013
b) 2014
c) 2015
d) 2016
e) 2017
f) 2018
g) 2019
h) 2020
B8 reflectance
1
0,9
0,8
0,7
0,6
0,5
0,4
0,3
0,2
J F M A M J J A S O N D
σ_ρ
ρ_AWS
ρ_mean

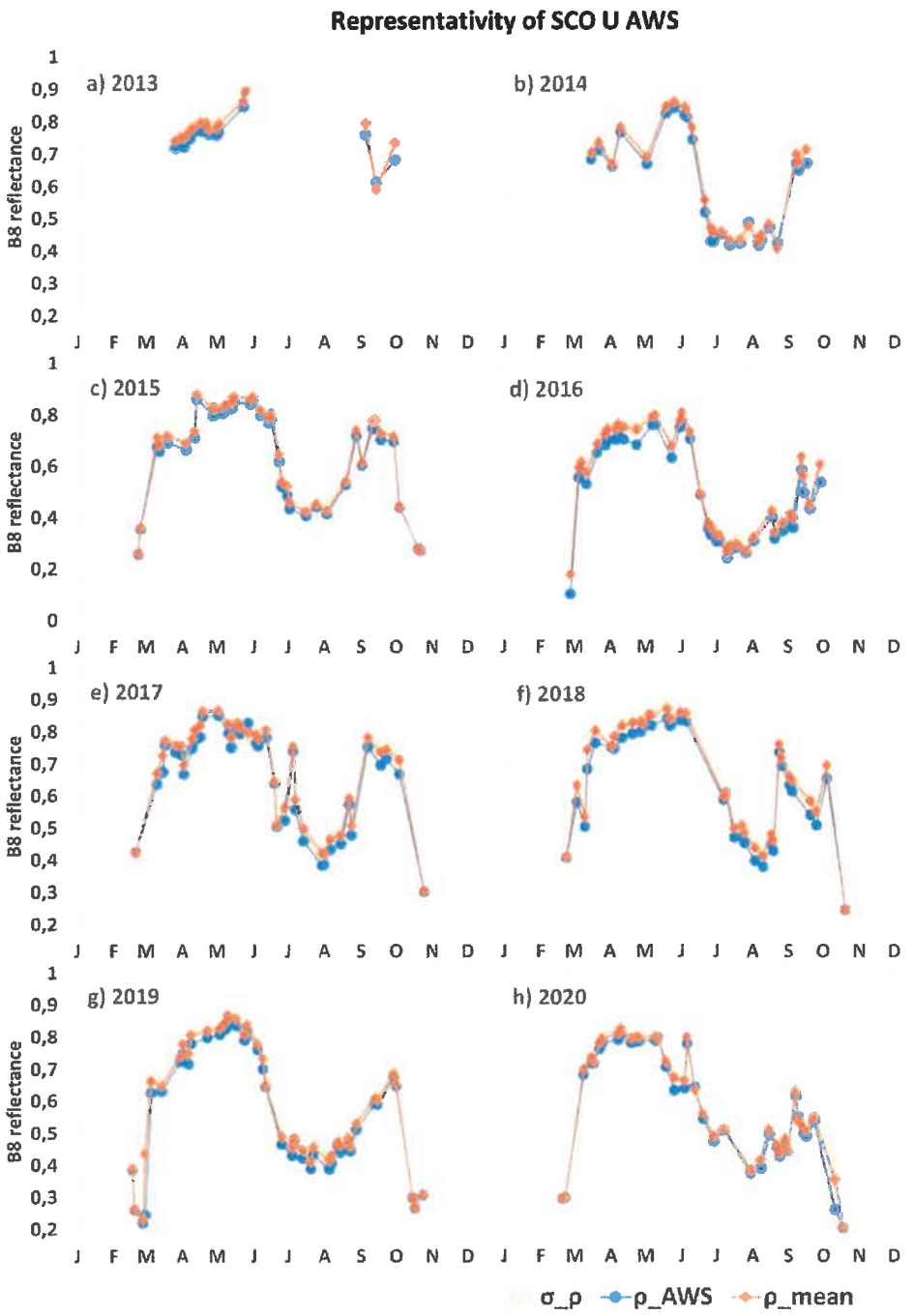
Representativity of SCO U AWS
a) 2013
b) 2014
c) 2015
d) 2016
e) 2017
f) 2018
g) 2019
h) 2020
B8 reflectance
J F M A M J J A S O N D
σ_ρ
ρ_AWS
ρ_mean

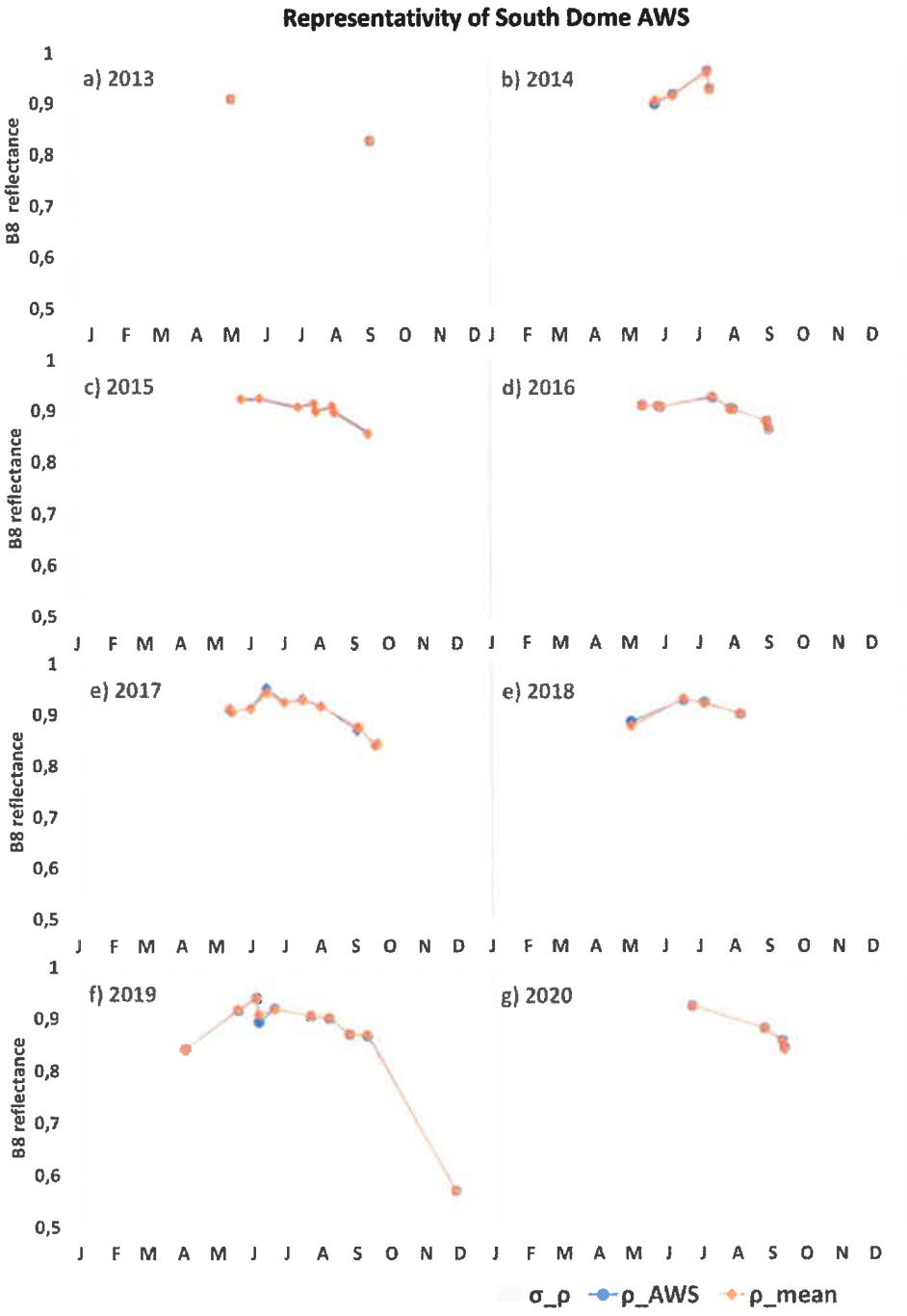
Representativity of South Dome AWS
a) 2013
b) 2014
c) 2015
d) 2016
e) 2017
e) 2018
f) 2019
g) 2020
B8 reflectance
1
0,9
0,8
0,7
0,6
0,5
J F M A M J J A S O N D
σ_ρ
ρ_AWS
ρ_mean

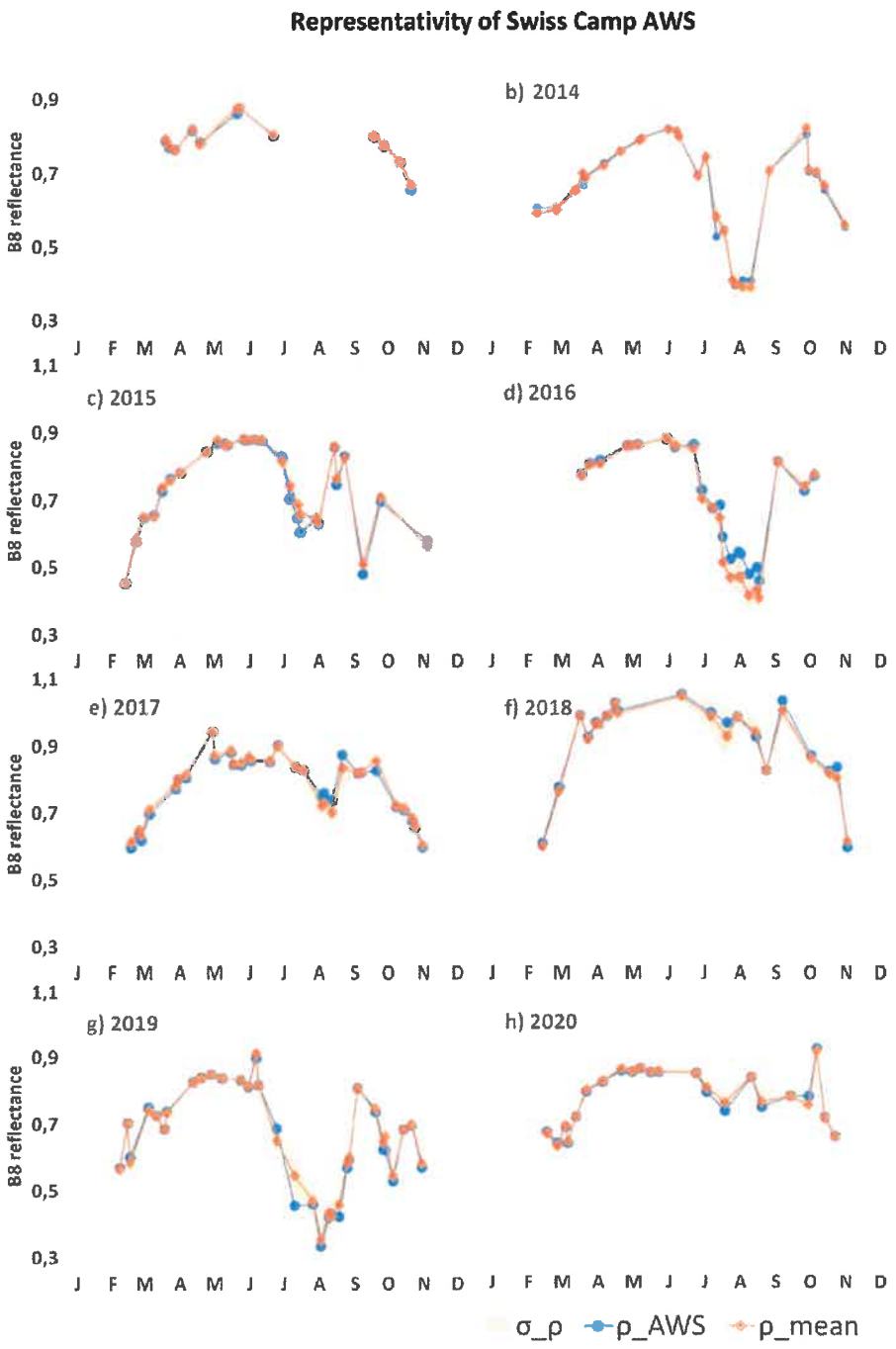
Representativity of Swiss Camp AWS
b) 2014
c) 2015
d) 2016
e) 2017
f) 2018
g) 2019
h) 2020
B8 reflectance
0,9
0,7
0,5
0,3
1,1
J F M A M J J A S O N D J F M A M J J A S O N D
σ_ρ
ρ_AWS
ρ_mean

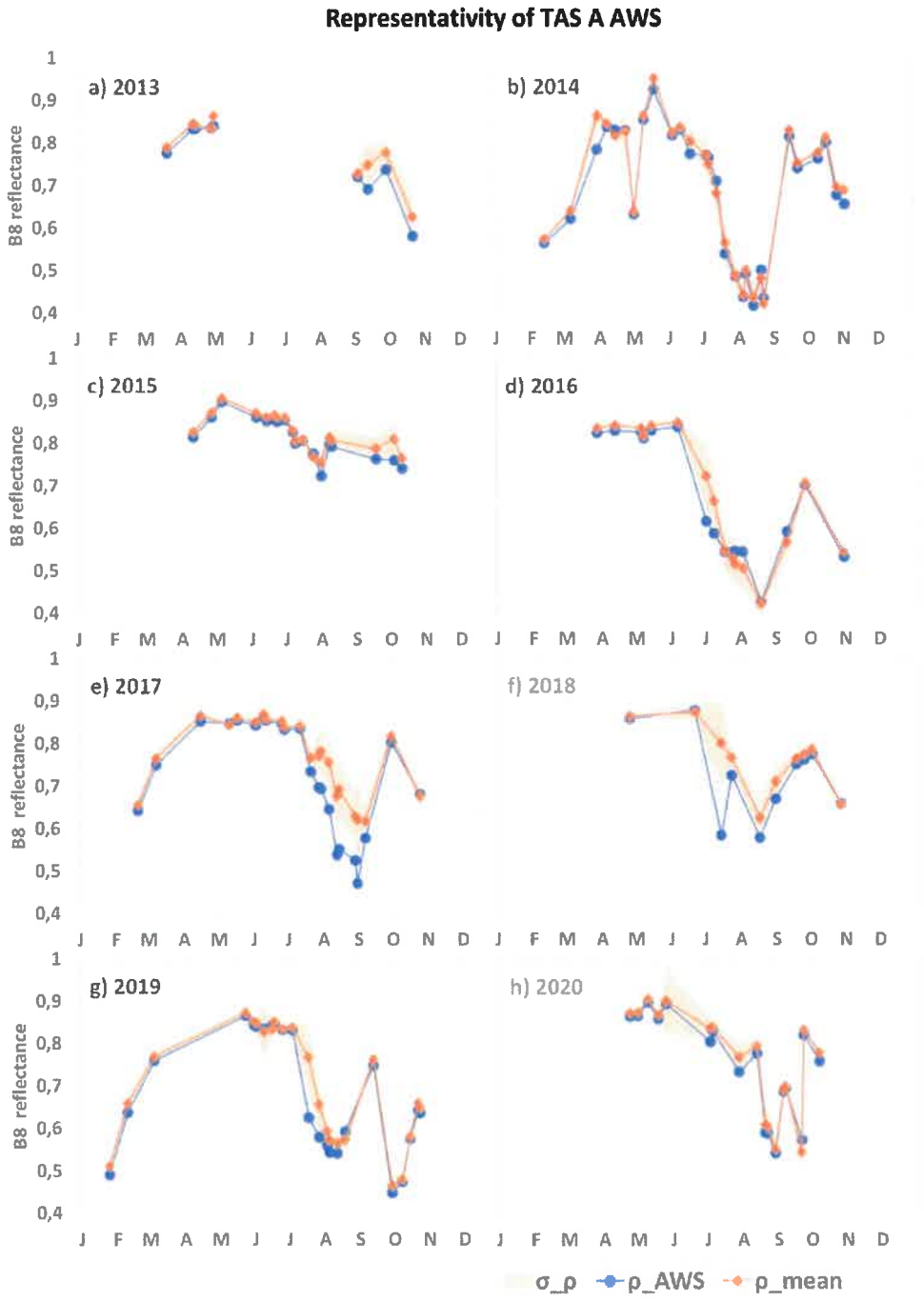
Representativity of TAS A AWS
a) 2013
b) 2014
c) 2015
d) 2016
e) 2017
f) 2018
g) 2019
h) 2020
B8 reflectance
1
0,9
0,8
0,7
0,6
0,5
0,4
J F M A M J J A S O N D
σ_ρ
ρ_AWS
ρ_mean

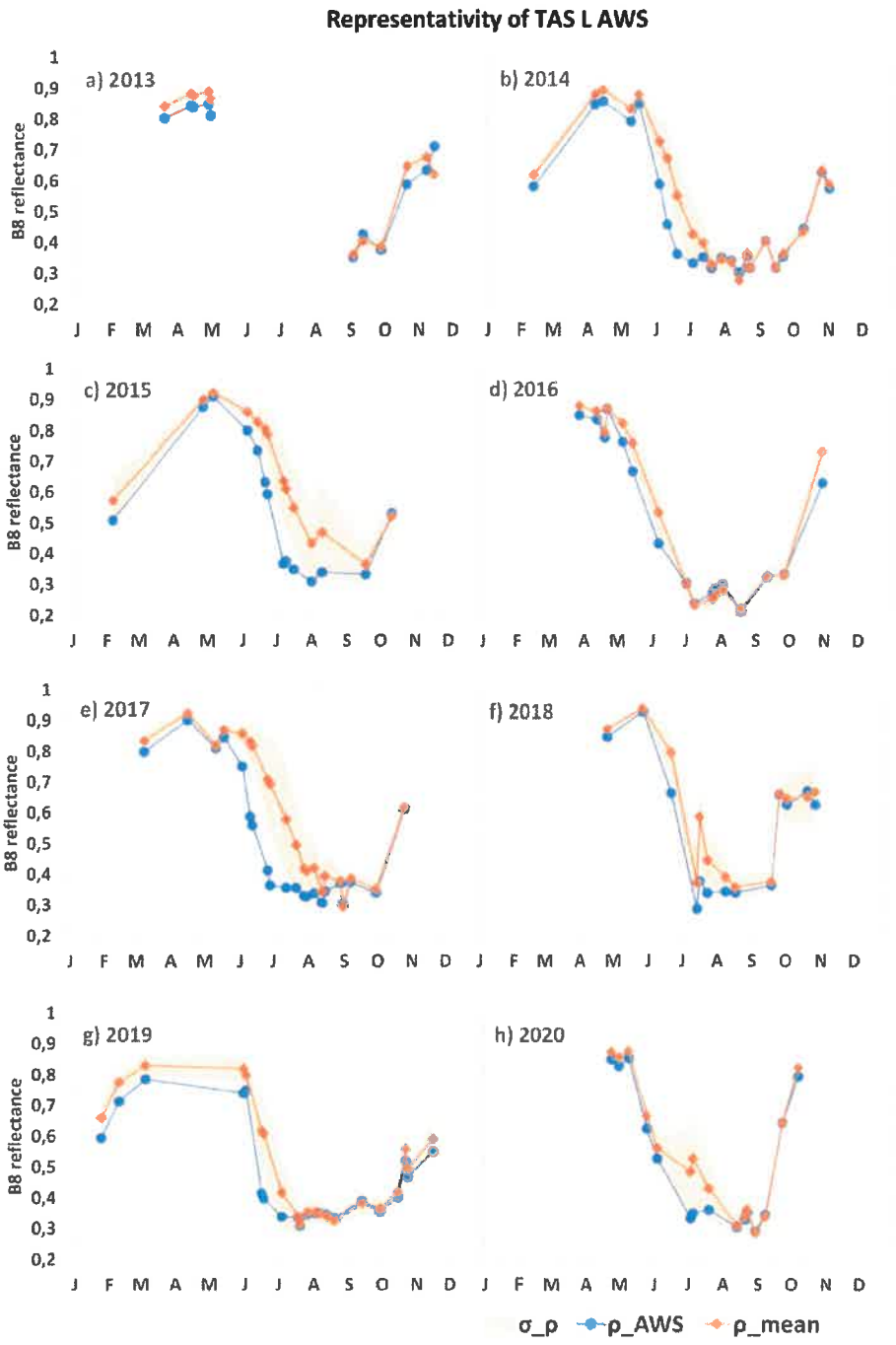
Representativity of TAS L AWS
a) 2013
b) 2014
c) 2015
d) 2016
e) 2017
f) 2018
g) 2019
h) 2020
B8 reflectance
1
0,9
0,8
0,7
0,6
0,5
0,4
0,3
0,2
J F M A M J J A S O N D
σ_ρ
ρ_AWS
ρ_mean

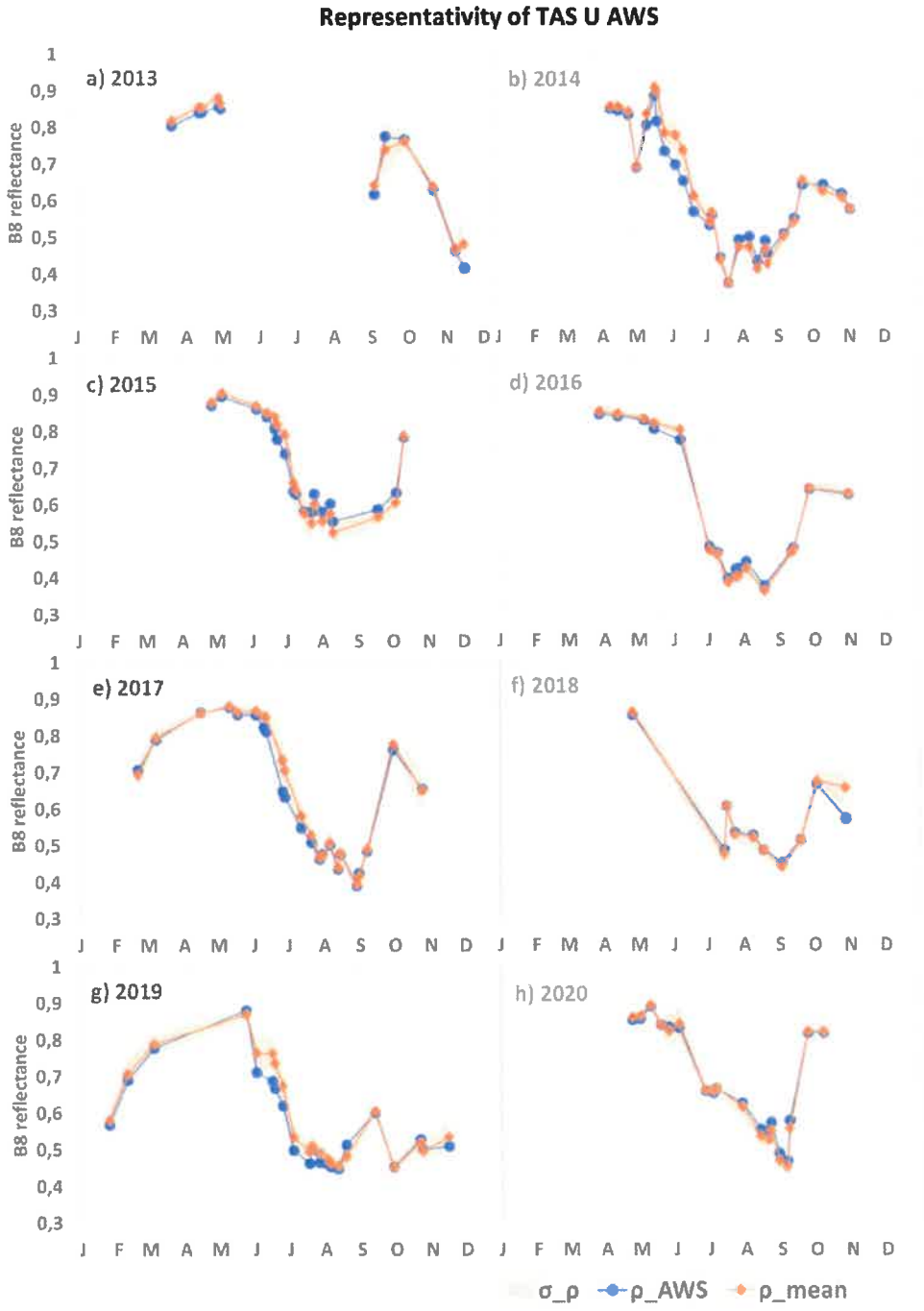
Representativity of TAS U AWS
a) 2013
b) 2014
c) 2015
d) 2016
e) 2017
f) 2018
g) 2019
h) 2020
B8 reflectance
1
0,9
0,8
0,7
0,6
0,5
0,4
0,3
J F M A M J J A S O N D
σ_ρ
ρ_AWS
ρ_mean

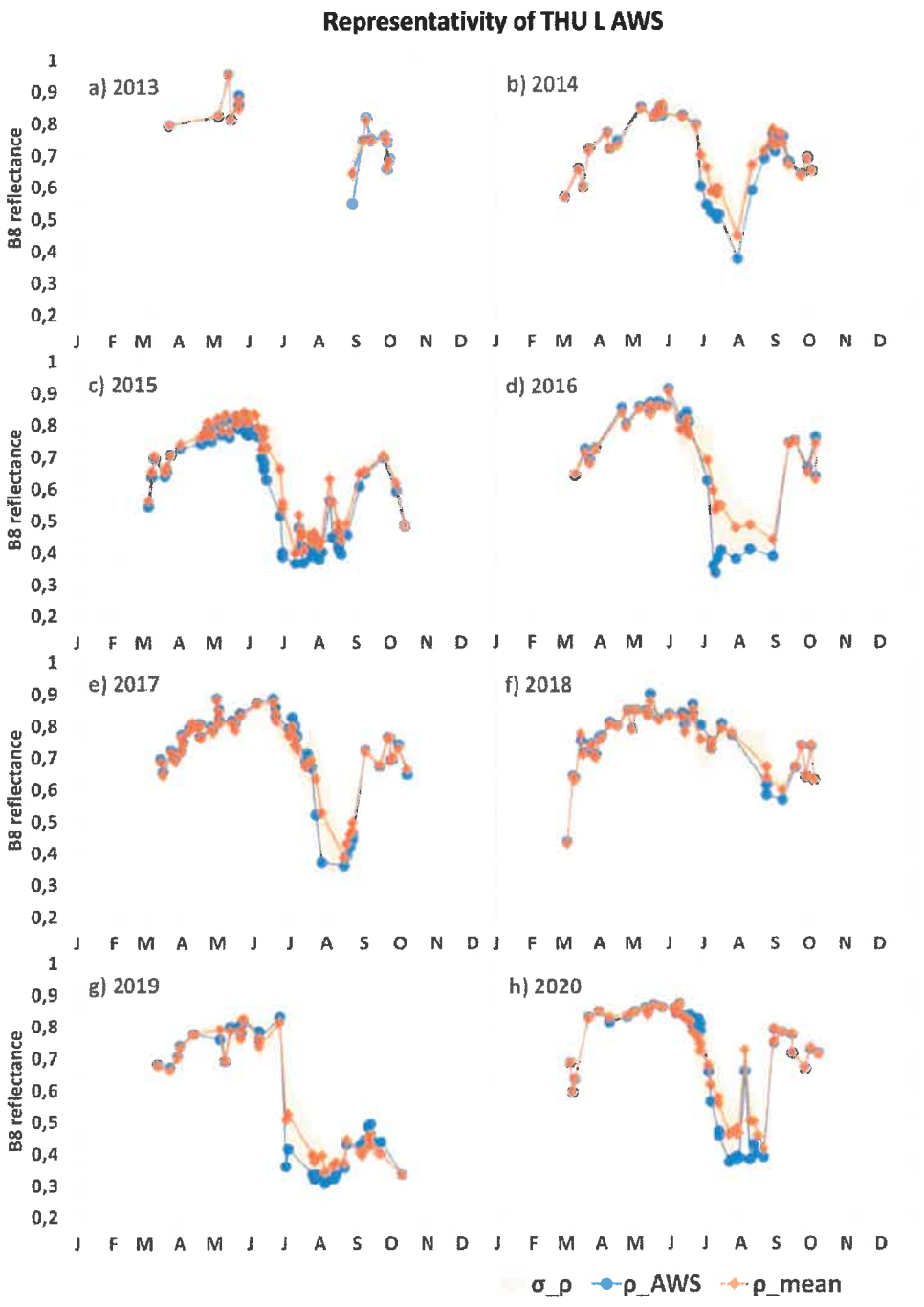
Representativity of THU L AWS
a) 2013
b) 2014
c) 2015
d) 2016
e) 2017
f) 2018
g) 2019
h) 2020
B8 reflectance
1
0,9
0,8
0,7
0,6
0,5
0,4
0,3
0,2
J F M A M J J A S O N D
σ_ρ
ρ_AWS
ρ_mean

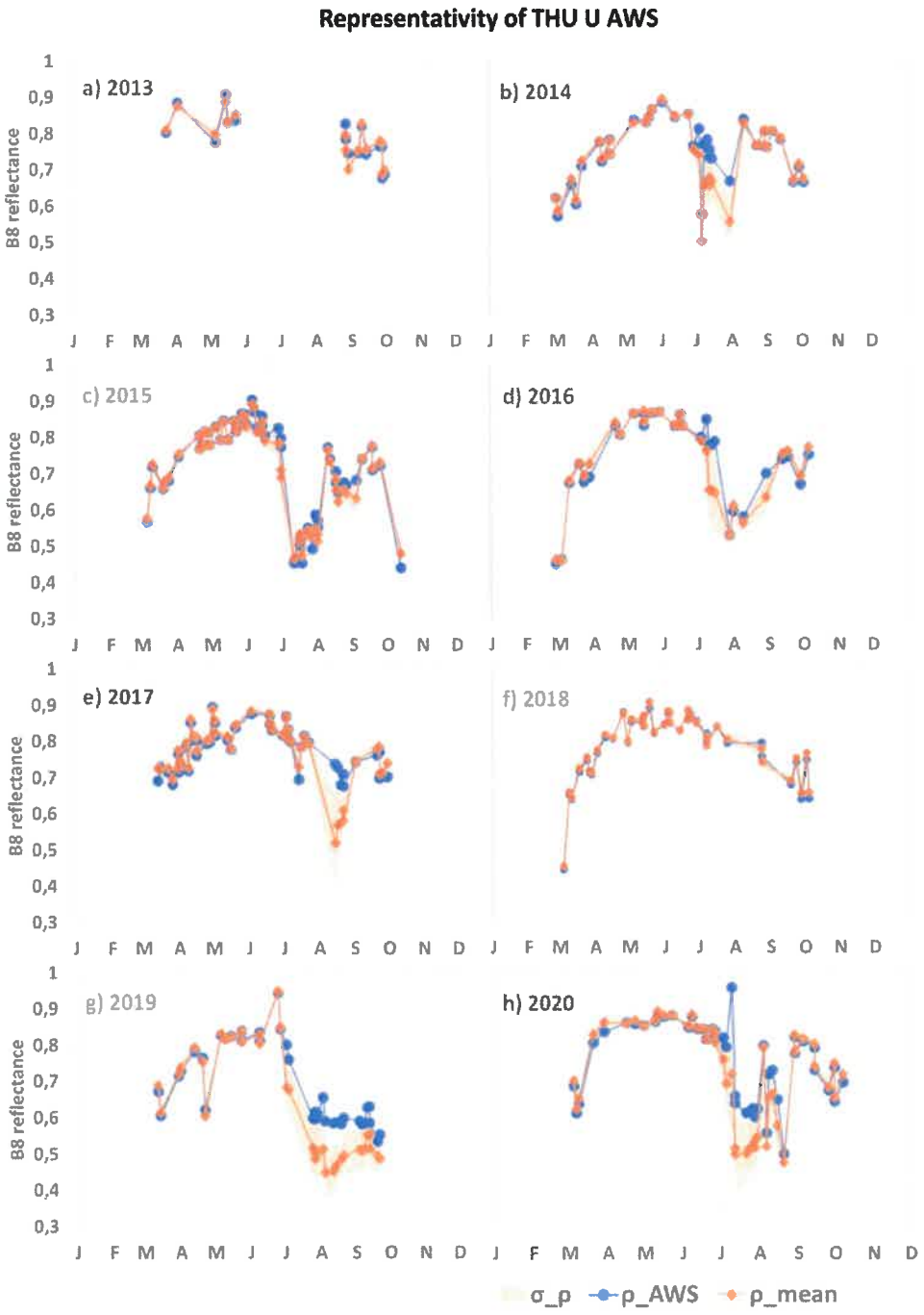
Representativity of THU U AWS
a) 2013
b) 2014
c) 2015
d) 2016
e) 2017
f) 2018
g) 2019
h) 2020
B8 reflectance
1
0,9
0,8
0,7
0,6
0,5
0,4
0,3
J F M A M J J A S O N D
σ_ρ
ρ_AWS
ρ_mean

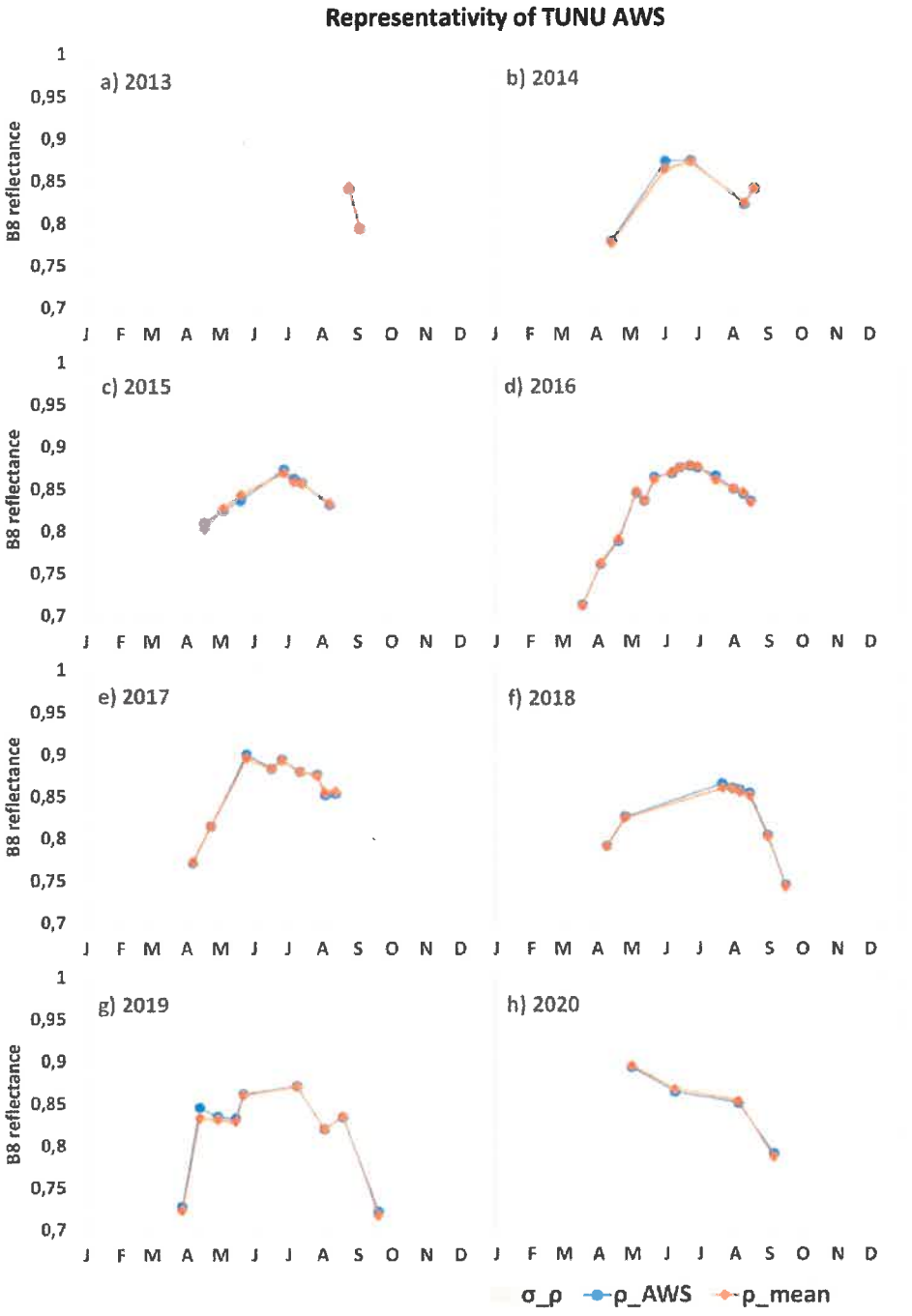
Representativity of TUNU AWS
a) 2013
b) 2014
c) 2015
d) 2016
e) 2017
f) 2018
g) 2019
h) 2020
B8 reflectance
1
0,95
0,9
0,85
0,8
0,75
0,7
J F M A M J J A S O N D J F M A M J J A S O N D
σ_ρ
ρ_AWS
ρ_mean

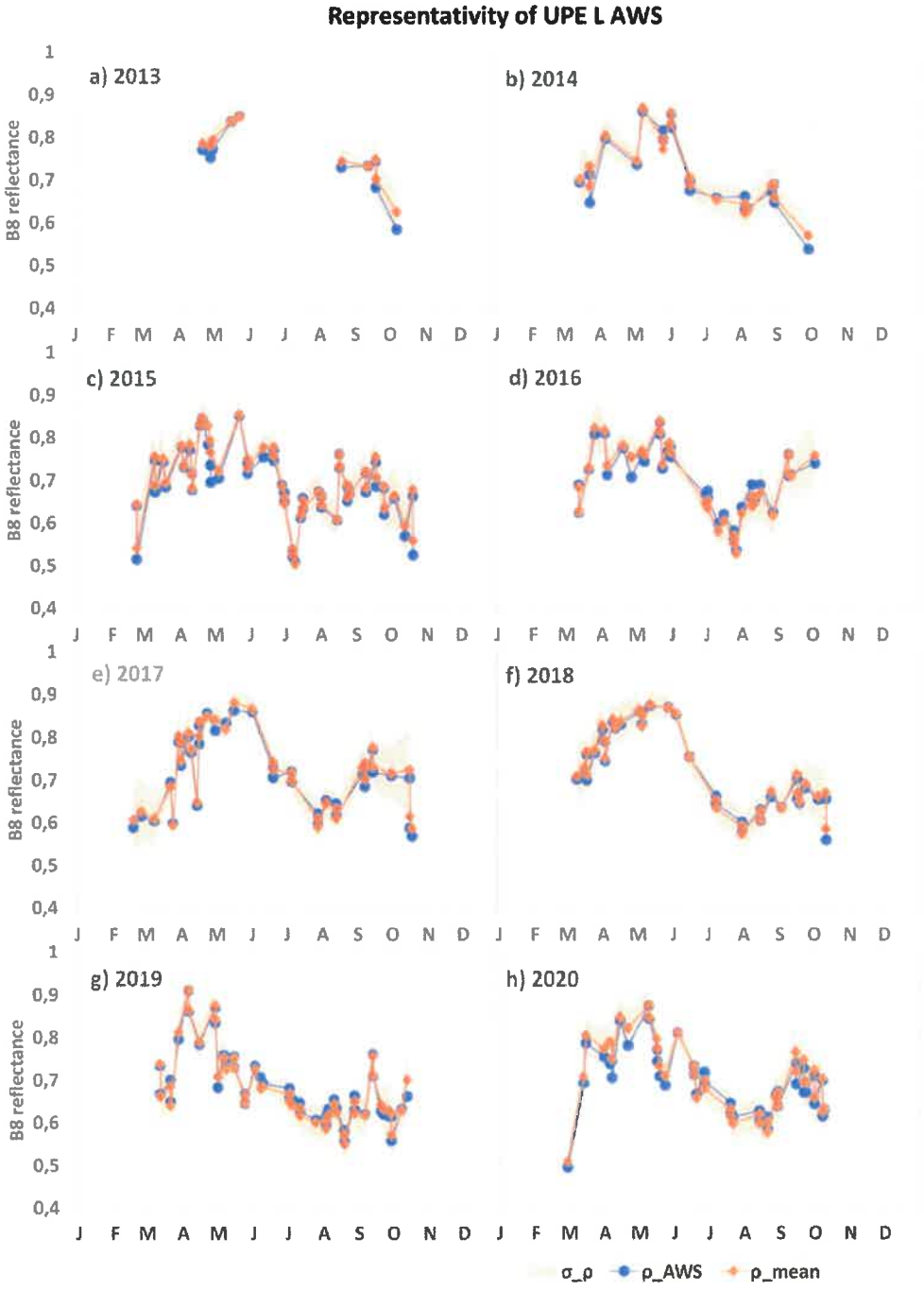
Representativity of UPE L AWS
a) 2013
b) 2014
c) 2015
d) 2016
e) 2017
f) 2018
g) 2019
h) 2020
B8 reflectance
1
0,9
0,8
0,7
0,6
0,5
0,4
J F M A M J J A S O N D
σ_ρ
ρ_AWS
ρ_mean